D D C

APR

B

APPLIED SCIENCE DIVISION
LITTON SYSTEMS, INC.
LITTON INDUSTRIES

20 November 1965

ELECTROHYDRODYNAMIC REMOVAL
OF MICROORGANISMS
FROM HYDROCARBON FUELS

FINAL REPORT

Covering Period:

25 June 1963 - 20 November 1965

Prepared for:

HQ QM Research and Engineering Command, U.S. Army
QM Research and Engineering Center
Natick, Massachusetts

Submitted by: *L.H. Ruhnke*
L.H. Ruhnke, Manager
Atmospheric Electricity

Prepared by:

   L. Ruhnke
   E. Will
   P. Pederson

Approved by: *A. A. Anderson*
A.A. Anderson, Director
Applied Research

Contract No: DA-19-129-AMC-141(N)
Project No: 1k012501A031(05)
ASD Project No: 51508
ASD Report No: 2905

APPLIED SCIENCE DIVISION
Litton Systems, Inc.
2003 East Hennepin Avenue
Minneapolis, Minnesota 55413

FOREWORD

This technical document report is the Final Progress Report
by the Applied Science Division of Litton Systems, Inc. (as successor
in interest to General Mills, Inc. as defined by Contract No.
DA-19-129-AMC-141(N), Modification No. 2).

ABSTRACT

The feasibility of removing microorganisms and other
particulates from hydrocarbon fuels by electrostatic precipitation
was studied. Theoretic investigations describe the physics of
electrohydrodynamic precipitation and essential parameters
influencing collection efficiency. Measurements of fuel character-
istics and filter parameters have been made which led to the
development of an electrohydrodynamic filter. Particulates and a
liquid are unipolarly charged in a corona edge ionizer and then are
flushed into a precipitation tube in which particulates are moved by
Coulomb forces into porous non-conducting walls. A 10-gpm model
showed filter efficiencies of a least 85 percent by number of
particles larger than 1 micron diameter. The basic advantages of the
method investigated are the low pressure drop over the filter
element and the small size of the unit.

TABLE OF CONTENTS

TABLE OF CONTENTS (continued)

TABLE OF CONTENTS (continued)

LIST OF ILLUSTRATIONS

LIST OF ILLUSTRATIONS (continued)

LIST OF ILLUSTRATIONS (continued)

ELECTROHYDRODYNAMIC REMOVAL OF MICROORGANISMS FROM HYDROCARBON FUELS

I. INTRODUCTION

A program to study electrohydrodynamic removal of microorganisms from hydrocarbon fuels was initiated by the U.S. Army Quartermaster Research and Development Command. The investigation's objective was to study electrostatic filter techniques which possess, as their major advantage, a very low pressure drop across the filter element while maintaining a high filter efficiency. Electrostatic filtering of atmospheric air has become widely known and used in industrial operations for removal of smoke and dust. Any suspended particles are electrically charged by corona currents and then are precipitated to a collecting electrode in a strong electric field. Similar mechanisms are applicable in nonconducting liquids, e.g., hydrocarbon fuels.

Two principal mechanisms can be employed to electrically precipitate suspended particles from insulating liquids: 1) electrical forces on non-charged particles in nonuniform electric fields or, 2) electrical forces on charged particles. The problem of precipitating uncharged particles has been sufficiently treated by Pohl[1], who demonstrated the behavior of larger-than-molecular-sized particles in strong divergent electric fields. This effect is known as dielectrophoresis. Of more importance for filter application, particles charged in strong unipolar ionization are forced to move in the direction of the electric field (Coulomb forces). As will be shown later, both effects (dielectrophoresis and Coulomb forces) act in opposite directions in a commonly used coaxial arrangement. Such an arrangement has the advantage that ionizer and precipitator are combined in one unit. The arrangement which was investigated in this research program used a highly efficient corona ionizer and a separate precipitator. This results in dielectrophoretic and Coulomb forces acting in the same direction. Such an arrangement evolved from

other applications of ion dynamics in hydrocarbons described elsewhere.
The expression electrohydrodynamic precipitator, in analogy to magneto-
hydrodynamics, has become useful for describing this kind of electrostatic
precipitator.

Preliminary tests fully demonstrated the feasibility of the method[5]
but many questions pertinent to operational use for the removal of micro-
organisms remained unanswered. Such vital parameters as filter effi-
ciency, filter saturation, rate of fuel flow, deposit removal, and operational
hazards needed to be investigated before development of operational-type
filter systems. While substantial progress can be achieved by analytical
study of the involved problems, it was believed that a considerable effort
must be spent on experimentation.

This report deals with a description of the experimental setup made
to investigate several parameters of the CIE fuel to be tested, to establish
design criteria for an operational-model precipitator, to develop a proto-
type model, and to test the instrument by using microorganisms and inert
particles as test agents.

In a theoretic analysis, simplifying assumptions are made to estimate
the influence of particle size, flow rate, charge density, water content,
and other factors on filter efficiency. In this way, a basis for experimen-
tation was evolved from which more sophisticated theories could be de-
veloped or experimental results could be interpreted meaningfully. One
of the major difficulties in experimenting with fuel slightly or heavily
contaminated by microorganisms is that an accurate sampling method
to enable the counting of living or dead suspended particulates had to be
employed. Considerable efforts were made, therefore, to develop a
reliable, but easy method for counting microorganisms over a wide
range of concentrations. The experimental setup is constructed as a
semipermanent installation--not only to measure and vary-at-will the
flow parameters and material constants, but also to serve as a test stand
for different models of precipitators.

Theoretical expressions show that large particles, low liquid viscosity, low ion mobility, and low electrolytic conductivity favor collection efficiency of such electrohydrodynamic filters. Collection efficiencies for a one-stage filter of close to 100 percent for particles down to 1 micron in diameter are technically feasible. For a particular liquid, however, it was necessary to study each parameter that influences collection. This is essential, not only to estimate obtainable filter efficiencies, but also to design the most proper arrangement for reliable and effective operation. An investigation was made to measure electrical, as well as other quantities, of the liquid and of the filter.

The precipitator wall material was found to be of great importance. While most of the particles within the liquid could be forced to the wall by electrostatic forces, it was found that at high Reynolds numbers the wall deposit was washed off easily by the liquid. A porous nonconducting wall material was found suitable to retain the deposited particles.

Tests were then made with a 10-gpm filter to obtain filter characteristics. Filter efficiency and its size dependence were investigated. It was found that for particles larger than 1-micron diameter filter efficiency is at least 85 percent, but probably higher than 95 percent by number and better than 99 percent by mass when using any commonly found size spectrum.

These tests were followed by the construction of a 50-gpm prototype filter. The prototype has a pressure drop of 8 psi which is determined by the pressure drop over the ionizer section. Much lower pressure drops are feasible through proper design.

In a last phase of the program, the electrostatic precipitator was used in a biological experiment in which the growth of microorganisms in filtered and unfiltered CIE fuel was investigated.

II. PHYSICS OF ELECTROHYDRODYNAMIC PRECIPITATION

A. Unit System

The unit system used throughout this study is the meter-kilogram-second system. Wherever comparisons of data from other sources demand conversion from other well-adopted units, both unit systems will be used in parallel. Electrical quantities are given in volts and amperes. The unit of force will be the newton (equal to $m \times kg \times sec^{-2}$), with 1 newton x meter equal to 1 volt x amp x sec. Dimensions of derived quantities such as mobility, viscosity, dielectric constant, and the like, are mentioned whenever first used. For conversion to other units, consult the Appendix. Vectors are denoted by arrows.

B. Analysis of Electrostatic Precipitator

According to Coulomb's law, the force $\vec{F}$ (newton) on a suspended particle is given by its charge Q (amp sec) and the electric field $\vec{E}$ (volt m^{-1}):

$$\vec{F} = Q \vec{E} . \tag{1}$$

For a particle of radius a (m) in a medium with viscosity η (newton sec m^{-1}), this force is balanced by Stokes friction force when moving at velocity v (m sec^{-1}):

$$\vec{F} = 6 \pi \eta a \vec{v} . \tag{2}$$

The velocity a particle will obtain against its surroundings is therefore proportional to its charge, electric field, and is inversely proportional to size and viscosity:

$$\vec{v} = \frac{Q \vec{E}}{6 \pi \eta a} . \tag{3}$$

From this, mobility b $(m^2 v^{-1} sec^{-1})$ can be derived which states how fast a particle moves in a given electric field:

$$b = \frac{Q}{6 \pi \eta a} .$$ (4)

For an electrostatic precipitator that uses Coulomb forces, it is necessary therefore to charge up the particles to be removed and to build up an elec-tric field, which is directed towards the precipitating walls.

The charging mechanism, as it applies to charging with corona ionizers, is described sufficiently in the literature.[6] Particulates stream through a region of high electric fields and high unipolar current densities. By bombardment with ions, the particulates obtain a maximum charge Q_{max};

$$Q_{max} = 4 k \pi a^2 \epsilon E,$$ (5)

where k is a dimensionless constant depending on the relative dielectric con-stant of a particle and liquid. ϵ (amp sec volt^{-1} m^{-1}) is the dielectric constant of the liquid.

The maximum electric field which can be applied is given by the break-down field of the liquid. For safe operation this field will be maintained somewhat below the breakdown point. The particles are then flushed out into the precipitating tube where they are discharged according to the con-ductivity σ (amp volt^{-1} m^{-1}) of the liquid and the remaining field strength. For reasons of simplicity we will assume a model where the charge is lost only due to attraction of ions of opposite sign and with no additional charging mechanism present. Then Q is determined by:

$$dQ/dt = Q \sigma/\epsilon$$ (6)

$$Q = Q_{max} \exp(-t \sigma/\epsilon) .$$ (7)

For deriving particle trajectories in the precipitator and, consequently, filter efficiency, it is necessary to know the electric field-line pattern caused by the space charge being flushed out from the ionizer. Figure 1 illustrates the notations used in relation to the operation of the precipitator.
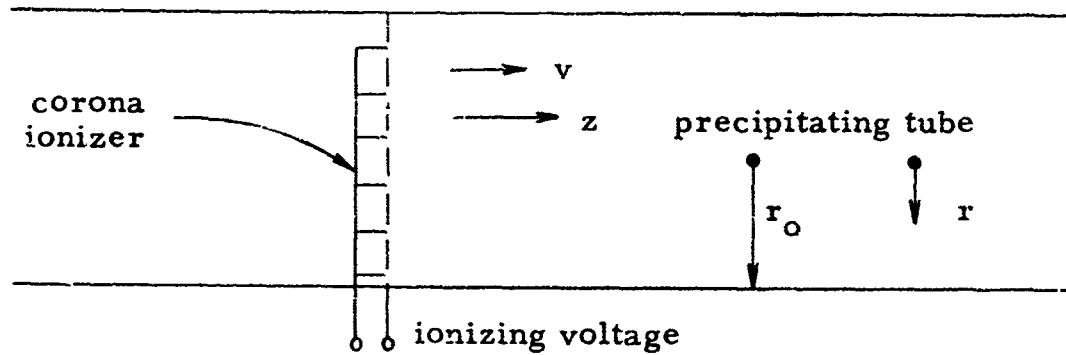
Figure 1. Operating Principle of the EHD Filter

At $z = 0$, liquid with charge density q_o (amp sec m^{-3}) is entering a cylindrical pipe of radius r_o (m) with velocity v. The maximum charge density in the liquid depends on the ionizer properties and maximum electric field. At the entrance of the tube, space charge density q can be assumed constant over the whole cross section. With time, q is decreasing hyperbolically:

$$q(t) = q_o/(1 + t/t_c) \quad , \qquad (8)$$

with t_c (sec) a time constant given by the dielectric constant, the electrolytic conductivity of the liquid, and the space charge induced conductivity qb. We will assume that this latter conductivity is not influenced by particulates so that the mobility b is that given by the liquid:

$$t_c = \epsilon/(\sigma + qb) \quad . \qquad (9)$$

After t_c seconds, the liquid has moved a distance of z_c:

$$z_c = v \, t_c \, .\tag{10}$$

Using Equation (8) we obtain a distance dependence of q:

$$q(z) = q_o \, 1/(1 + z/z_c) \, .\tag{11}$$

The hyperbolic decay of the space charge is exactly true only where the gradient of the space charge can be neglected. This is fulfilled only approximately for our model when the space charge is streaming through the precipitator.

Electric field strength is now given by Poisson's equation

$$\text{div } \epsilon \, \mathbf{E} = q \qquad .\tag{12}$$

For a cylindrical pipe we obtain the radial component $\mathbf{E}_r$ from Equation (12) which is:

$$\mathbf{E}_r = q_o \, r/2\epsilon \, (1 + z/z_c) \, .\tag{13}$$

To estimate the order of magnitude of the longitudinal field $\mathbf{E}_z$, we will neglect the boundary effects and assume only a change of space charge with z. We obtain from Equations (11) and (12) in approximation:

$$\mathbf{E}_z = -q_o/\epsilon \, z_c \, \exp(-z/z_c)\tag{14}$$

and

$$\mathbf{E}_z/\mathbf{E}_r = 2 \, z_c/r \qquad .\tag{15}$$

It seems, therefore, that the electric field vector has an appreciable longitudinal component because z_c and r are in the same order of magnitude. This means that the force vector on the particle is not directed exactly perpendicular to the flow direction. The longitudinal component will not alter principally the filter efficiency. It will, however, change the apparent viscosity of the fluid[7] and influence hydrodynamic characteristics. A more rigid attempt to calculate particle flow pattern will not be made because of the mathematical burden involved.

C. Dielectrophoretic Forces

For comparison with the corona-wire ionizer-precipitator, we will discuss dielectrophoretic forces. The radial field in a coaxial precipitator with a center electrode of radius r'_o is strongest at the center and decreases with increasing distance from the center (Figure 2). Assuming constant conductivity over the cross section, the radial field strength E'_r is given by

$$E'_r = E_{max} r'_o/r \quad . \tag{16}$$

For the electrohydrodynamic case, we obtain from Equation (13)

$$E_r = E_{max} r/r_o \quad . \tag{17}$$

For the dielectrophoretic force F_d, Kao[8] gives an expression for spherical particles of radius a:

$$F_d = 2 \pi a^3 \epsilon \nabla E^2 \tag{18}$$

For the total force on a particle, the Coulomb force F_c and dielectrophoretic forces F_d have to be added:

$$F = F_c + F_d \tag{19}$$
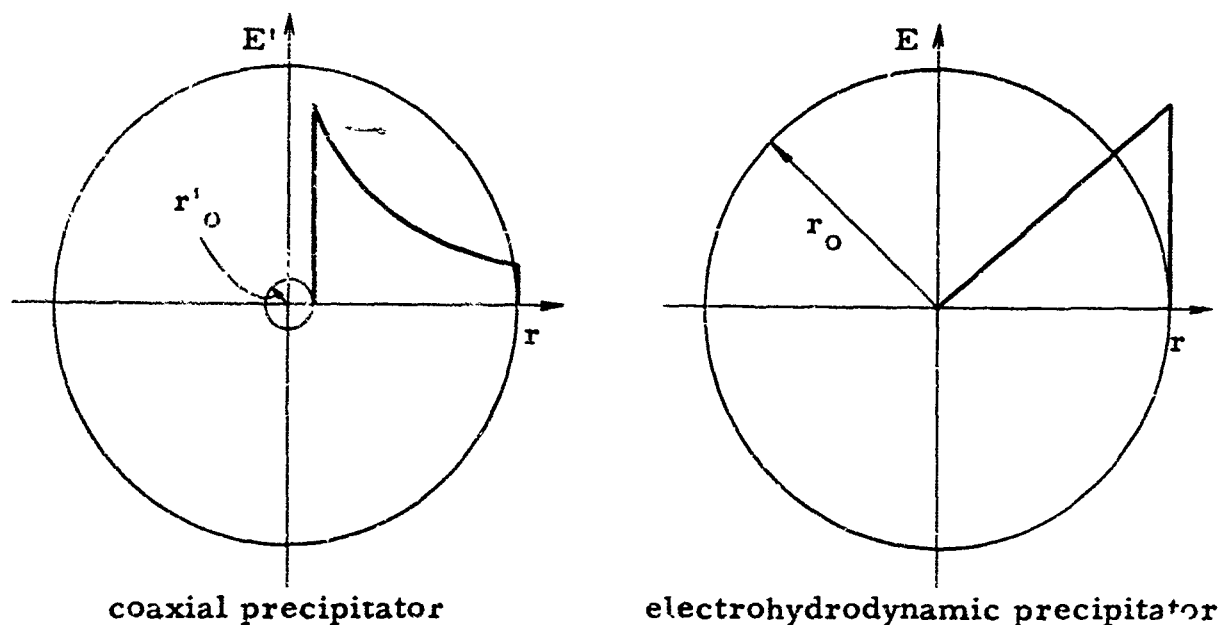
Figure 2. Comparison of Electric Fields in Corona Wire and
Electrohydrodynamic Precipitators

For a coaxial arrangement, we obtain

$$F' = Q E_{max} r'_o/r(1 - 4\pi a^3 \epsilon E_{max} r'_o/Q r^2) \quad . \qquad (20)$$

While, for the electrohydrodynamic case, Equations (17) and (18) yield:

$$F = Q E_{max} r/r_o (1 + 4\pi a^3 \epsilon E_{max}/Q r_o) . \qquad (21)$$

The second terms within the brackets are standardized dielectrophoretic
forces. In the coaxial arrangement these decrease the Coulomb forces,
while in the electrohydrodynamic case, both forces have the same direction.
Considering high charges and comparatively small particles, we can
neglect the dielectrophoretic component for practical considerations.

III. THEORETICAL COLLECTION EFFICIENCY

To consider collection efficiency, we must calculate particle trajectories. A particle injected at $z = 0$ and $r = r'$ will flow toward the wall by Coulomb forces. At a given z it will reach the wall. Assuming that all particles which will reach the wall are collected, we can express collection efficiency η as

$$\eta = 1 - (r'/r)^2 , \tag{22}$$

where r/r' may be obtained from the radial velocity of the particle. Combining Equations (3), (10), and (13) we get

$$dr/dt = q_0 Q r/12 \pi \epsilon \eta \ a (1 + t/t_c). \tag{23}$$

For Q, we will assume the maximum charge Q_{max} (as derived and given in Equation (5)) will decay exponentially as stated in Equation (7):

$$dr/dt = K qb/\epsilon \ r \ \exp(-t/T)/(1 + t/t_c). \tag{24}$$

Whereby K is a collection parameter given by

$$K = kaE \ \epsilon/3 \eta \ b. \tag{25}$$

Parameter K contains all the important properties of the liquid and the particulate, except electrolytic conductivity. Its value strongly influences the characteristics of the filter. Equation (24) can be separately integrated and yields with r' the location of the particle at $t = 0$,

$$\ln r/r' = K qb/\epsilon \int_0^t \exp(-t/T)/(1 = t/t_c) \ dt. \tag{26}$$

The remaining integral yields an infinite series which, however, converges rapidly for small values of t_c/T. t_c/T is another important parameter. It expresses the ratio of the electrolytic conductivity σ to total conductivity.

$$t_c / T = \sigma/qb + \sigma \tag{27}$$

For high space-charge concentrations and good insulating properties of the liquid, t_c/T can be neglected. Liquid hydrocarbons contaminated with water as well as chemical additives might not always yield a high insulating liquid. The influence of t_c/T on collection efficiency is therefore considered an important study.

Equation (26) can be expressed as

$$\ln r/r' = K(1 - t_c/T) \exp (t_c/T) \left\{ \ln(1 + t/tc) \right.$$
$$- t/T + 1/T^2 \left[\frac{(t_c + t)^2 - t_c^2}{2 \cdot 2} \right] !$$
$$\left. - \frac{1}{T^3} \left[\frac{(t_c + t)^3 - t_3^3}{3 \cdot 3} \right] + \ldots \right\} \tag{28}$$

For relatively good insulating liquids ($t_c/T < .2$), for times comparable to the critical time of the precipitator ($t/t_c < 5$), and for accuracies of at least 10 percent, Equation (28) can be simplified to

$$r/r' = \left\{ (1 + t/tc) \exp (-t/T) \right\}^K . \tag{29}$$

Using Equations (22) and (29), collection efficiency can be expressed as

$$\eta = 1 - \left\{ (1 + t/t_c) \exp (-t/T) \right\}^{-2K} . \tag{30}$$

Or, expressing time in terms of filter length and flow velocity:

$$\eta = 1 - \left\{ (1 + z/z_c) \exp (-z/vT) \right\}^{-2K} . \tag{31}$$

Figures 3, 4, and 5 show theoretical filter efficiences when using the exact formula of Equation (28) as a function of the standarized filter length z/z_c, with K and t_c/T as parameters. It can be seen that for fairly good insulating liquids (as will be the case for operational CIE fuel), the

filter efficiency is not markedly changed by small amounts of water or additives. Of much importance, however, is parameter K. Values of K = 0.8 (or better) are required to obtain good filter efficiencies with a reasonable filter length.

For an estimation of the magnitude of K we will assume values for kerosene, which can be assumed similar to CIE

k = 3 (for conductive particles).

$E = 3 \times 10^7$ V/m.

$\epsilon = 2 \times 10^{-11}$ amp sec V^{-1} m^{-1},

$\eta = 2 \times 10^{-3}$ newton sec m^{-2},

$b = 3 \times 10^{-7}$ m^2 V^{-1} sec^{-1},

$a = 10^{-6}$ m .

With the values above, we obtain K = 1 for particles of 1 micron in diameter. For larger particles, K increases in proportion to the diameter. This means there are excellent collection properties for particles larger than 1 micron.

To estimate the influence of water on electrolytic conductivity and therefore, on collection efficiency it is best not to rely on theoretical assumptions. The number of dissociated water molecules in solution within the hydrocarbon is difficult to estimate. Experimental investigation will easily enough give exact measures as to the dependence of electrolytic conductivity or water content. A slight change in approximating the analytical approach can be made for the case of relatively low space charge density and relatively high electrolytic conductivity as is probably the case when the liquid is saturated with water. For that case Equation (30) changes to

$$\eta = 1 - \exp\left\{ -2K\ qb/\sigma \left[1 - \exp(- t/T) \right] \right\} . \qquad (32)$$
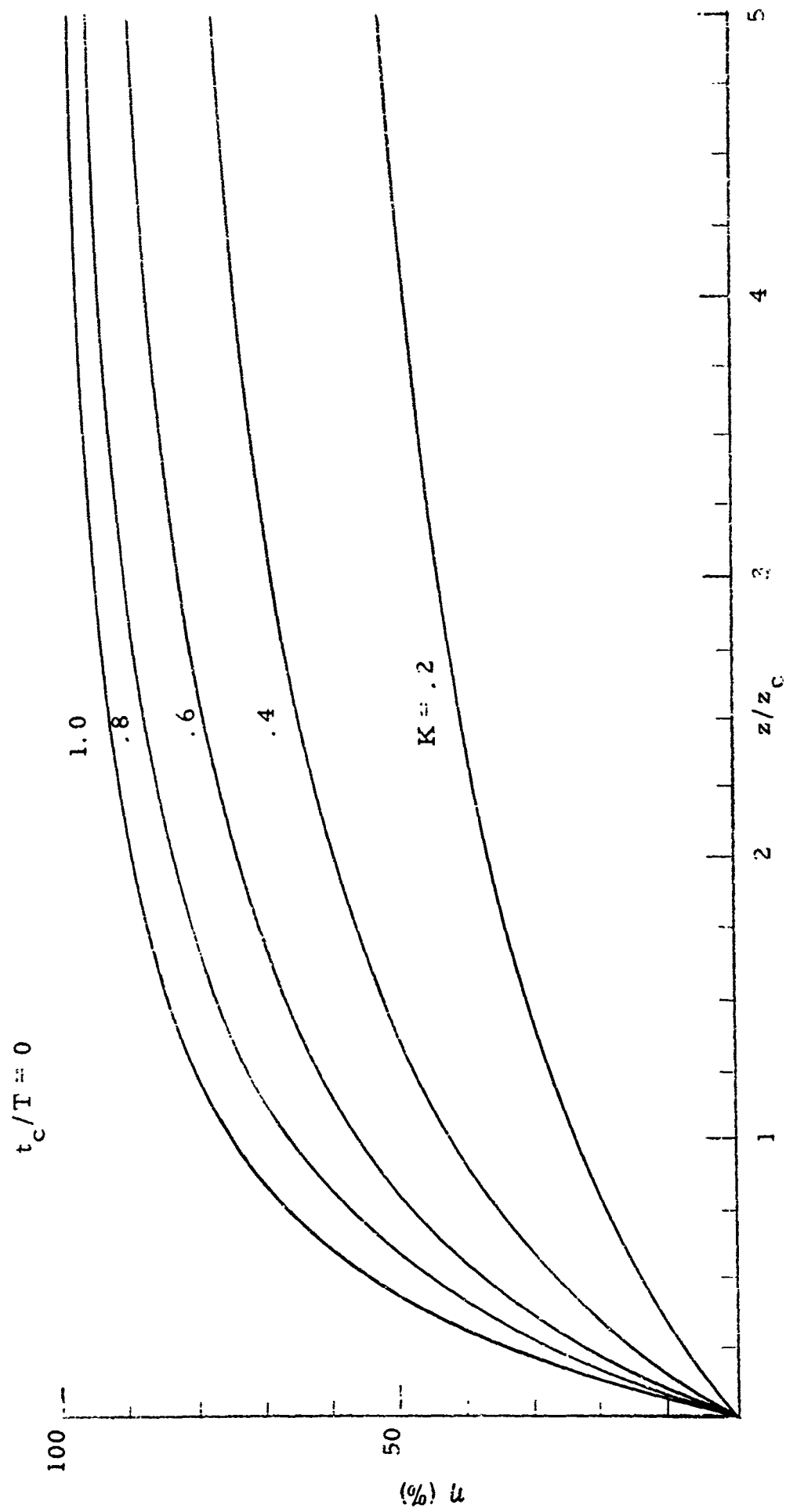
Figure 3. Filter Efficiency as a Function of Filter Length
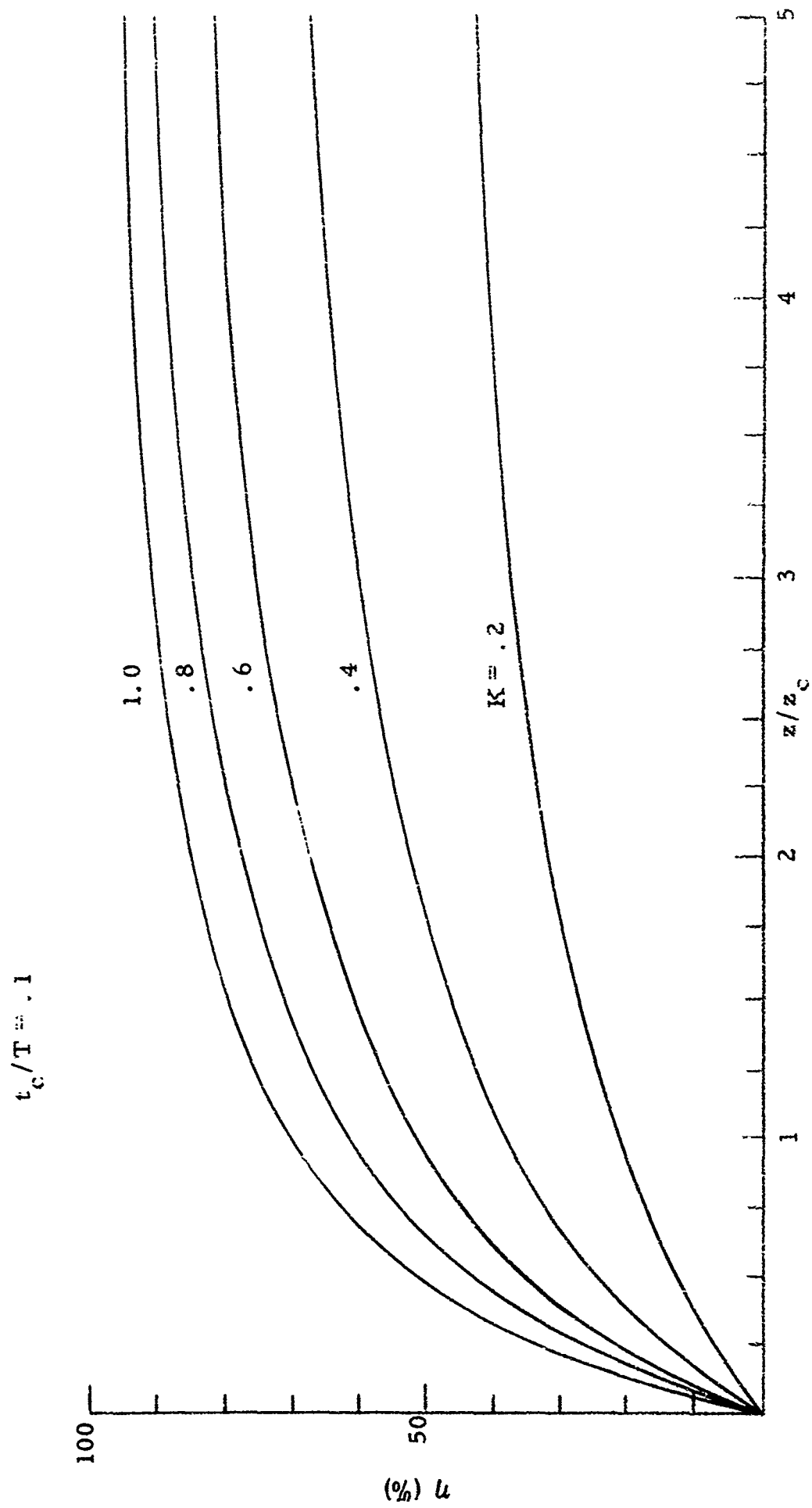
Figure 4. Filter Efficiency as a Function of Filter Length

- 14 -
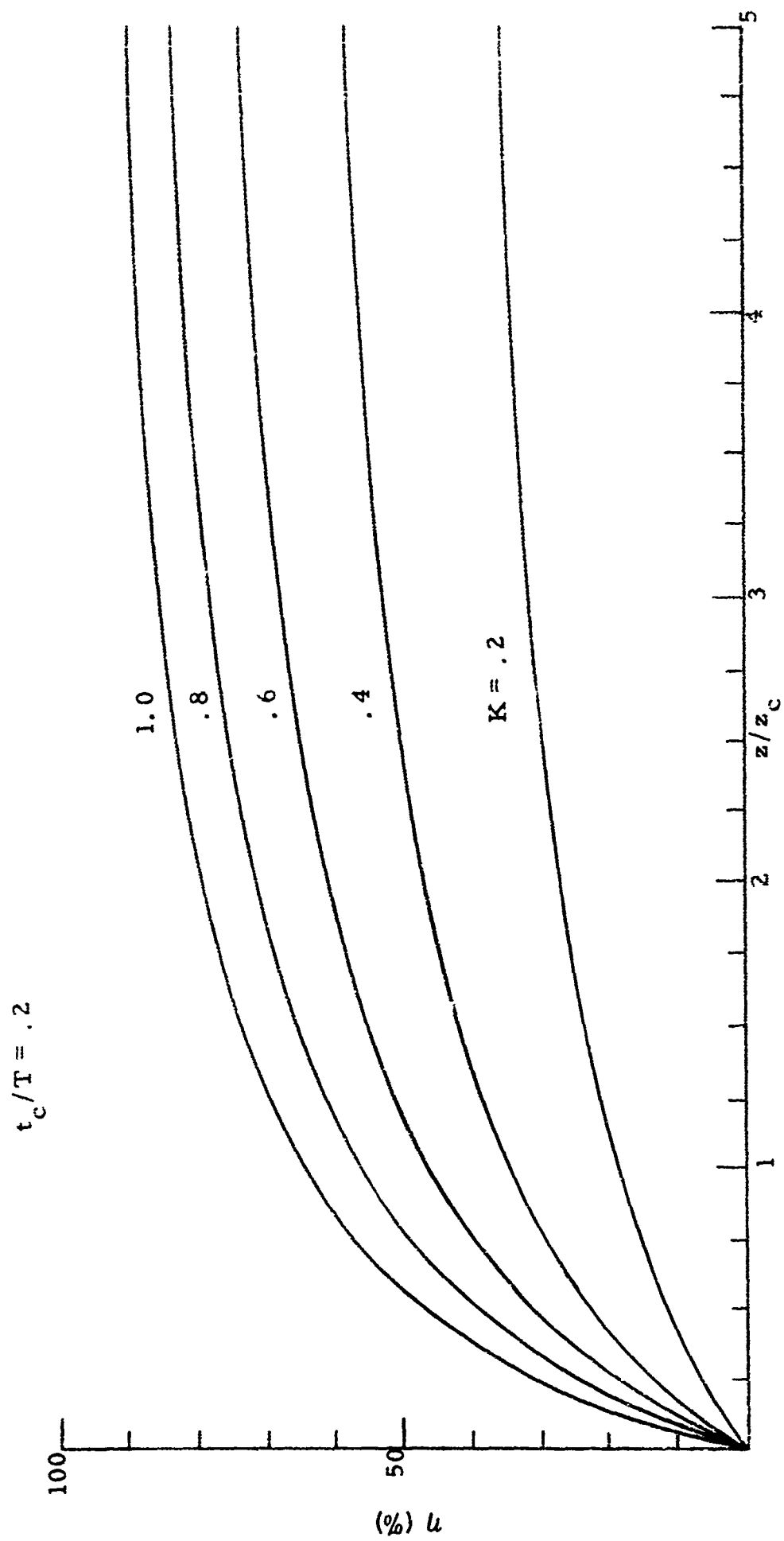
Figure 5. Filter Efficiency as a Function of Filter Length

$t_c/T = .2$

η (%)

100

50

z/z_c

1.0
.8
.6
.4
K = .2

IV. ANALYSIS OF WALL EFFECT ON COLLECTION

For the velocities and particle sizes used in our experiments, we
found that no adhesion occurred without electrical forces. From this we
concluded that we can neglect all forces other than electrical and drag
forces when considering collection properties of the wall. A particle
reaching the wall will stay charged there in the presence   of strong elec-
trical fields and unipolar ion densities. Its charge, besides depending on
the electric field and ion density, depends on the electrical properties of
the particle, the wall and of the liquid film between them. The electric
field component perpendicular to the wall will exert a Coulomb force on
the particle to press it to the wall. This force and a friction coefficient
will determine the drag forces necessary to flush the particle away. An
additional force is exerted by an electric field component in the flow-line
direction. If this resultant force component is strong enough, it will
overcome frictional and drag forces and the particle will move against the
flow of liquid. Because the electric field decreases with increasing dis-
tance from the ionizer, we will find a distance z_1, below which no collec-
tion takes place due to strong longitudinal electric fields, and a distance
z_2, beyond which no collection is possible because of the radial electric
fields which become too low. The efficiency formulas discussed (Section III)
have to be modified to take the influence of this wall effect into account.
As pointed out earlier, the efficiency formulas were derived under the
assumption that every particle reaching the wall is collected. Our ex-
periments have shown that the influence of the wall and wall material is
extremely important to the overall efficiency of the system. As a matter
of fact, collection properties of the wall are the major factors influencing
total efficiency. In the following therefore, we present an analysis of this
problem and a discussion of the experimental results.

To consider the forces acting upon a particle which is close to the
wall, we will make the following assumptions: 1) the particle is of spheri-
cal shape and is a very good electrical conductor compared to the

conductivity of the liquid; 2) the wall material has electrical properties similar to the liquid; 3) inertial forces can be neglected; 4) the coefficient of friction is a constant; and 5) high Reynolds numbers exist for the flow through the precipitator tubing with well developed turbulence. In order to organize the analysis, we will consider the drag force, frictional force, and the force due to longitudinal electric fields separately and then estimate their effect on collection efficiency.

A. Drag on Particles at the Wall

In regions very close to the wall, the flow around particles is laminar due to the very low Reynolds numbers involved. The drag force F_D, therefore, can be calculated from the Stokes equation for viscous flow around a sphere:

$$F_D = 6\pi\mu a v .\tag{33}$$

Viscosity μ and particle radius a are unambiguous quantities, while the velocity v is difficult to determine due to the fact that it changes considerably over one particle diameter.

The velocity profile over the precipitator can be divided into three parts: a turbulent flow in the center with uniform velocity distribution, a turbulent boundary layer, and a laminar sublayer. In this laminar sublayer, the velocities increase linearly with distance from the wall. The thickness of this sublayer as given by Hoerner[9] is:

$$\delta = 37.5 \ x/R_x\tag{34}$$

with R_x the Reynolds number of length x. Replacing the Reynolds number R_x by

$$R_x = xv\rho/\mu\tag{35}$$

- 17 -

yields:

$$\delta = 37.5 \, \mu/v\rho \qquad (36)$$

with ρ the density of the liquid. For our range of velocity and viscosity this sublayer has a thickness of 10 to 100 microns. Because all of our particles are between 1 and 10 microns, we only have to consider this sublayer for drag computations as long as deposition depth does not exceed a few particle diameters. To take into account the increase of velocity with distance from the wall, we can define an effective uniform velocity as approximately the velocity at one-half diameter from the wall. Hoerner has given the velocity distribution in this sublayer as

$$v/v_{max} = 0.116 \cdot (y/r)R^{1/2}. \qquad (37)$$

where y is the distance from the wall and r is the cylinder tube radius. The velocity acting on a resting particle at the wall is therefore given by

$$v/v_{max} = 0.116 \, (a/r) \, R^{1/2} \, . \qquad (38)$$

Using Equation (33), we can now express the drag force on a particle resting at the wall:

$$F_D = \kappa a^2 \, \mu^{1/2} \, v^{3/2} \, \rho^{1/2} \, r^{-1/2} \, . \qquad (39)$$

B. Friction Force at Wall

The drag force is counterbalanced by frictional force F_F whose magnitude depends on the friction coefficient κ and the Coulomb force F_r which acts perpendicular to the surface walls. F_r is given by

$$F_r = E_r \, q \, . \qquad (40)$$

An expression for the radial field E_r has been derived previously:

$$E_r = q_o \, r/2\epsilon \, (1 + z/z_c) \, . \qquad (41)$$

The charge q of the particle can easily be calculated from the electric field and the particle size a by using White's formula

$$q = 12 a^2 \epsilon E_r .$$ (42)

Friction force F_F is therefore given by

$$F_F = \frac{q_o^2 r^2 3 \pi a^2}{\epsilon . (1 + z/z_c)^2} . \kappa$$ (43)

The magnitude of the friction coefficient κ depends strongly on surface material and conditions at the wall, on liquid properties, and on the shape of particles. No good estimate could be obtained either from a literature search or experiment. The range, however, will be between 0.5 and 0.001 with 0.1 being a realistic value when assuming rolling friction at the wall.

C.   Additional Coulomb Forces

As pointed out in our first quarterly report, there is a longitudinal component of the electric field present in the precipitator section. Therefore, a longitudinal Coulomb force F_L resulting from this field component and the charge of the particles will be evident. This force will be directed opposite to the drag force. The magnitude of this electric field for small distances z from the ionizer can be expressed by

$$E_z = q_o z_c / \epsilon (1 + z/z_c) .$$ (44)

This leads to the magnitude of F_L:

$$F_L = 6 \pi a^2 q_o^2 z_c r/\epsilon (1 + z/z_c)^2 .$$ (45)

D. Influence on Collection Efficiency

From the foregoing discussion it is obvious that whenever drag forces or longitudinal Coulomb forces exceed the frictional force, particles will move along the wall (away from the regions of electric fields) until they are swept into the stream of liquid. Collection will take place only in a limited range. To calculate the two limits z_1 and z_2, we have to satisfy the next equation which states that collection takes place whenever friction force F_F is stronger than the absolute difference between drag force F_D and longitudinal force F_L:

$$F_F \geq \left| F_D - F_L \right| . \tag{46}$$

Using Equations (39), (43), and (45) we find the two values of the distance from the ionizer to be

$$z_{1,2} = z_c \left\{ \frac{(z_c \pm r\kappa)^{1/2} 6^{1/2} r^{3/4} q_o}{\epsilon^{1/2} \mu^{1/4} \rho^{1/4} v^{3/4}} - 1 \right\}. \tag{47}$$

Collection efficiency can be derived from particle trajectories in a way similar to a method previously shown in Section III. Again, using the case of relatively high electrolytic conductivity of the CIE fuel, we derived the following expression which now includes adhesion properties of the precipitator walls:

$$\eta = \exp \left\{ -2Kqb/\sigma \; (1 - \exp [-z_1/vT]) \right\}$$
$$- \exp \left\{ -2Kqb/\sigma \; (1 - \exp [-z_2/vT]) \right\}. \tag{48}$$

In Figure 6, filter efficiency is plotted against flow velocity in the precipitator tubing. Realistic values of variables were used as also discussed before in Section III. The following additional parameters were used in plotting this figure:
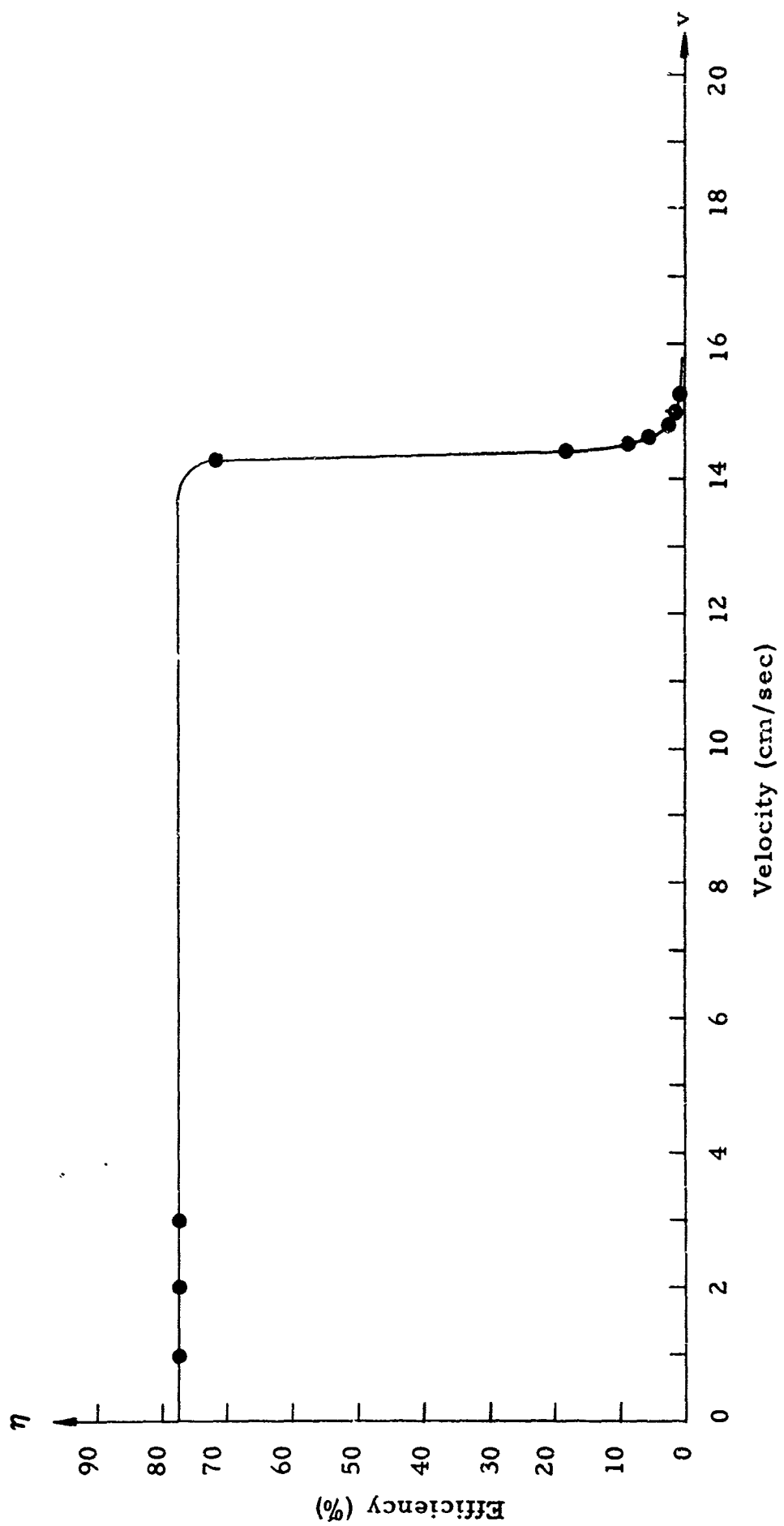
Figure 6. Collection Efficiency

Collection parameter $K = 1$,

Precipitator tube radius $r = 10^{-2}$ m,

Friction coefficient between particles and wall $\kappa = 0.1$.

As has been expected, a maximum velocity exists at which efficiency drops to zero. This maximum for velocity varies strongly with the frictional coefficient.

V. ANALYSIS OF FILTER EFFECTS ON SIZE DISTRIBUTION

Because of the frequent use of probability terms in this report, a short discussion and definitions of the more important terms are presented in the following.

A. Normal Distribution

Most of the measurements taken in this experiment can be approximated as a normal or lognormal distribution of the variable. The normal distribution is defined by the following frequency distribution function:

$$F(x) = \frac{1}{\sigma \sqrt{2\pi}} \cdot \exp{\frac{1}{2} \frac{x^2}{\sigma^2}} , \tag{49}$$

We will show here that when two measurements are taken, each of which gives rise to a normal distribution, the result is again a normal distribution function. The standard deviation of this function is the square root of the squares of the two original standard deviations. This case occurs, for instance, when samples which have a normal distribution are filtered by our electrostatic filter which has a normal distribution characteristic.

In Figure 7 consider a strip of width dx and a height $F_1(x)$ after it has been modified by F_2. This will give rise to an element of the new distribution:

$$dF_3 = F_1(x) \, dx \, F_2(x-a) . \tag{50}$$

$$F_1 = \frac{e^{-\frac{1}{2}\left(\frac{x}{\sigma_1}\right)^2}}{\sigma_1\sqrt{2\pi}} \qquad\qquad F_2 = \frac{e^{-\frac{1}{2}\left(\frac{x}{\sigma_2}\right)^2}}{\sigma_2\sqrt{2\pi}}$$
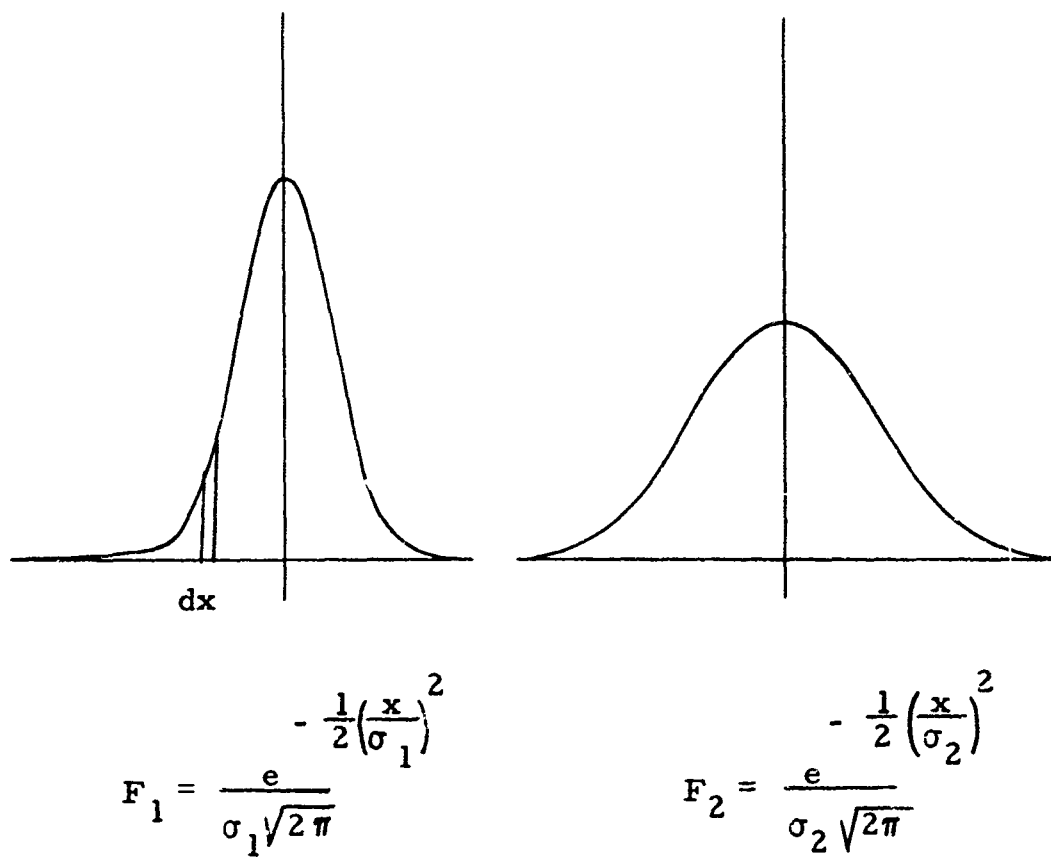
Figure 7. Normal Distribution

In order to get the resulting distribution function $F_3(a)$, we have to integrate (50) from $-\infty$ to $+\infty$ as follows:

$$F_3(a) = \int_{-\infty}^{+\infty} \frac{1}{\sigma_1 \sqrt{2\pi}} \, e^{-1/2 \left(\frac{x}{\sigma_1}\right)^2} \, \frac{1}{\sigma_2 \sqrt{2\pi}} \, e^{-1/2 \left(\frac{x-a}{\sigma_2}\right)^2} dx$$

$$\tag{51}$$

$$= \frac{1}{\sigma_1 \sigma_2 \, 2\pi} \int_{-\infty}^{+\infty} e^{-1/2 \left\{ \left(\frac{x}{\sigma_1}\right)^2 + \left(\frac{x-a}{\sigma_2}\right)^2 \right\}} dx$$

The integral can only be evaluated if the power of the exponential can be expressed as 1/2 of a full square. This can be accomplished by adding and subtracting a constant to the power so that it now consists of a full square and a constant. The constant term can then be brought outside the integral sign, which leads to the following expression.

$$F_3(a) = \frac{e^{-1/2 \frac{a^2}{\sigma_1^2 + \sigma_2^2}}}{\sigma_1 \sigma_2 \, 2\pi} \int_{-\infty}^{+\infty} e^{-1/2 \left\{ \frac{\left(\sigma_1^2 + \sigma_2^2\right)^{1/2} x - \frac{a \sigma_1^2}{\left(\sigma_1^2 + \sigma_2^2\right)^{1/2}}}{\sigma_1 \sigma_2} \right\}^2} dx \ . \tag{52}$$

Now the integral can be evaluated by changing the variables.
Let

$$u = \left(\sigma_1^2 + \sigma_2^2\right)^{1/2} x \tag{53}$$

then

$$dx = \frac{du}{\left(\sigma_1^2 + \sigma_2^2\right)^{1/2}} \tag{54}$$

and the integral becomes

$$\frac{1}{(\sigma_1^2 + \sigma_2^2)^{1/2}} \int e^{-1/2 \left\{ \frac{u - \frac{a\sigma_1}{(\sigma_1^2 + \sigma_1^2)^{1/2}}}{\sigma_1 \; \sigma_2} \right\}^2} dx \qquad (55)$$

which has the value

$$\frac{\sigma_1 \; \sigma_2 \; \sqrt{2\pi}}{(\sigma_1^2 + \sigma_2^2)^{1/2}} \quad .$$

Finally, we obtain the following expression for the distribution function:

$$F_3(a) = \frac{e^{-1/2 \frac{a^2}{\sigma_1^2 + \sigma_2^2}}}{\sqrt{\sigma_1^2 + \sigma_2^2} \; \sqrt{2\pi}} \qquad (56)$$

which is of the same form as (49) with

$$\sigma_3 = \sqrt{\sigma_1^2 + \sigma_2^2} \qquad (57)$$

and is again a normal distribution.

B. Lognormal Function

The probability function which most frequently occurs in this work is the lognormal function, which is rather typical for small-particle statistics[10]. Because of the nature of the work, an error of -50 percent is as likely to occur as an error of +100 percent and counts of both zero and infinity are equally unlikely. These two considerations cause the lognormal distribution to appear skewed when plotted on rectangular paper and as straight lines when plotted on lognormal paper which indicates that the lognormal distribution is the closest approximation to the experimental data.

The lognormal distribution is defined by the normal distribution of the natural logarithm of its variate x. If we let $y = \ln x$, then y will have a normal distribution with a mean m and a variance σ^2 as follows:

$$f(y) \, dy = \frac{1}{\sigma \sqrt{2\pi}} \exp{-\frac{1}{2} \left(\frac{y-m}{\sigma}\right)^2} dy. \tag{58}$$

Expressed in x, this will then become:

$$f(x) \, dx = \frac{1}{x\sigma \sqrt{2\pi}} \exp{\frac{1}{2} \left(\frac{\ln x - m}{\sigma}\right)^2} dx. \tag{59}$$

In writing this expression we have to take into account that we can only take logarithms of dimensionless numbers, so that x, σ, and m have to be divided by one unit of whatever is being measured in order to make Equation (59) meaningful.

Two important parameters in probability distributions are the mean and the mean deviation. The mean is the straight arithmetic mean, which, for a distribution with a continuous probability density curve, is calculated by:

$$m = \int_{-\infty}^{+\infty} x \, f(x) \, dx. \tag{60}$$

The mean deviation of a distribution is defined as the square root of the mean of the squares of the deviation of the variable from its mean value:

$$\sigma = \left(\int_{-\infty}^{+\infty} (x-m)^2 \, f(x) \, dx \right)^{1/2} \tag{61}$$

For the normal distribution, as defined by the right hand side of Equation (58), the mean is equal to m, and the standard deviation is equal to σ .

When considering the lognormal function, however, a more meaning-ful quantity than the mean is the median. With a continuous probability law, the median m_e satisfies the equation

$$\int_{-\infty}^{m_e} f(x) \, dx = 1/2 \quad , \tag{62}$$

and 50 percent of all observations occur at either side of this value. By using this quantity rather than the mean, the higher values measured (found in the tail end of the lognormal distribution) will not be weighed too heavily. In the normal distribution, the mean and the median are equal because of the symmetry of the curve.

Further, we will be considering the 16 and 84 percentile points in dis-cussing the lognormal function instead of the standard deviation. For the normal distribution we know that the range from m - σ to m + σ goes from 16 percent of all observations to 84 percent of all observations. This will enable us to calculate the same percentile points for the lognormal distri-bution. Let us consider (58) with respect to y. Because of the known pro-perties of the normal distribution, we know that the median (which, in this case, equals the mean) occurs at m and that the 16 and 84 percentiles occur at y = m - σ , and y = m + σ , respectively. Going from (58) to (59) involves only a change of variable. That is, a change in the magnitude of the quantities measured is involved but not in the number of measurements so that the quantiles will still occur at the same points. This mean thus

occurs at $y = \ln, \; x = m$ or at $x = e^m$, and the 16 and 84 percentile points at $\ln x = m - \sigma$ and $\ln x = m + \sigma$, or $x = e^{m - \sigma}$ and $x = e^{m + \sigma}$, respectively.

If the lognormal distribution is plotted on lognormal paper, we can immediately obtain the value for m and σ. The value of m is equal to ln x at the 50 percentile point, $m = \ln x_{50\%}$. Similarly from the 16 or 84 percentile we get

$$\sigma = \ln x_{50\%} - \ln x_{16\%} = \ln x_{84\%} - \ln x_{50\%} . \tag{63}$$

Another property that we will make use of is one of the reproductive properties in the lognormal distribution. It can be shown that if f_1 and f_2 are independent lognormal distributions, then the product $f_1 \, f_2$ is also a lognormal distribution for which $m = m_1 + m_2$ and $\sigma^2 = \sigma_1^2 + \sigma_2^2$.

VI. DESCRIPTION AND TESTING OF EXPERIMENTAL SETUP

A. Layout of EHD Precipitator

The electrohydrodynamic (EHD) precipitator test stand is shown in the block diagram (Figure 8). It is especially designed to meet the requirements discussed in the theoretical sections and outlined in the contract's statement of work. This setup contains a model precipitator to remove biological and other suspended material from CIE fuel and to determine by measurements essential filter characteristics. The instrumentation is capable of measuring quantities like flow rate, flow velocity, temperature, pressure drop, ion density, electrolytic conductivity, dielectric constant, and other parameters as required. The arrangement is made very flexible in order to incorporate new sensors if need be and to allow quick exchange of ionizer, precipitator, and other parts for evaluation of different filter configurations.

The entire precipitator assembly is mounted on an aluminum plate. All the essential parts of the arrangement are flanged and sealed with O-rings to assure fast and simple assembly, disassembly, cleaning, and

Figure 8.   Block Diagram of EHD Precipitator

1 Tank
2 Cooling Coil
3 H.V. Power Supply
4 Pump
5 Filter
6 Gate Valve
7 Bellow
8 Test Tube
9 Solenoid Valve
10 Ionizer
11 Precipitator
12 Flow Meter
13 Microammeter
14 H.V. Terminal
15 Pressure Gauge
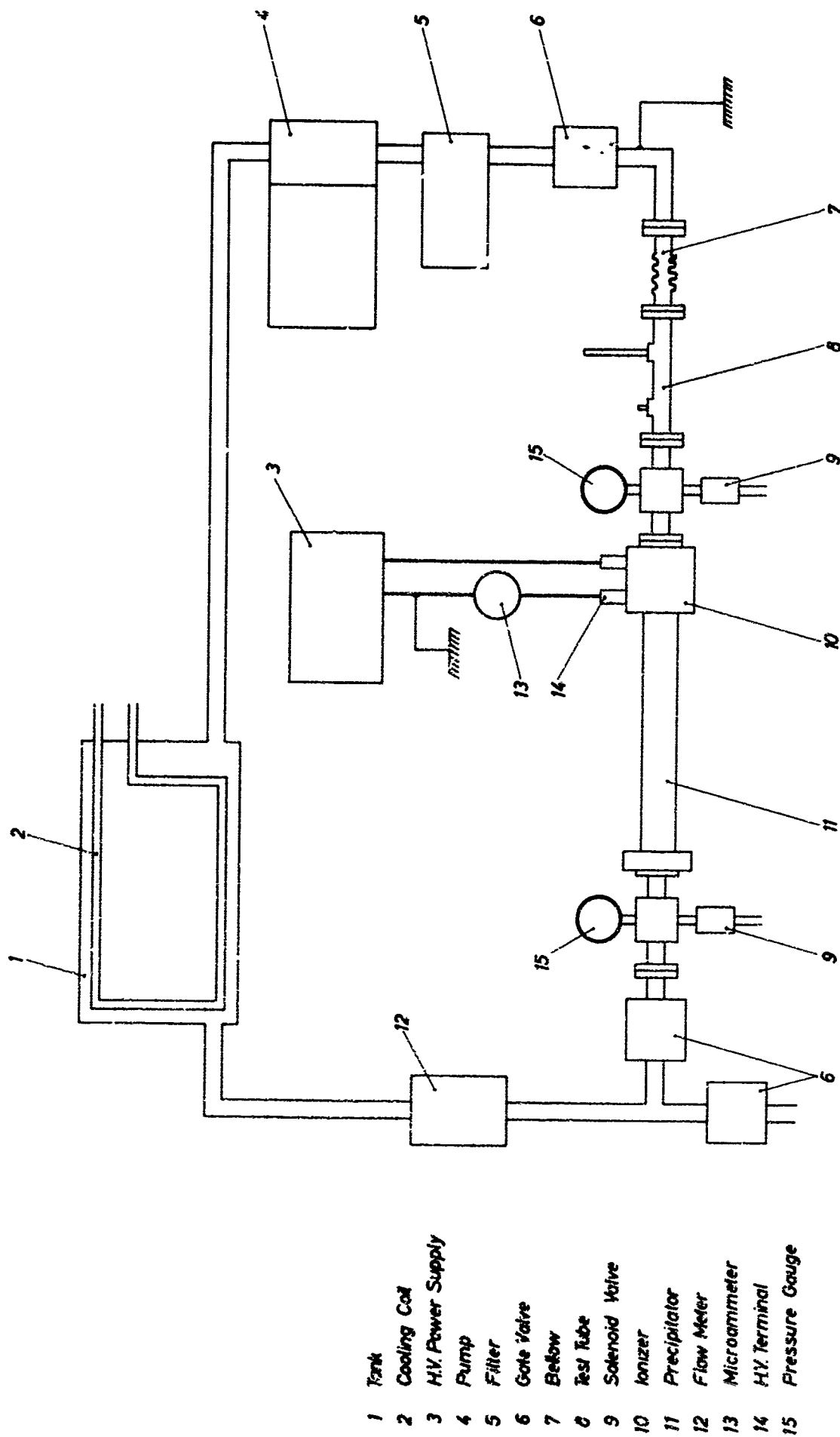
inspection. Furthermore, great care has been taken to assure an entirely leak-proof system.

The fuel is contained in a 12-gal tank(1).[*] Inlet and outlet of the tank can be closed off by gate valves. The transparent hoses leading to the precipitator assembly are equipped with quick-connector nipples. Coils (2) made from copper tubing are immersed in the liquid. Cooling or heating of the fuel by water can be achieved by this means.

A centrifugal pump (4) manufactured by Eastern Industries, Hamden, Connecticut, is used for circulating the fuel at 20 gal/min and 15 psi maximum. The pump is equipped with an enclosed motor (115 Vac, 1 phase, 1/2 hp), and is suitable for operation over the entire range of performance. The flow rate will be controlled by several gate valves (6), according to the desired pressure differential and to avoid cavitation in the valves at very low flow rates.

The entire flow of liquid passes through a mechanical filter (5) (approximate size, 50 microns) to remove any large foreign matter which might have entered the system. Larger particles tend to cause electrical breakthrough in the ionizer which, in time, may damage the emitters. Furthermore, larger particles would introduce operational errors when testing efficiency as it depends on particle size.

Further downstream, a test tube (8) is inserted in the line which will be used to measure the dielectric constant and temperature of the fuel, for example. The probes are exchangeable with others, if desired. Just before the ionizer and immediately after the precipitator tube, pressure gauges (15) and solenoid valves (9) are connected to the circuit. The use of the gauges is obvious. The solenoid valves provide a clean, predictable, and (in particular) a simultaneous sampling of the fuel before and after the precipitator.

_____

* Refers to Figure 8, item 1.

The ionizer (10) uses the latest design of corona emitter (razor-edge emitters)[11] and is completely enclosed in a heavy-wall housing made of DuPont Delrin, a high-quality insulating material. The high-voltage terminals (14) of the ionizer are also sufficiently insulated.

Ionizer and precipitator tube (11) are connected as closely as possible to obtain highest possible agreement with theory. The other end of the tube is connected to a sealing and mounting assembly. The tube can easily be removed and reinserted. A variety of metallic and non-metallic tubes were prepared to test the influence of wall material on filter efficiency. Immediately after the precipitator tube, an electric filter for small ions is put into the line. This makes sure all charges have been removed from the fuel and avoids precipitation at other sections of the circuit.

Two drain valves have been incorporated into the system. One can be used to drain part of the assembly, the other one enables the operator to flush the precipitator tube and collect the filtered matter in another container for further testing and evaluation. Furthermore, this valve could be used as an outlet to hook up a second precipitator to the system, if desired.

The final portion in this pipe arrangement is the flow meter (12). It is a piston-type meter and is equipped with a roller register. Two bellows (7) are built into the system to compensate for longitudinal tolerances and small misalignments.

The few required controls for motor and solenoid valves are mounted in the control box. A high-voltage power supply (3) (0-20 kV) was connected to the ionizer. The best precipitation effect was expected with negative ionization; however, the polarity can be changed easily by exchanging the leads to the ionizer. A microammeter (13) in this electrical circuit indicates the current and the field strength can be computed from this measurement. When a metallic precipitator tube is used, it is also of great interest to evaluate the charges carried to the tube by the flowing liquid. The entire assembly is well grounded. The photograph in Figure 9 shows the physical layout.
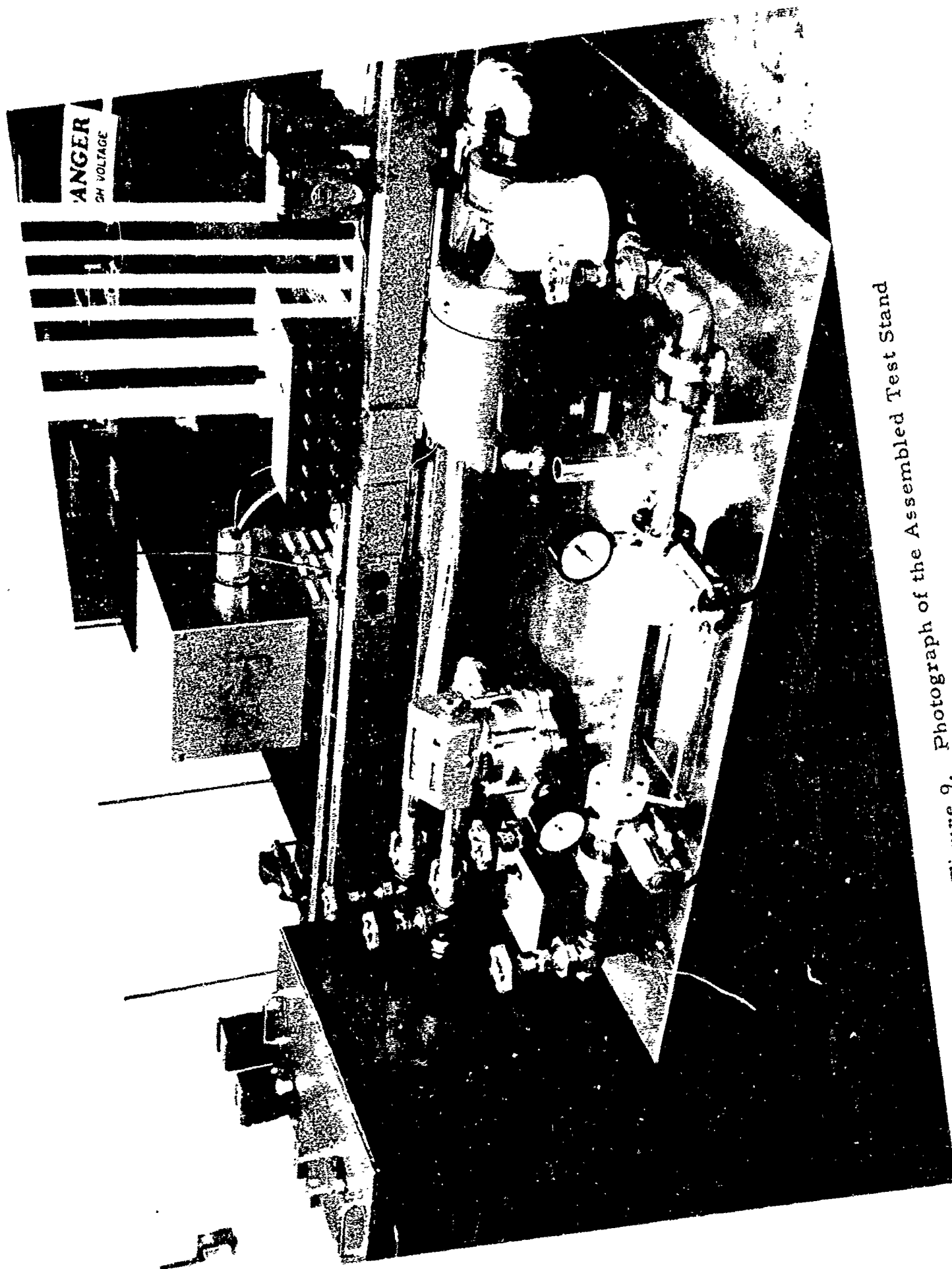
Figure 9. Photograph of the Assembled Test Stand

B. Preliminary Tests

Several parameters had to be tested in order to establish quantities of the fuel and the experimental setup which were necessary to compare analytical and experimental results.

1. Voltage Current Characteristic of Ionizer

For a given configuration of the ionizer and a given liquid, the relationship of voltage U versus current I is expected as follows:

$$\sqrt{I} = (U - U^*) \, gfh. \tag{64}$$

U^* thereby is the voltage necessary to start corona ionization, g is a constant geometric factor, f is a liquid and a time-dependent term, and h is a term dependent on the flow rate through the ionizer.

Figure 10 shows typical behavior of the ionizer used in the experimental apparatus. Part of the current from the corona edge is flushed out into the precipitating tube (I_1), and part flows to the catcher electrode opposite the corona edge (I_2). It can be seen that for low ionizing voltages almost the total current is available for the precipitator. For very high voltages, the flushed-out ion current is constant and depends strongly on flow rate. The influence of flow rate on total ion current I_t is shown in Figure 11. This also shows the flushed-out current I_1 and the catcher current I_2 plotted against flow rate. For this test, the applied voltage was kept constant.

As observed by other investigators[12], many dielectric liquids change their electric parameters with the length of the experiment. Because in our test stand, CIE fuel is circulated again and again through the ionizer, we found it necessary to investigate the possibilities of errors due to this setup. We measured the ion current versus voltage relationship of a small amount of fuel that was being subjected continuously to corona ionization.

Figure 10. Voltage-Current Characteristic of Ionizer
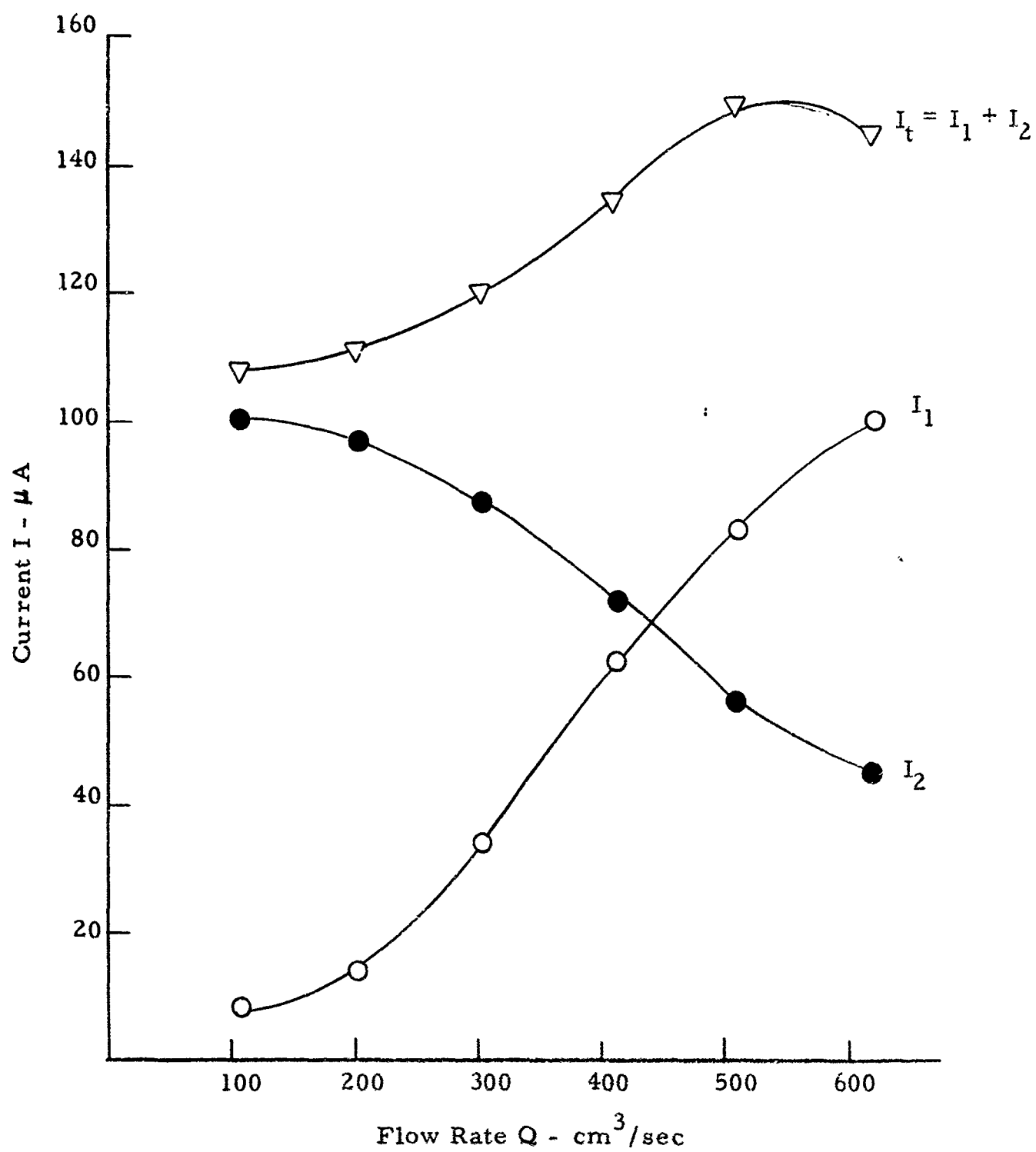
Figure 11. Influence of Flow Rate on Ion Current

We found a definite relaxation phenomenon in that the ion current continuously decreased and approached a stable but quite low value. The explanation of thi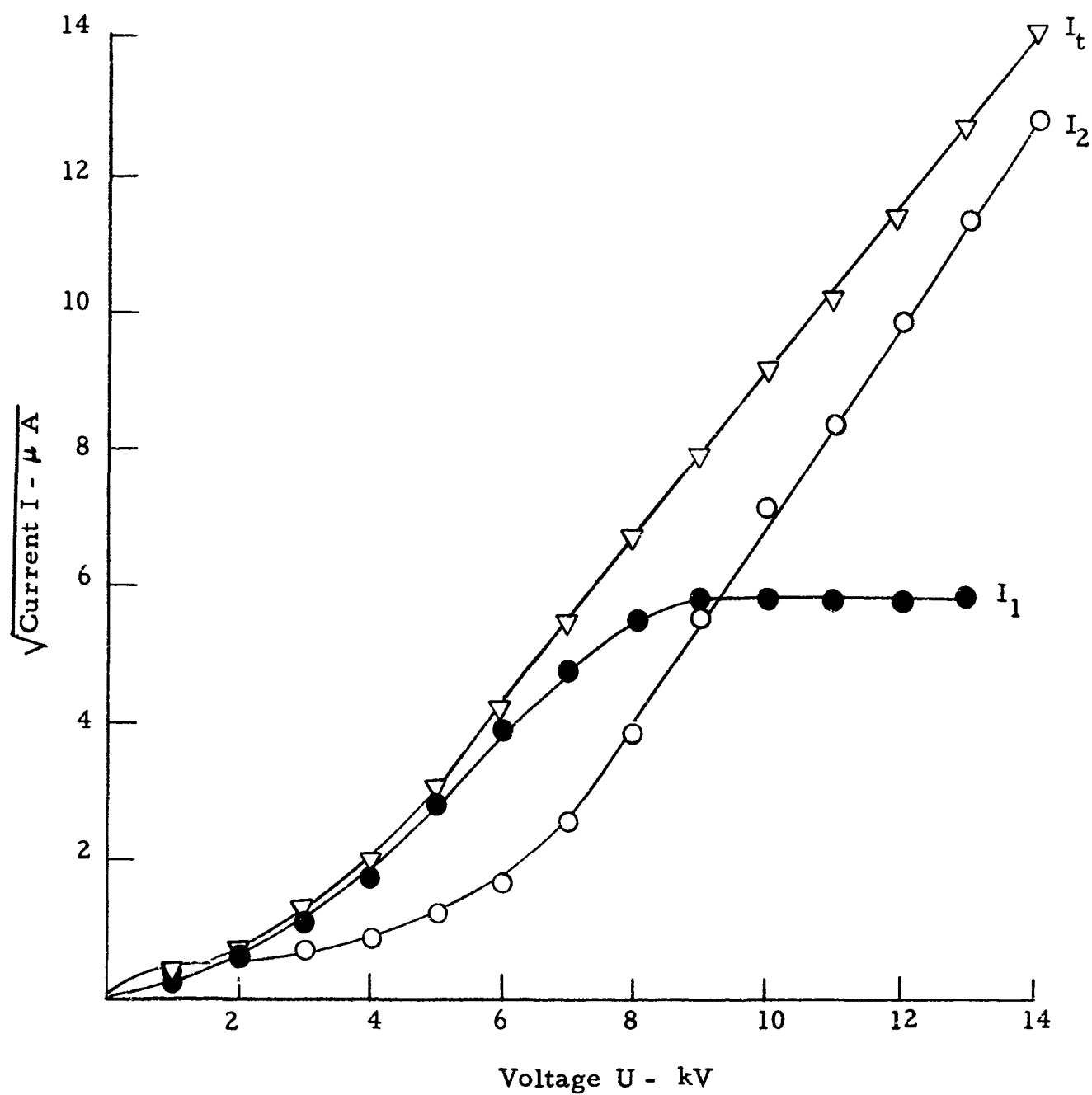s phenomenon is of vital importance in understanding basic ionization mechanisms in dielectric liquids, but is only of secondary interest to the scope of this contract; therefore, a thorough investigation was not believed justifiable.

Figure 12 shows data on a sample of about 500 cc CIE fuel which was repeatedly flushed through an ionizer. After only 10 minutes an effect was noticeable. Comparisons of the curve at $t = 0$ and $t = 5$ hours indicate principally that the voltage U* (at which ionization starts) changes with time; but there is also a possibility that ion mobility changes. The phenomenon suggests that the energy necessary to create an ion is very low in fresh liquid. Comparable conditions are found in kerosene where sometimes U* seems to be nonexistent in a virgin liquid. Our explanation is that molecules are often clustered very loosely so that they are easily broken up by electrical forces. The presence of such cybotactic groups has already been suggested by Stewart[13]. It seems possible, then, that in a fresh liquid, ionization by dissociation of cybotactic groups is responsible for carrying the major portion of the ion current. When sufficient ionization per volume has taken place, most of the groups are broken up thus diminishing ion current to a level determined by molecular ionization. In a matter of hours or days, a liquid at rest will recover to a state equal to fresh liquid.

Figure 13 shows the time dependence of ionization current with the application of constant voltage. A volume of 500 cc CIE fuel was used. It can be seen that in the first 10 minutes the steepest decrease in ionization current occurs. Assuming total ionization due to time-dependent cybotactic dissociation and stable molecular dissociation, we can estimate that an electric charge of 230 amp-sec/cm^3 can be created from fresh CIE fuel before it becomes time-independent. With the 10-gallon capacity of our experimental setup and an ion current of 100 microamperes we could
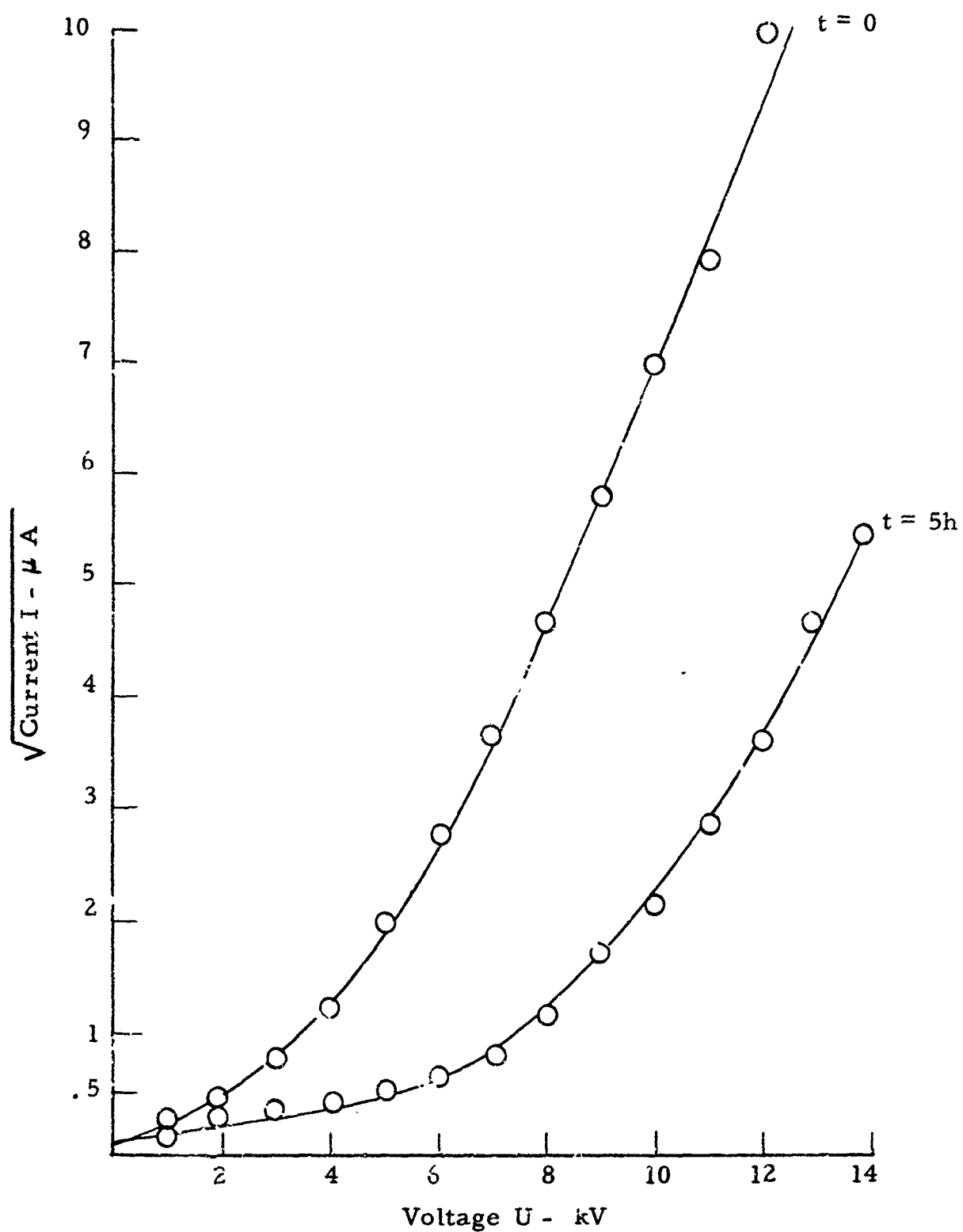
Figure 12. Time Dependence of Voltage-Current Relationship
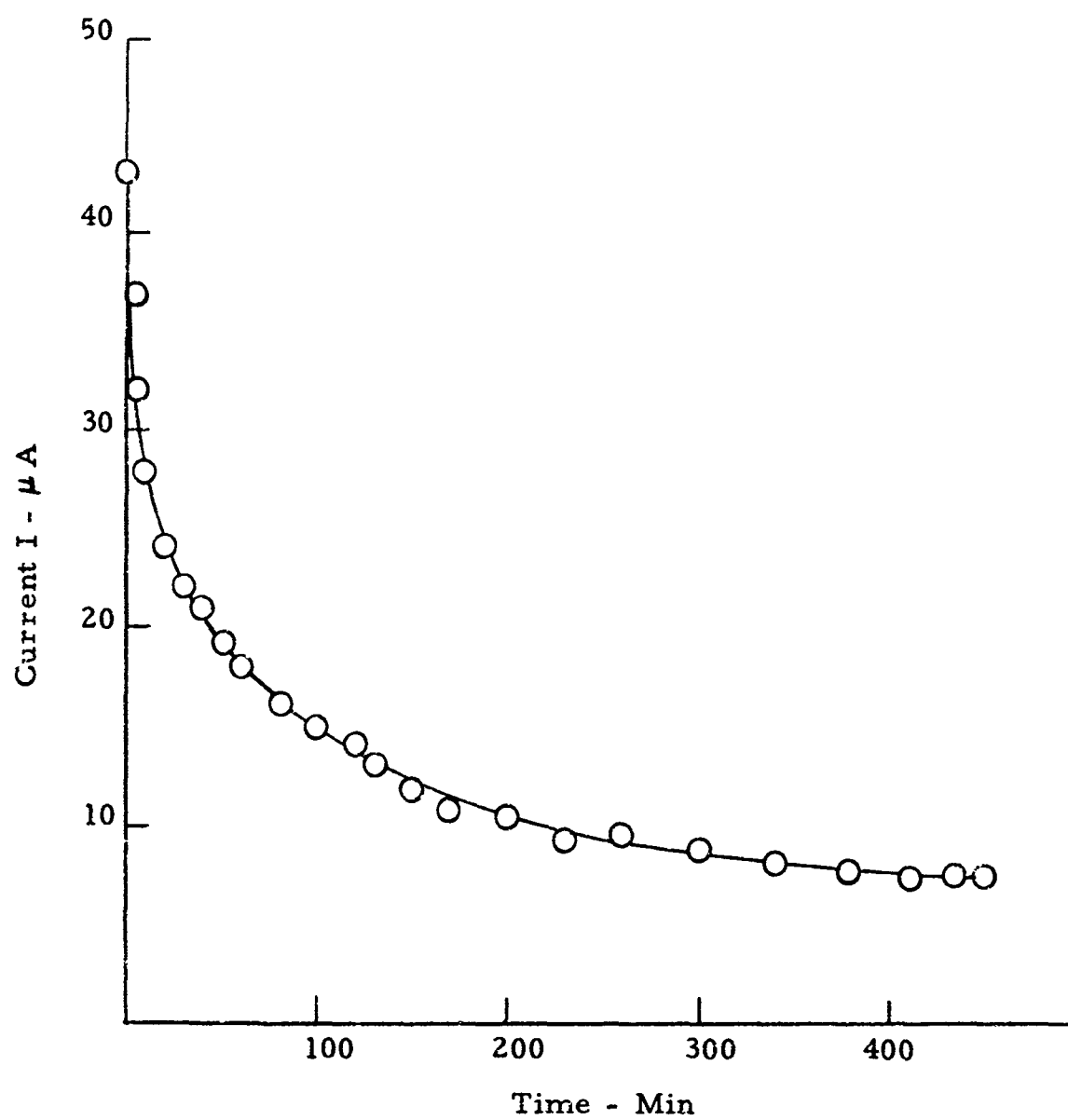
Figure 13. Time Dependence of Ionization Current

run the test stand for 1 hour per day without considering effects from relaxation phenomena.

Comparisons of CIE fuel with other hydrocarbons revealed that CIE cannot be ionized as easily as kerosene or octane, but there will be no special problems in developing sufficiently strong ionizers for CIE fuel. Table 1 lists the liquids used for comparison; all test conditions were kept constant.

Table 1. Ionization of Several Hydrocarbons Under
Identical Conditions (u = 10 kV, 20°C)

Liquid	J (μA)
Kerosene	81
Octane	62
Dodecane	47
CIE Fuel	43
Isooctane*	34
Decane	32
Cyclohexane	30
Hexane	27
Heptane	25

*2, 2, 4 - trimethylpentane

2. Relative Dielectric Constant

Formulas for collection efficiencies contain the relative dielectric constant which influences the time needed to dissipate charges under given space-charge conditions and electrolytic conductivity. The dielectric constant is the factor which determines the increase of capacitance of a condenser if dielectrics different than air are used. For CIE fuel, we used a probe with a capacity carefully measured by considering all stray and lead capacitances. For air, this probe had a capacitance of 3.4×10^{-12} F. By replacing air dielectric by CIE fuel, the capacitance increased to 7.35×10^{-12} F. yielding a dielectric constant of 2.16. At different temperatures no change of this value was observed.

3. Electrolytic Conductivity

One of the more important parameters involved in electrostatic pre-
cipitation is electrolytic conductivity. For electrostatic precipitation in
air, as well as in most pure hydrocarbons, this measure can be neglected.
This is not true for industrial grade hydrocarbons with chemical additives
and an appreciable water content. A high conductivity can have the effect
that electricity from charged particles is leaking away faster than the
particle can travel to the precipitating wall. Also, the dissipation of the
space charge, from which electric fields originate to force charged parti-
cles to the wall, is enhanced by electrolytic conductivity. For this reason
no electrostatic principles can be employed in water or other highly con-
ducting liquids.

Research on electrical conduction in hydrocarbons has recently been
made by Zaky, et al[14] who investigated, in particular, conduction at very
high electric field strengths. In general, conductivity in hydrocarbons is
extremely sensitive to impurities, apparently decreasing indefinitely with
continued purification. To some degree, measured conductivity depends
on electrode material; its influence, however, is not significant at the
impurity levels of industrial CIE fuel. Furthermore, measured conduc-
tivity values depend on the electric fields used. Similar to voltage-cur-
rent characteristics in air, there exists a linear region (ohmic conduc-
tivity), a saturation region (where conduction is limited to the rate of ion
production), and a breakdown region (where ionization takes place by high
electric fields). In our measurements as in our calculations, we restrict
ourselves to the linear region which for CIE fuel extends up to fields of
3×10^6 volts/m.

Another consideration is the stability and reproducibility of measure-
ment results. As pointed out by prior investigators, frequent irregular-
ities appear that make an accurate measurement impossible. For our
interest, however, a $\pm$ 10 percent accuracy is adequate and, within this
limit, data are reproducible.

For our purposes, we used a probe of capacitance C and measured the resistance R of this probe while immersed in the liquid by monitoring the current at a specified voltage. For such a arrangement, Kasemir and Ruhnke[15] have stated that:

$$RC = \epsilon/\sigma \ . \tag{65}$$

Therefore, it is

$$\sigma = \epsilon/RC. \tag{66}$$

Probe capacity was $3.4 \times 10^{-12} F$, ϵ was $8.86 \times 10^{-12} F/m$, the applied voltage was about 3 volts, and the recorded current was in the neighborhood of 2×10^{-10} amp. An average value of conductivity of 2.6×10^{-10} 1/ohm m was found. A temperature dependence could be easily ob. rved as illustrated in Figure 14. It seems that the conductivity is directly proportional to the water content of saturated fuel. Apparently, for the temperature range investigated, there was at all times sufficient water available to saturate the liquid.

The conductivity values found for CIE fuel lie in the order of magnitude of chloroform or chlorobenzene and cannot be considered very satisfactory. Kerosene, octane, heptane, and other fuels frequently used in electrohydrodynamic work, have conductivities in the order of 10^{-13} to 10^{-16} 1/ohm m. The effect is that for analytical calculations, electrolytic conductivity can no longer be neglected. This high conductivity of CIE fuel might be caus_d by a high water content dissolved in the liquid, as compared to kerosene or other fuels.

4. Time Constant

With the measured dielectric constant and values for conductivities, we are able to determine the time constant T.

$$T = \epsilon/\sigma . \tag{67}$$
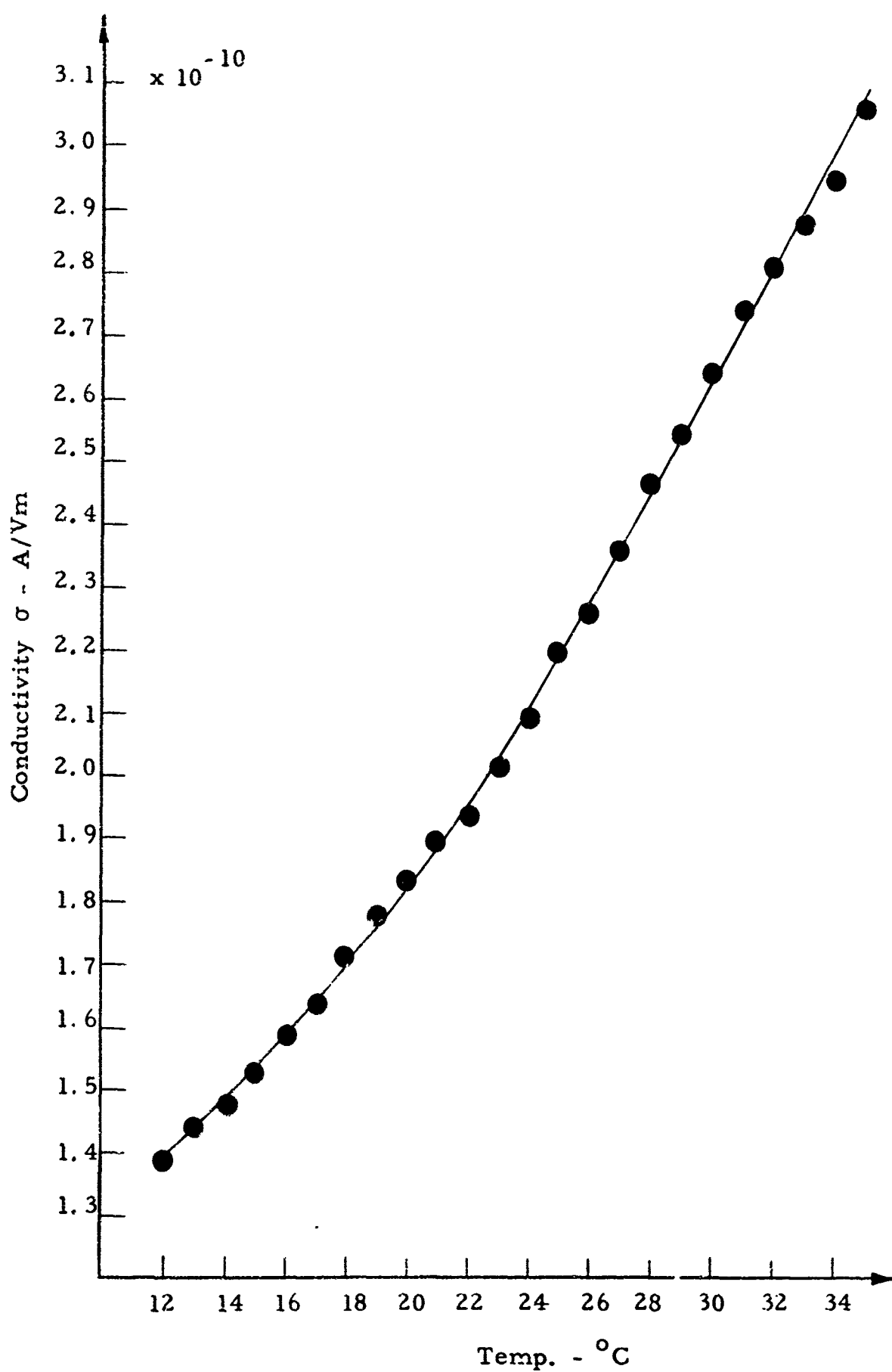
Figure 14, Temperature Dependence of Electrolytic Conductivity

This time constant, as pointed out, determines how fast electrical charges disappear in a liquid. Neglecting dissipation by diffusion and Coulomb forces, a charge q_o will dissipate exponentially:

$$q(t) = q_o \exp(-t/T). \tag{68}$$

Out time constant according to Equation (68) is 0.1 sec for a temperature of the liquid at 22°C. This means that charged particles should have a residence time in the precipitator comparable to this value; that is, approximately 0.1 sec. Furthermore, this gives a clue as to the necessary space charge densities for good collection efficiency.

5. Ion Mobility

A knowledge of the magnitude of ion mobility is important because this parameter is involved in space charge calculations and appears in the efficiency formula--in the exponent as well as in the base. Values for hydrocarbons range widely among investigators and liquids. Adamczewski[16], as well as Bragg, et al[17], gives values between 10^{-8} and 10^{-7} m^2/volt sec while Stuetzer[18], measuring freshly created ions on corona points, found mobilities ranging from 10^{-5} to 10^{-7} m^2/volt sec. For certain industrial mineral oils, Gemant[19] found values in the order of 10^{-11} m^2/volt sec--an appreciable deviation from finds of other investigators. This wide spread of values can be attributed to the method of measurement, the strong influence of impurities, and the age and nature of the investigated ions.

To be compatible with the nature of precipitation, the method we used was one in which ion mobility was determined in its natural environment, i.e., under the electric fields which will normally be found in the precipitating tube. Small probes were inserted into the precipitating tube and initial space charge density q and time function were measured when the charges traveled through the tubing. Several important conclusions can be drawn from such measurements. For high initial space charge densities

and negligible electrolytic conductivity, Whitby[20] has proved that charge density, after sufficient time, is independent of the injected space charge density and decreases in inverse proportion to t and mobility.

$$q(t) = q_o / (1 + q_o \, bt/\epsilon). \tag{69}$$

Unfortunately, electrolytic conductivities were not small enough to be neglected, so that Whitby's equation had to be modified. Thus, we obtained an approximation by combining Equations (68) and (69):

$$q(t) = q_o \exp(-t/T)/(1 + q_o \, bt \exp(-t/T)/\iota). \tag{70}$$

This relation yields, for low enough mobilities, values of q(t) which are at all times proportional to the initial values. For two values of space charge densities q_o and for different ion mobilities, Equation (70) is plotted in Figure 15. Experimental values found for these space charge densities could now be compared with theory, and conclusions on the effective mobility could be drawn which apply directly to our model precipitator. We derived a mobility of 3×10^{-9} m^2/volt sec as the most probable value. This value is close to those given by Gemant[19] for hydrocarbons containing a high dose of impurities.

It is realized that no discrete ion mobility value exists; rather, a broad spectrum of mobilities is present at any time in the liquid. This one value, however, can be used to estimate collection efficiency.

6. Maximum Space Charge Density

Besides ion mobility, it is important to know the highest possible space charge density that can be obtained with CIE fuel in our ionizer. The applied maximum voltage is based on the dielectric strength of the liquid and a safety factor in order to avoid possible breakdown in the ionizer. Although occasional sparking is not considered dangerous (nor will it affect chemical constituents of the liquid), it should be avoided to increase the life of the ionizer edges. For such safe voltages, obtainable space charge densities
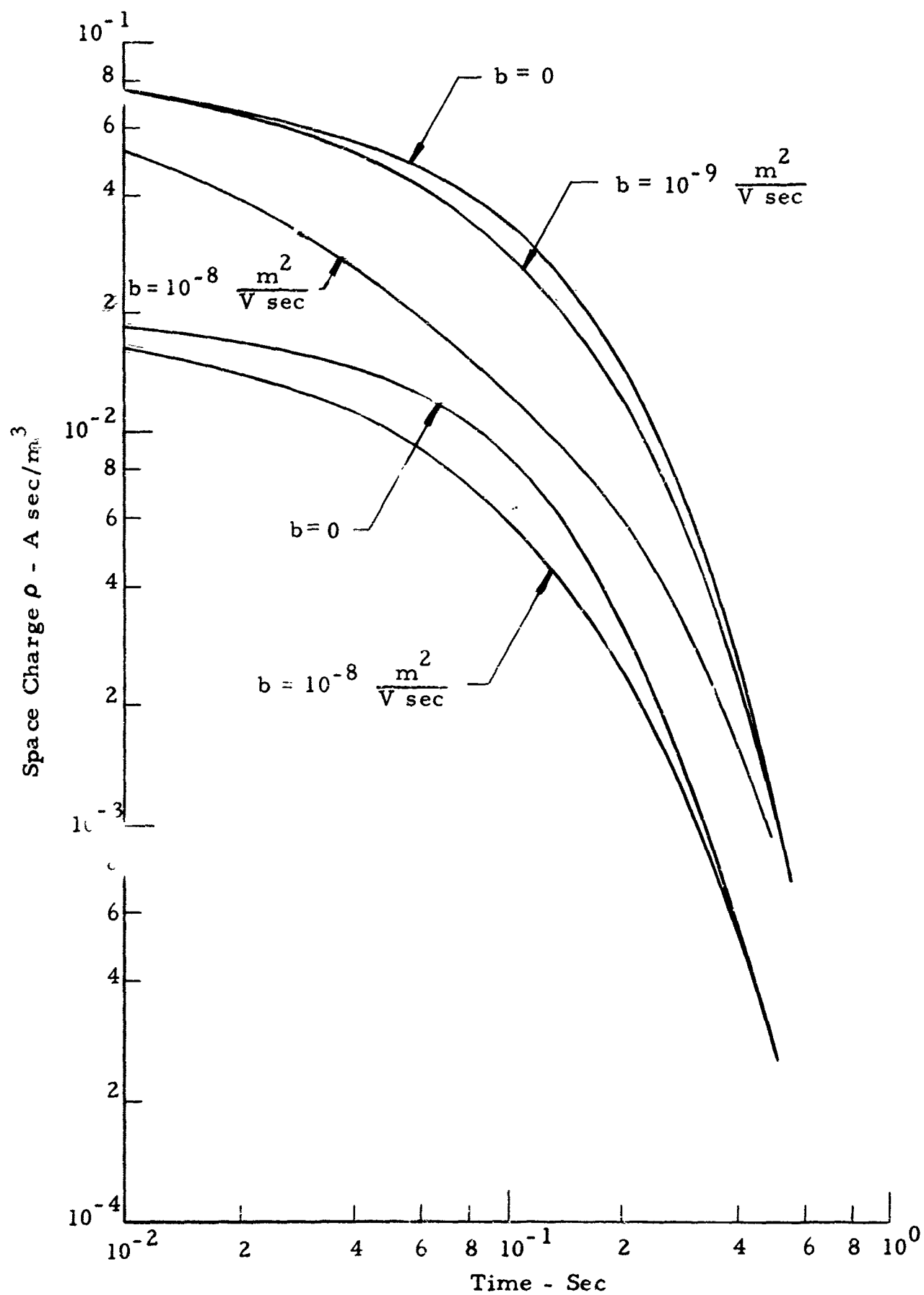
Figure 15. Decay of Space Charge Density in Precipitator Tubing

depend only slightly on flow rate as can be seen from Figure 16. A value
of at least 0.08 amp/m^3 can be obtained with all flow rates.

7. Dielectric Strength of CIE Fuel

Experimenting with the electrohydrodynamic (EHD) precipitator re-
quires the knowledge of the maximum dielectric strength of the CIE fuel.
The dielectric strength is of great importance as a measure of the fuel's
ability to withstand electric stress without failure and, when low values
are found by test, may also serve to indicate the presence of excessive
contaminants such as water or chemicals in the fuel. It is well known
that the contaminants may considerably lower the electrical breakdown
strength of liquid insulators.

Within the ionizer, the fuel itself is used as an insulating medium and,
furthermore, it is exposed to the high electric field between the emitter
and collector. An occasional breakthrough in the ionizer does not damage
the emitter severely, but such should be avoided. Tests show that the
average maximum dielectric strength of CIE fuel is $E_{max} = 3 \times 10^6$ volt/m.
This was calculated from the breakdown voltage and the gap between the
emersed electrodes.

A number of clean and filtered samples of CIE fuel have been tested
between two polished metal electrodes (1 inch in diameter), mounted with
axes horizontal. The gap between the electrodes was varied between
0.1 mm and 0.5 mm. Tests were performed with dc and ac, 60 cycles, at
68°C. These are the conditions to which the fuel is likely to be subjected
in the model precipitator.

The values in the literature[21] for the dielectric strength E_{max} of trans-
former oil are found to be 1.2 to 1.8×10^6 volt/m; for very pure hydro-
carbons, the dielectric strength reaches values up to $E_{max} = 1.6 \times 10^8$ volt/m. [12]
The dielectric strength of the CIE fuel is most satisfactory in the EHD
precipitator.
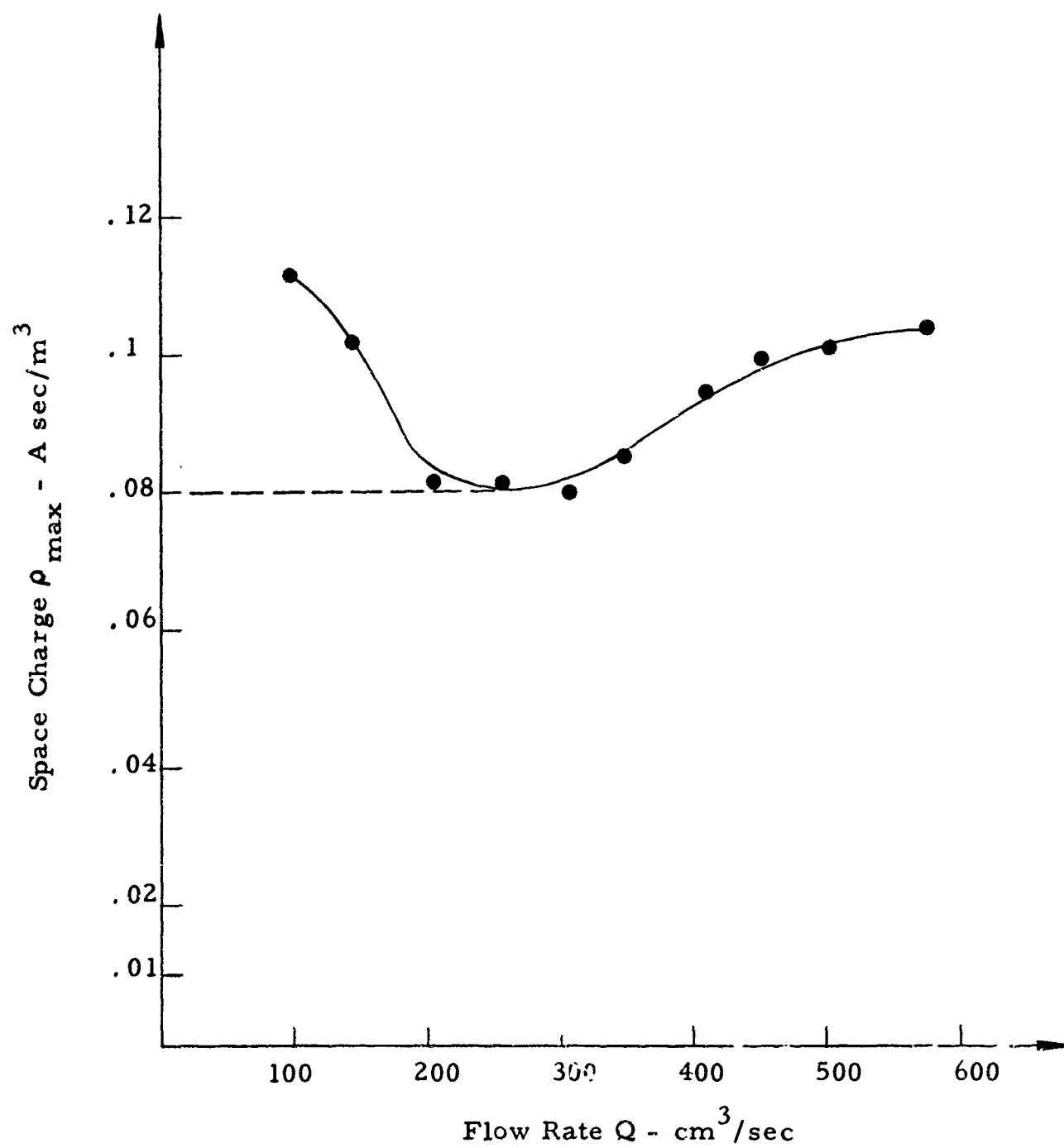
Figure 16. Space Charge Density in Relation to Flow Rate

8. Pressure Drop Across the Filter

It has been pointed out that the pressure drop across the filter is very low compared to pressure drop across equivalent mechanical filters. Using the flow rates for which the EHD filter was designed, we obtain pressure drops as illustrated in Figure 17. From these values it is possible to calculate the power of a pump necessary to flush the liquid through the filter, i.e., for 10 gpm a mechanical power of 40 watts is necessary. Using similar units in parallel for higher flow rates and a motor-pump efficiency of 80 percent, we might need 5 watts per gpm electrical power for pumping the liquid through the filter. Additionally, 0.1 watt per gpm would be needed to supply the ionizer with high voltage power.

9. Viscosity

Data on kinematic viscosity of CIE fuel, together with its temperature dependence, have been supplied by QMR&E, Natick, Massachusetts. For our considerations of collection efficiency, dynamic viscosity in mks units must be obtained. Figure 18 gives values of dynamic viscosity using the following equation of conversion as applicable for CIE fuel:

dynamic viscosity (Newton sec/m^2) = kinematic viscosity (cs) x 0.775 x 10^{-3} (Newton sec/m^2 cs).

The values obtained are slightly higher than for kerosene. No difficulties due to viscosity are anticipated with our collection mechanism.

10. Collection Efficiency

It is now possible to derive collection efficiencies which can be expected by utilizing all the discussed parameters. An efficiency η very close to 100 percent can be calculated from the following values:
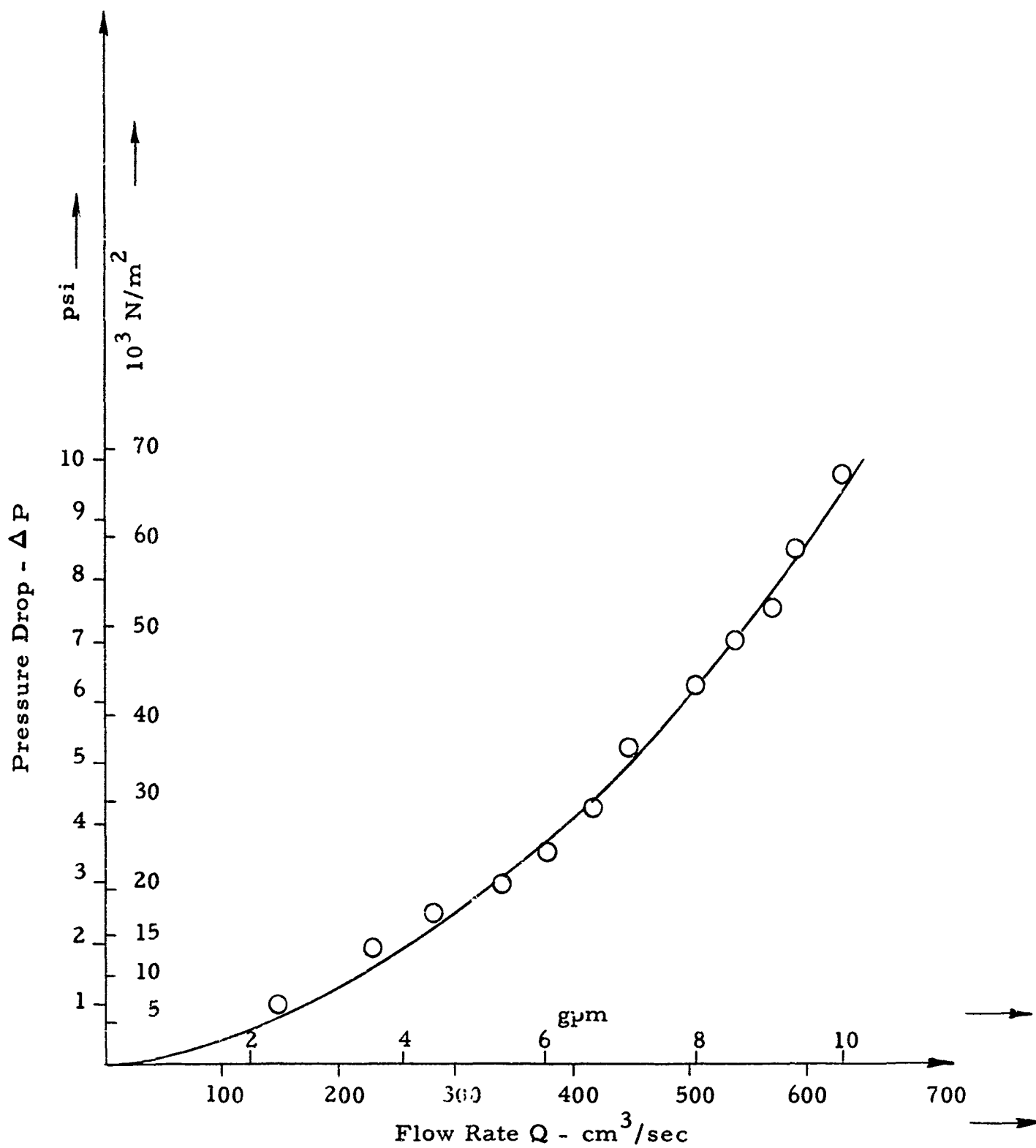
Figure 17. Pressure Drop Versus Flow Rate for the Model Precipitator
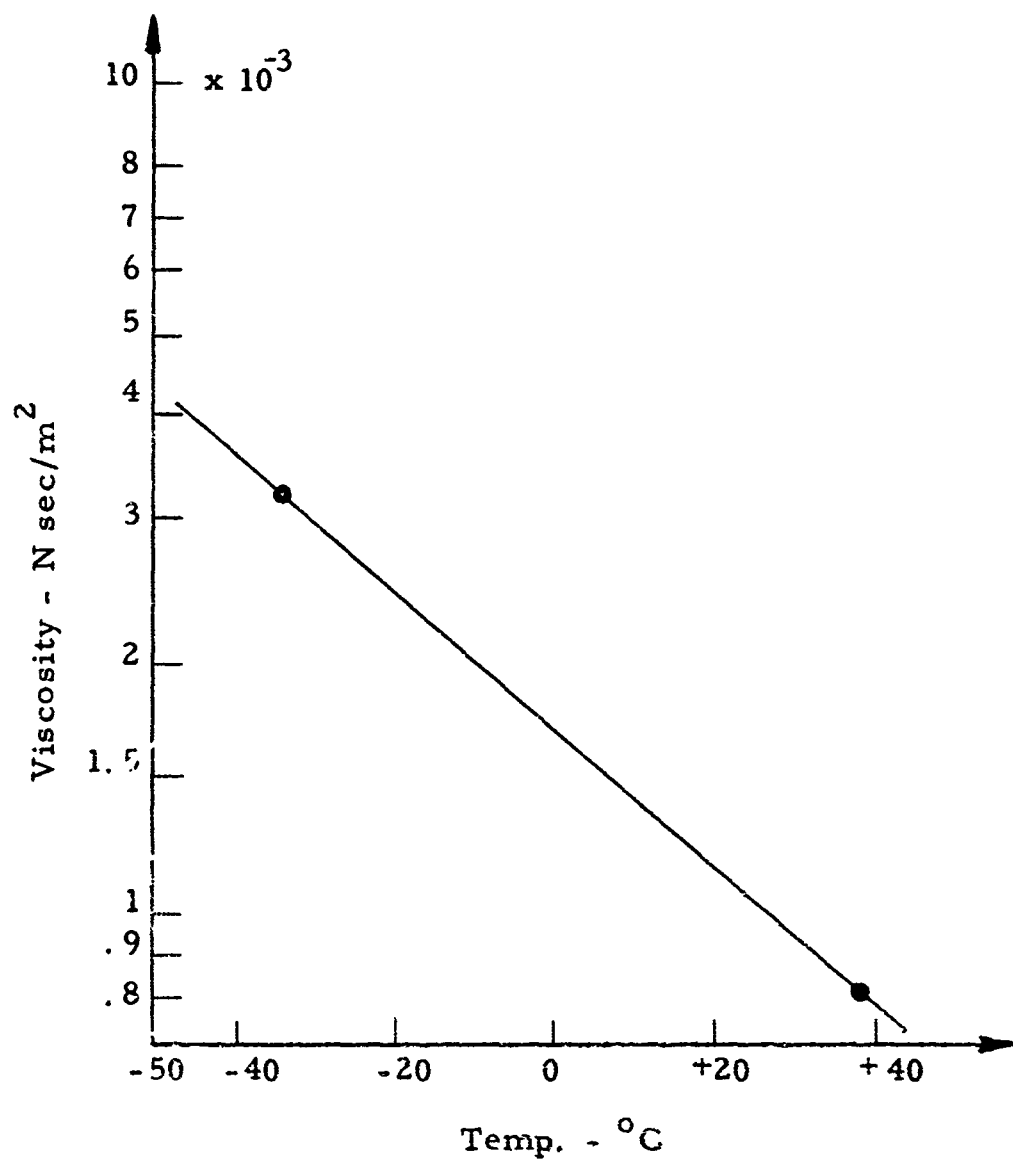
Figure 18. Temperature Dependence of Dynamic Viscosity

$$\epsilon = 8.859 \times 10^{-12} \text{ amp sec/volt m}$$

$$\epsilon_o \doteq 2.16$$

$$q = 0.08 \text{ amp sec/m}^3$$

$$b = 3 \times 10^{-9} \text{ m}^2/\text{volt sec}$$

$$\sigma = 1.95 \times 10^{-10} \text{ amp/volt m}$$

$$a = 0.5 \times 10^{-6} \text{ m}$$

$$E = 3 \times 10^6 \text{ volt/m}$$

$$\mu = 1.2 \times 10^{-3} \text{ Newton sec/m}^2$$

$$t_c = 0.07 \text{ sec}$$

$$T = 0.1 \text{ sec}$$

$$K = 8.$$

Using much more moderate values for E (10^6 volt/m), space charge density q (0.03 amp sec/m^3), and a residence time t of only 0.1 sec in the precipitator, we still arrive at an efficiency of 80 percent.

11. Wall Material of the Precipitator

Since all material of the precipitator tube is of great importance, a number of experiments were performed using various materials. The results from tests with metallic (brass, stainless steel, aluminum) and nonmetallic (glass, quartz, Plexiglas*, Territe II**) tubing were negative.

The only material which gave relatively good results was P. V. C.*** plastic tubing. This tubing is soft, crystal clear, and fairly flexible.

---

* Rohm and Haas Company, Philadelphia, Pennsylvania.

** Busada Mfg. Corporation, Flushing, New York.

*** Polyvinyl Chloride, Mayon Plastics, Hopkins, Minnesota.

The flexibility is obtained by a plasticizer. It was noticed that CIE fuel dissolves the plasticizer within several hours depending on the wall thickness of the tubing. The result is a considerable hardening, shrinking and hazing of the tube and unfortunately a rapid decrease in the filter efficiency to practically zero.

The loss of the precipitation effect can be explained by the coefficient of friction dropping with decreasing softness of the tube material. The coefficient is no longer high enough for the particles to resist the forces of drag and to adhere to the wall. Dissolving the plasticizer may also result in a change of an otherwise favorable conductivity of the plastic material. The negative results for tests with hard metallic and non-metallic tubes, as mentioned above, verify the assumption that the coefficient of friction at the wall of the P. V. C. tube has changed to a low number.

Efforts were continued to find a more suitable precipitator wall material in order to improve the efficiency and the reliability of the precipitator. Although plastic tubing has fairly good characteristics for a short length of time, the problem of hardening and also the random results obtained could not be overcome. Neoprene rubber, well known as oil resistant, was tested as precipitator wall material. Its resistance to CIE fuel is good, but the fine, non-regular deposit of precipitated particles did not adhere to the wall well enough to improve previous results in efficiency. O-rings made out of neoprene were used instead to create a corrugated surface when placed close to each other in a tube. It was anticipated that the corrugated surface would provide grooves and create almost turbulence-free areas. However, no precipitation was found. Several silicone rubbers were tested for resistance to CIE fuel. Unfortunately, their resistance is so very low that no precipitator test runs were possible.

A separator in combination with a precipitator was suggested. The device was built, but the experiments were discontinued because of turbulence problems. Turbulence-free flow and equal velocity in the area of separation are of great importance and these conditions could not be achieved easily in the present design.

The difficulty of retaining the precipitant on the wall of the precipitator finally led to the use of a commercial filter cartridge as the precipitator wall material (See Figure 19). Under the force of an electric field, particles deposit on and penetrate into the porous wall material and then remain there. This arrangement proved to be highly satisfactory. It was found that the precipitant easily penetrated into the porous material and was not worked out by the turbulent flow.
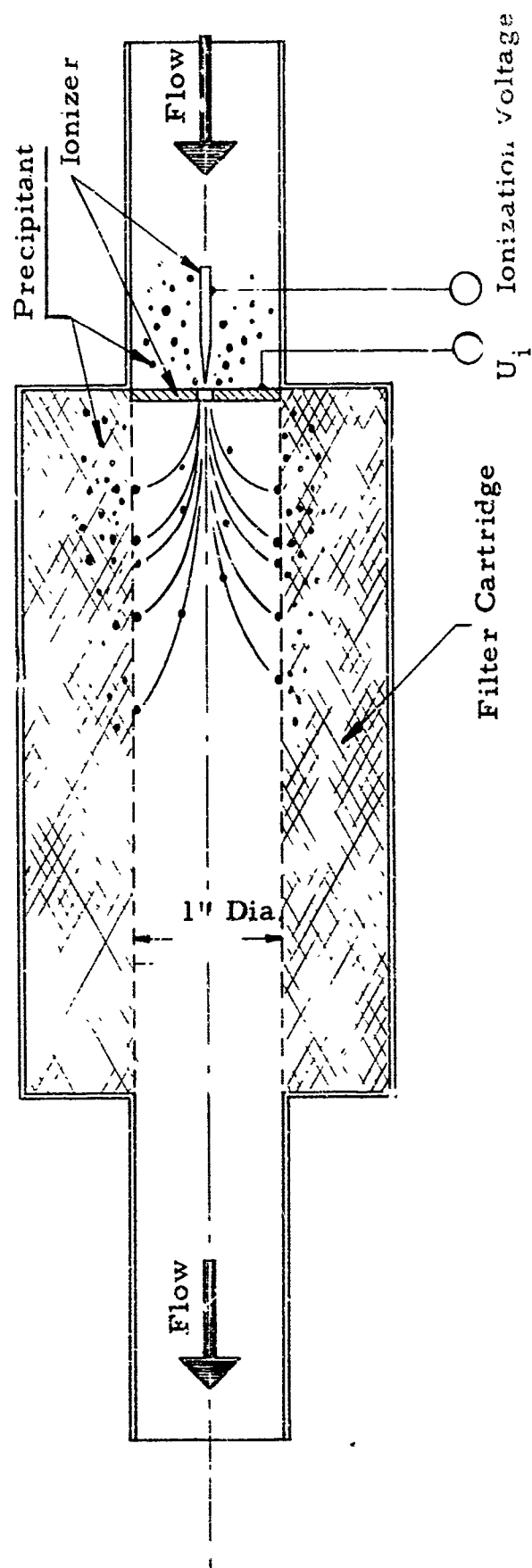
Figure 19. Precipitator

VII. SAMPLING OF CIE FUEL CONTAMINATED BY MICROORGANISMS

A. Development of Artificial Contamination and Analytical Techniques

We found that the most serious problem involved in culturing viable organisms from fuels utilizing the membrane filtration technique to develop a satisfactory artificial contamination technique and a routine analytical technique was growth inhibition by residual fuel in the membrane. Unless every trace of fuel was flushed out of the filter, uneven growth occurred on its surface, and replicability between samples was poor. The problem apparently was solved by using an excess of wetting agent as a flush. We achieved fair replication when we used 400 to 500 ml of a 0.5 percent Triton x-100 rinse, followed by a final rinse with a nutrient broth.

Other satisfactory plating procedures were tried:

1) After filtering the fuel through the membrane, the filter was disintegrated in 100 ml of Triton x-100 (0.5 percent) in a Waring Blender. Dilutions of this fluid could then be plated routinely. Although this technique is time-consuming, it is quite useful in cases where the original count is unknown and there is the danger of overgrowth of contaminants. Essentially, this procedure permits one to convert the fuel sample (which is implatable by classic methods) into an aqueous sample (which can be treated classically) by transferring the microbial load from the former quantitatively into the latter.

2) Centrifuge method: This technique was recently described in the SIM Handbook on Proposed Procedures for Microbiological Examination of Fuels (Refs. 23 - 25). Our modification used 15,000 rpm x 15 min (in a Spinco apparatus) on a semi-micro scale (1 ml of fuel and 2 ml Triton x-100); the results were satisfactory.

Microscopic examination of fuels was satisfactory for evaluating fungus contamination, but unsatisfactory for bacterial quantitation.

Several attempts were made to inoculate known number of contaminants into sterile fuels and to recover these contaminants quantitatively. Little success was noted when lyophylized Serratia marcescens (Sm) was added directly to the fuel. However, fairly satisfactory results were obtained when aqueous suspensions of organisms were shaken with the fuel, then allowed to partition themselves into the respective water-fuel layers. In order to reach a level of 10^3 organisms/100 ml of CIE fuel, 10 ml of water containing 10^7 organisms/ml were used. We experienced some difficulty in the preparation of homogeneous fungus contamination into the fuels. We solved this problem by actually growing the fungus in a fuel-medium mixture.

As preliminary tests, we sampled contaminated fuel upstream and downstream from the filter. Because of the long time needed for growing samples taken from background contamination, an appropriate dose of Serratia marcescens was added. Several samples taken and analysed during three days are shown in Table 2. Although the number of samples taken was not sufficient to give representative results, it is surprising that the count was higher in most cases after the liquid passed the filter than before. This was explained by dissociation of clusters of bacteria through high velocity gradients within the ionizer jet. It was not found easy to disseminate pulverized Sm material into the liquid as single bacteria. For these reasons, bacteria grown naturally in the liquid offered a more reliable source of samples.

Table 2. Sampling of Sm

Count before Filter (per 100 ml)	Count after Filter (per 100 ml)
3000	5000
3300	1700
710	1000

B. Sampling of Biological Material

After overcoming these difficulties to reliably disseminate Serratia
marcescens (Sm) into the CIE fuel, we tried to use only the natural
background as test material. We found only about 3 viable particles
per 100 ml. In Figure 20, the distribution of the background is plotted
on logarithmic probability paper. The distribution is best approxi-
mated by the lognormal distribution appearing as a straight line. A
standard deviation of 0. 86 can be derived and a median of 2. 7 bacteria
per 100 ml. This wide spread was first believed to be due to the inho-
mogeneity of the liquid. If was found. however, that stirring the liquid
as well as changing the sample volume did not change this distribution.
The sample volume could not be raised much higher than 100 ml for
reasons inherent in the total volume of liquid circulated in the system.
It appeared that 3 counts per sample is not enough to give a represen-
tative sample, even if averaged over many test runs. It seems possible
that a certain background count is unavoidable even if a well filtered fuel
is used. To estimate the background distribution. we assumed that
among 100 samples the average count will be 3 while 20 will be sterile.
This suggests an exponential probability law. Such a distribution is
shown in Figure 20. It explains the necessity of having samples with
higher counts and makes samples with low counts meaningless as the
one derived from measurements in Figure 20. We believe that 30
counts per sample are necessary for reliable evaluation of test
results.

For a test on reliability of samples, the distribution of counts
should be similar for bacteria and inert material on one row of samples.
Figure 21 shows the evaluation of 34 random samples of CIE fuel.
Each sample was evaluated by bioassay and microscopically examined
for fluorescent particles and inert black background material. The
much higher standard deviation of the bacteria count indicates that an
error process of appreciable magnitude is associated with the analysis
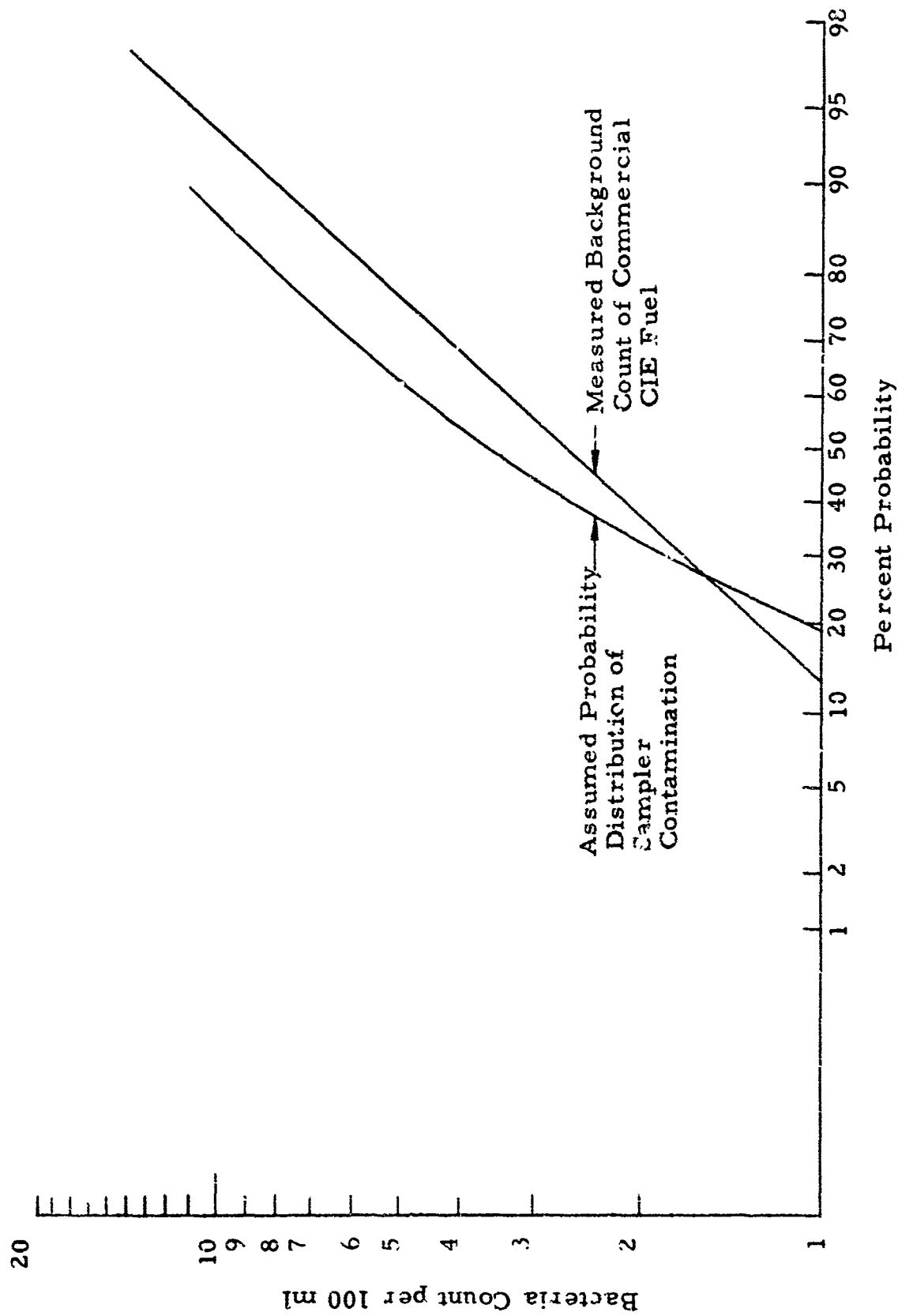
Figure 20. Distribution of Natural Background in CIE Fuel
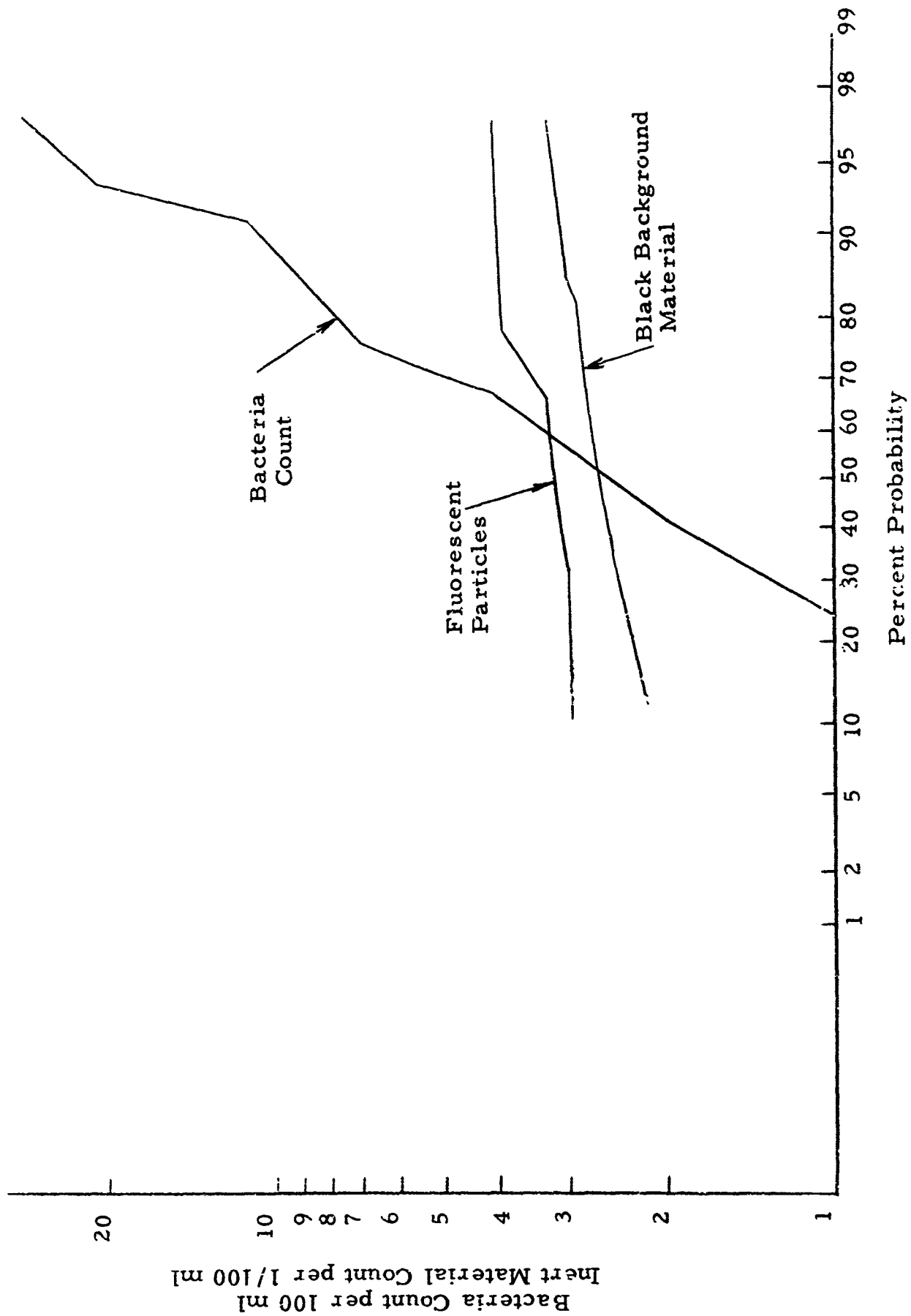
Figure 21. Test of Sample Reliability

of biological samples. Fluorescent particles and inert background
material show to a good degree equal probability distributions. These
data suggested that we increase the bacteria count artificially. We
mixed a quantity of contaminated CIE fuel with water and kept this
mixture at room temperature and agitated on a shaker table. In this
way the interface was kept constantly large. Very high counts of
bacteria were found after a few days. By adding some portion of this
culture to our test stand, we hoped to control the bacteria count.
The results were discouraging. Figure 22 shows the results of a
series of samples taken from CIE fuel after an artificial increase
of background bacteria. Each sample taken was divided into 1 ml,
10 ml, and 100 ml samples and analyzed. Not even on the average
was proportionality preserved. While the 10 ml samples showed
about 10 times higher count than the 1 ml sample, the 100 ml samples
showed only an insignificantly higher count than the 1 ml sample.
The proportionality is also not preserved when a sample-to-sample
comparison is made. Table 3 shows the data used to plot Figure 22.
The results suggest that a process is involved which makes the count
dependent on the amount of liquid used in the bioassay. The bacteria
present in 100 ml of CIE fuel is apparently killed when filtered through
the micropore filter while the bacteria present in 1 or 10 ml is not.
Samples with counts over 400 could not be analyzed because it was
not possible to distinguish between single colonies. From these and
other results it was concluded that: 1) a sample has to have at
least 30 counts; 2) a sample must not have more than 400 counts;
3) a sample must not be larger than 10 ml; 4) the concentration of micro-
organisms must be enriched in CIE fuel by at least a factor of 10;
and 5) at least 50 samples under the same conditions have to be made
to give one representative point of measurement.

In addition to the disadvantage of the time consumed in culture
growing processes, we found that in testing for the influence of various
parameters on filter characteristics, the bioassay technique is very
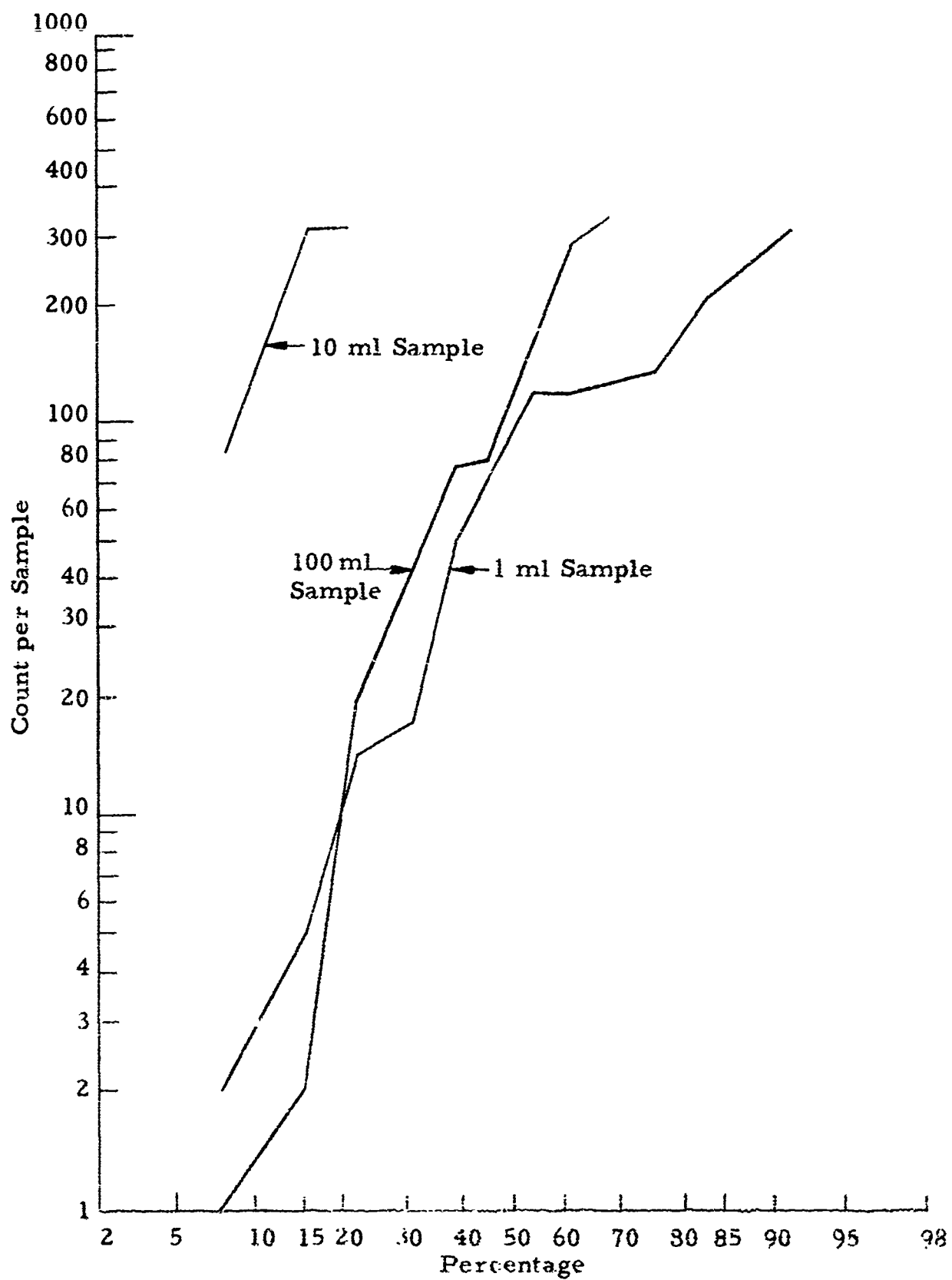
Figure 22.   Proportionality Test

expensive. Because of this, we then concentrated on experiments using the natural backgroun, of inert material. which we increased in some cases by adding ferric oxide.

A number of tests with the natural background contamination of CIE fuel and Serratia marcescens (Sm) as an artificial contaminant have been conducted. These experiments, however, were discontinued because of the long time required to grow samples for evaluation, the wide variation of counts, and indiscernibility of deposits at the precipitator wall due to the relatively low dispersion of the microorganisms in the fuel. Pulverized Sm could not be disseminated as single bacterium and clusters would dissociate in the ionizer to cause the count to be higher after passing the precipitator than before.

Table 3. CIE Fuel Bacteria Count

No. of Sample	Count at 1 ml	Count at 10 ml	Count at 100 ml
254	126	>400	339
255	14	>400	81
256	119	>400	1
257	50	313	>400
258	74	>400	148
259	210	>400	>400
261	2	>400	2
263	17	>400	78
265	332	>400	>400
267	132	>400	285
269	5	310	20
271	316	>400	>400
273	6	83	42
274	120	>400	>400

C. Sampling of Inert Particles

Following the tests which showed difficulty in using microorganisms as test particles, we discontinued the biological phase of this program for some time in order to arrive at design criteria for a prototype precipitator. Fluorescent ZnCds particles ($< 10 \mu$) and graphite ($< 30 \mu$) were used as artificial contamination instead of bacteria. Both kinds of contamination, filtered from 100 ml samples, were counted under the microscope. The fluorescent particles, when exposed to an ultraviolet light source, are easily and rapidly counted. This method reduces the time required from days to hours and has an added advantage in that the fine deposit at a transparent precipitator wall is easily observed by the naked eye. This observation is valuable in finding the apparent best ranges of flow rate and ionization voltage, and in turn gives a good indication of the collection efficiency. It immediately delineates the regions where no or very little precipitation can be expected. Furthermore, the observation of the precipitation effect is very helpful in explaining the hydrodynamic and electrical problems of these experiments.

Numerous samples have been taken from the precipitator under varying conditions to determine the collection efficiency using a plastic tubing for the precipitator walls. Every efficiency evaluation is based on the comparison of two samples taken just before entering the ionizer and shortly after leaving the precipitator tube. The test stand is equipped with two solenoid valves which allow simultaneous sampling. The results of two different test groups (Figures 23 and 24 and Figures 25 through 29) are given below. In order to compare the efficiencies for microbiological material, fluorescent and carbon particles, the numbers have been evaluated from the same samples within each test group.

Figures 23 and 24 show typical efficiency values for fluorescent particles and microbiological material ranging from zero to almost 100 percent. These numbers, however, are so random that distinct
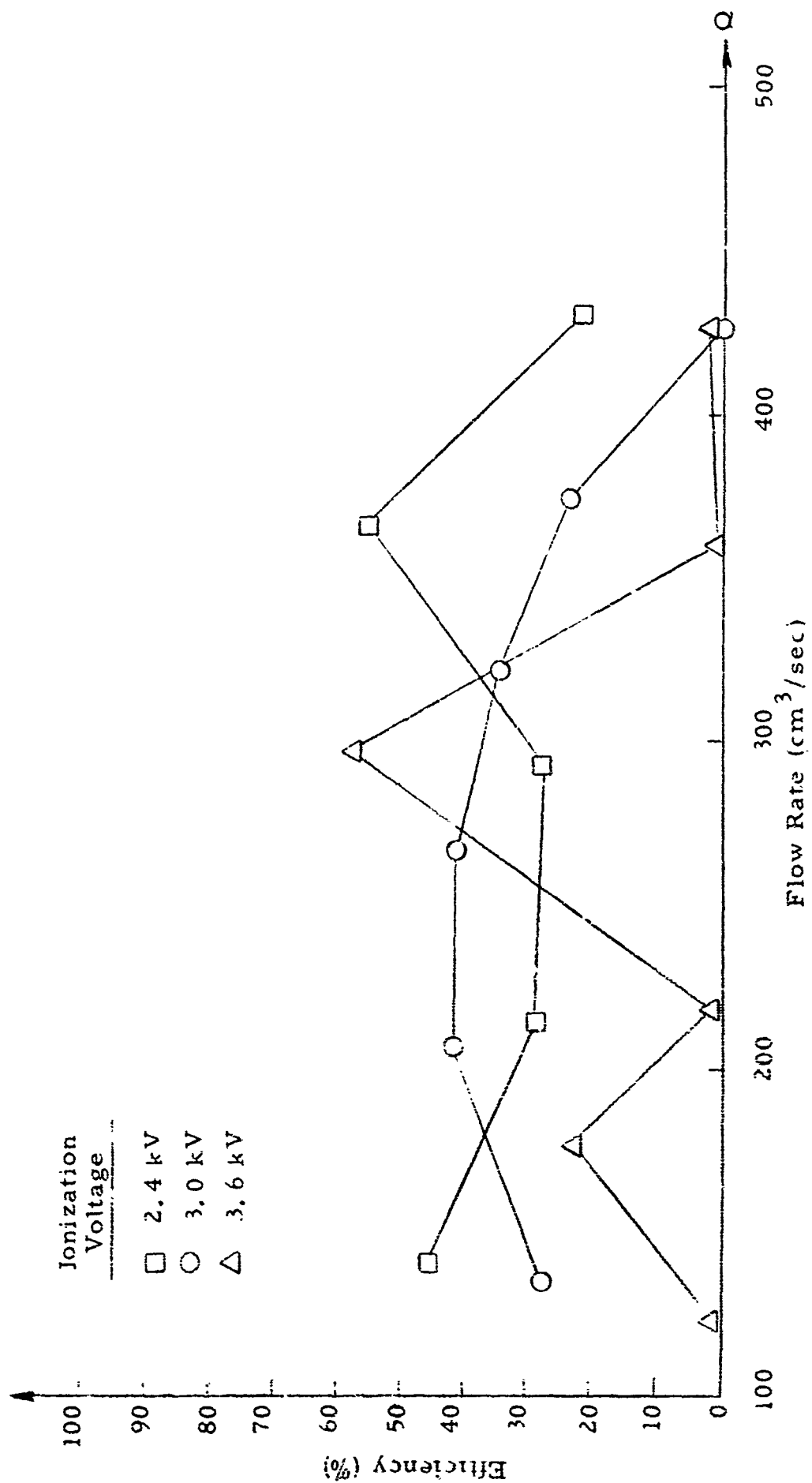
Figure 23. Collection Efficiency for Fluorescent Particles
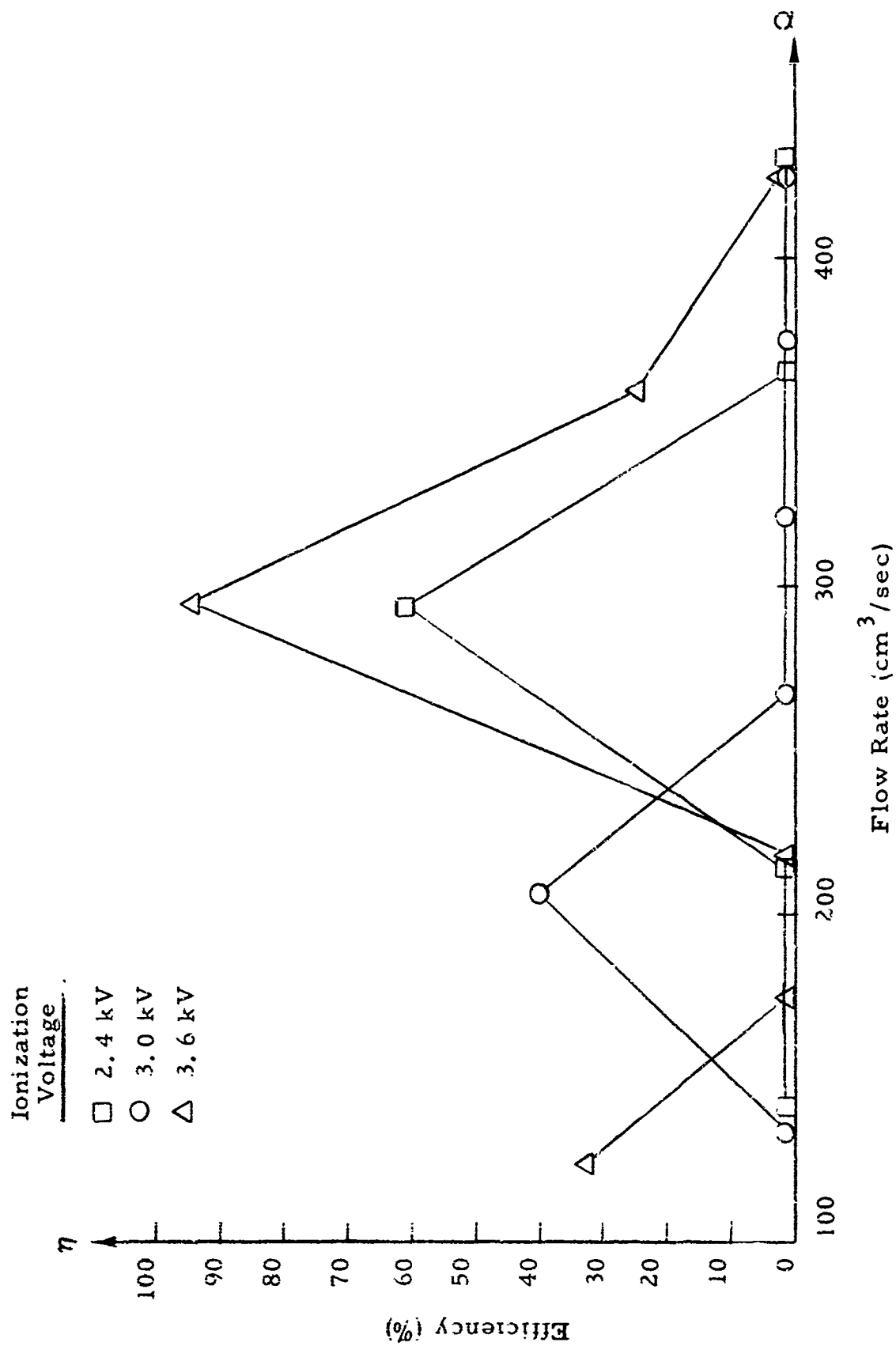
Figure 24. Collection Efficiency for Bacteria

Fig. 25.   Collection Efficiency for Bacteria

Ionization
Voltage

○   6 kV
△   8 kV
□ 10 kV
✕ 12 kV

Flow Rate (cm³/sec)
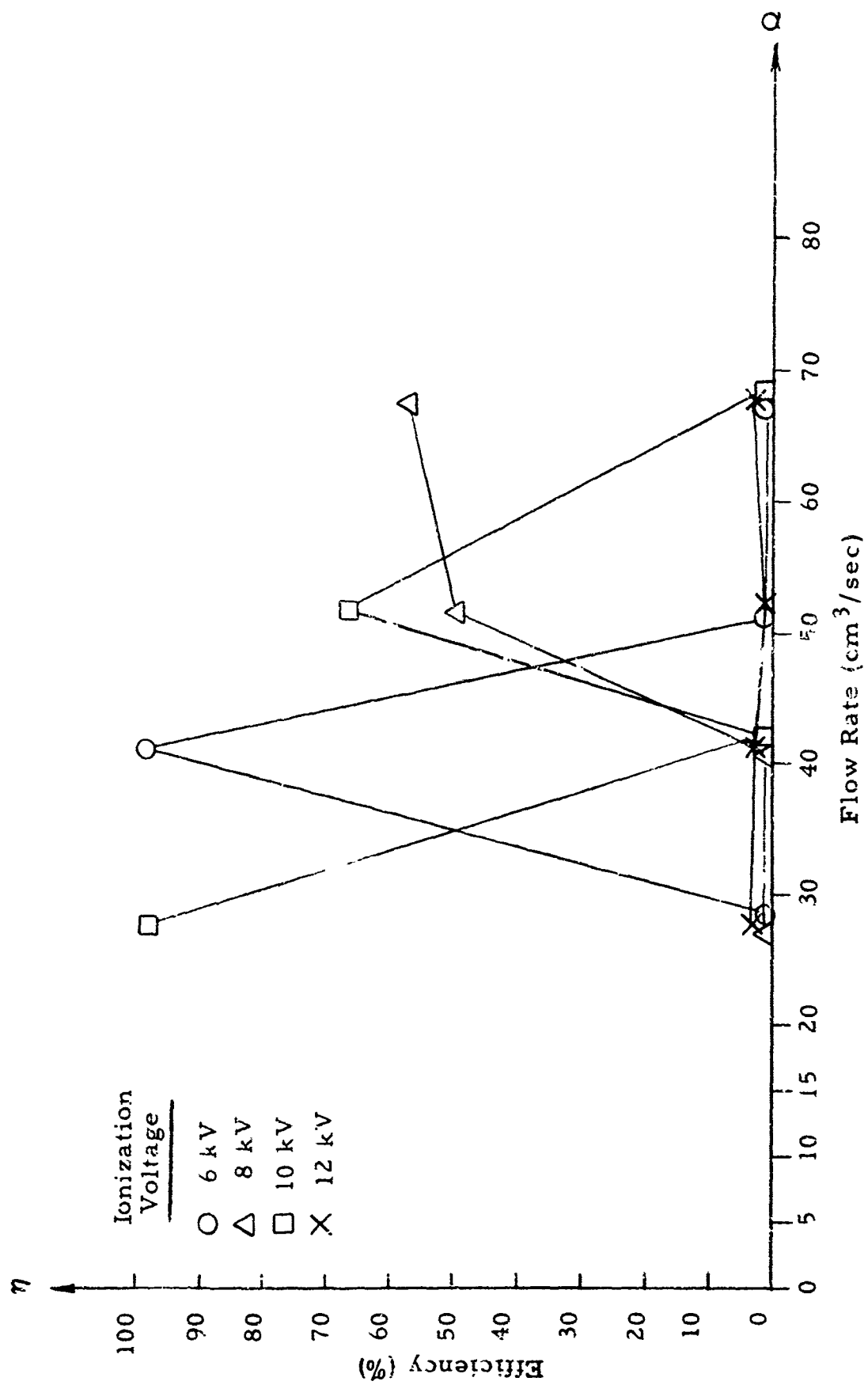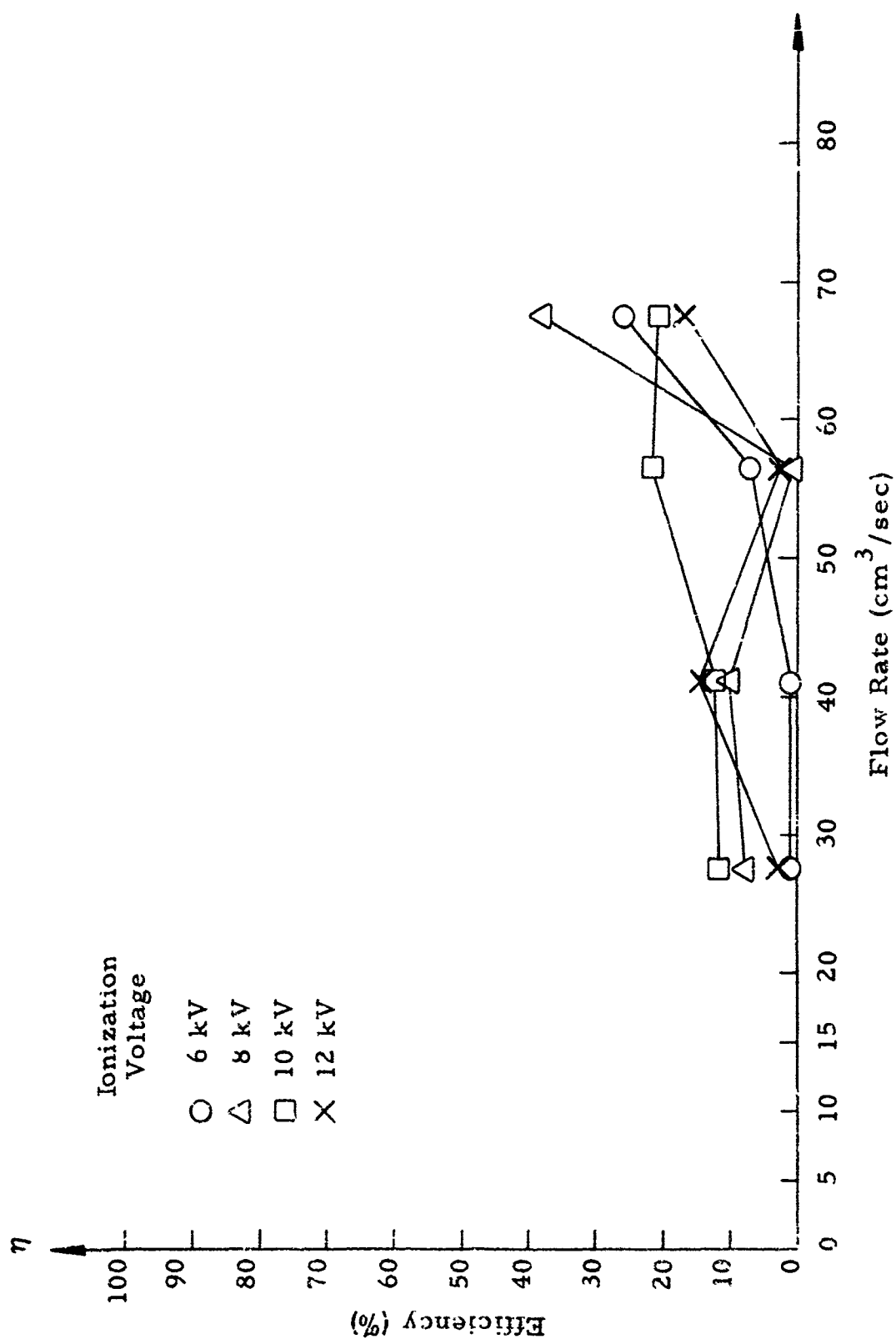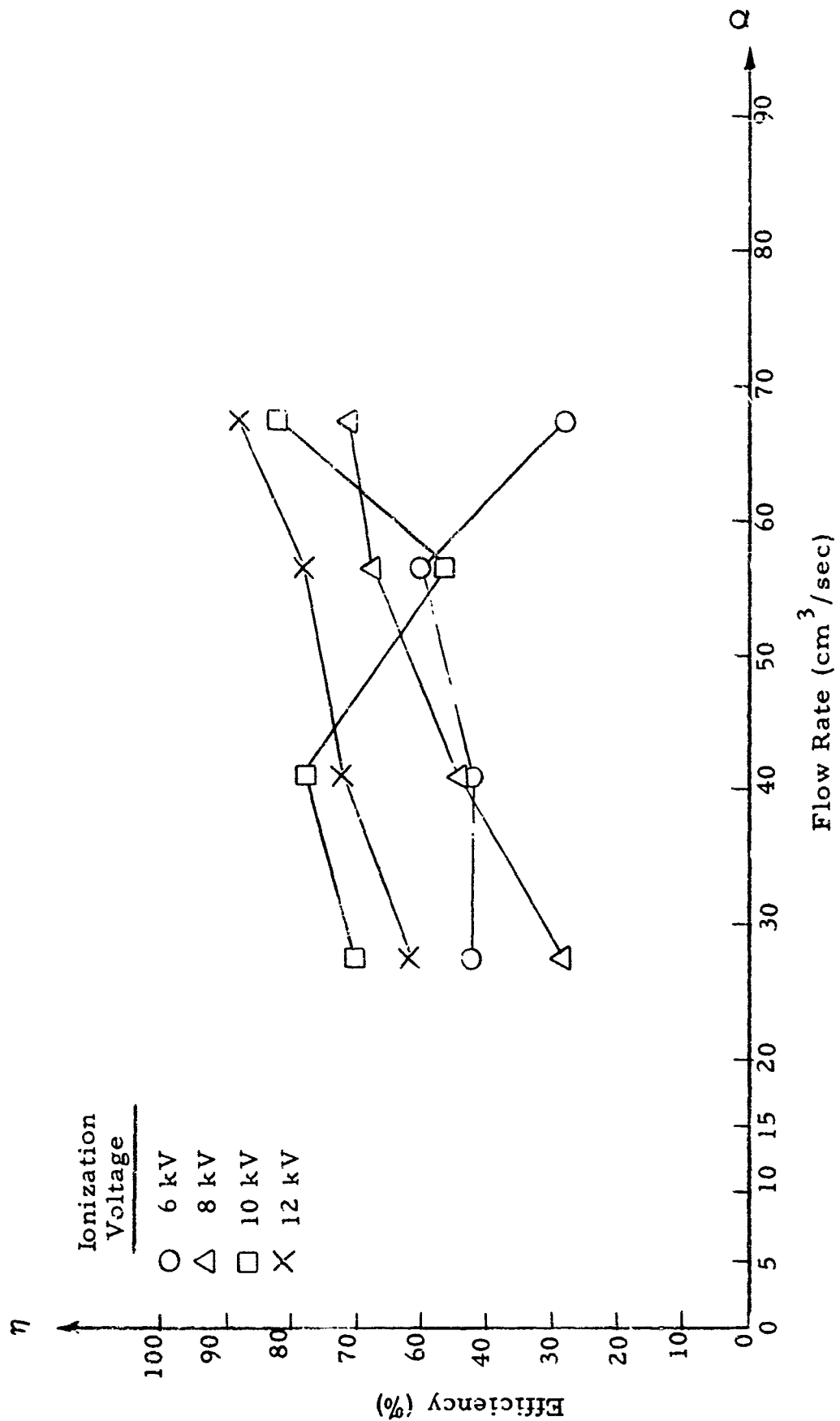
Efficiency (%)

Figure 26. Collection Efficiency for Carbon Particles

Figure 27. Collection Efficiency for Fluorescent Particles
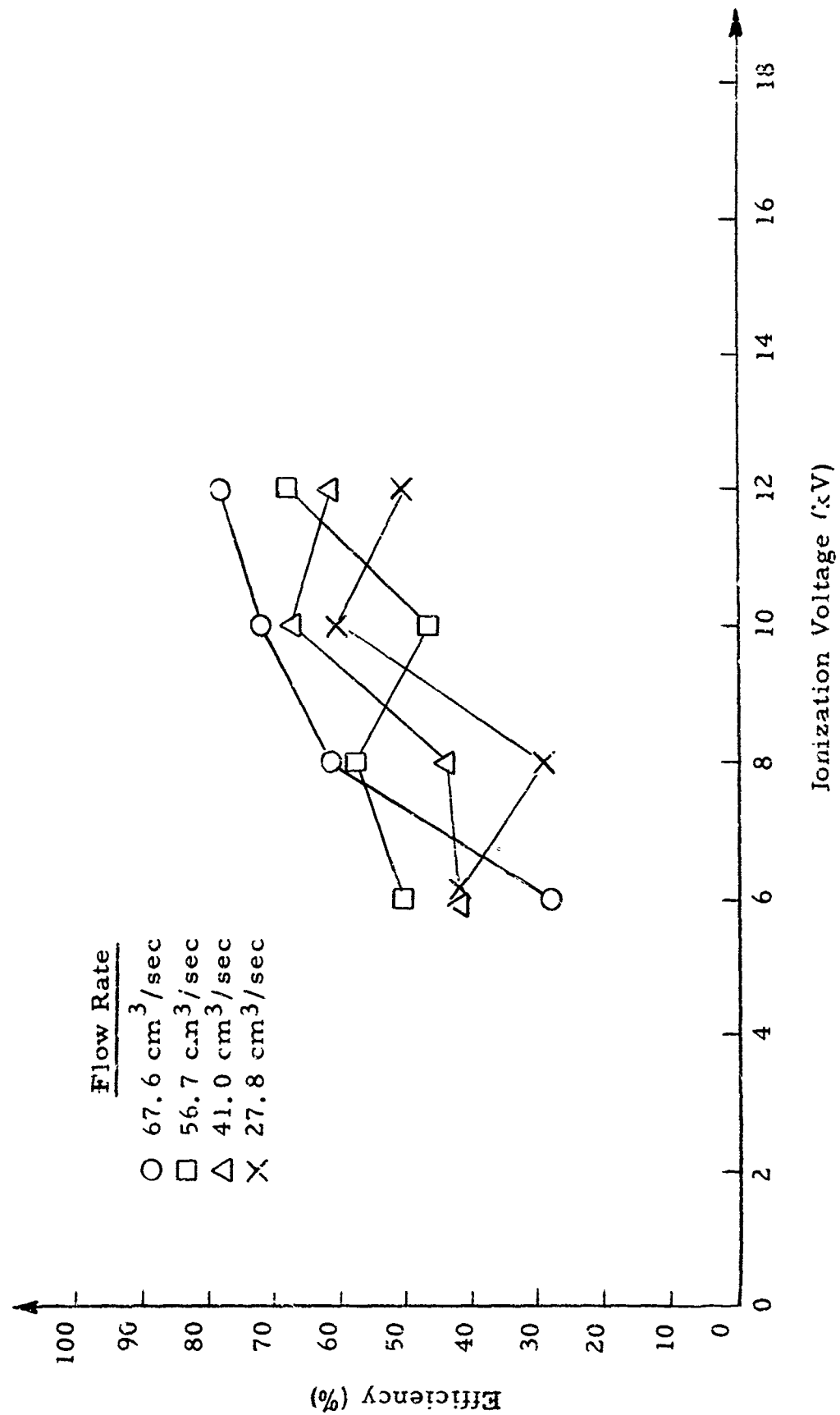
Figure 28. Collection Efficiency for Fluorescent Particles

Flow Rate

○ 67.6 cm³/sec
□ 56.7 cm³/sec
△ 41.0 cm³/sec
✕ 27.8 cm³/sec

Ionization Voltage (kV)
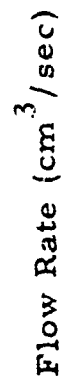
Efficiency (%)

Figure 29. Distribution of Collection Efficiency

curves or tendencies can hardly be interpreted. At a flow rate Q of approximately 300 cm^3/sec, a maximum seems to appear in these particular tests. Experiments for Figures 23 and 24 were performed by using P. V. C. tubing of 20 mm ID and a razor-edge emitter in the ionizer assembly.

Another ionizer design with a point emitter was used to perform the tests shown in Figures 25 through 29. While a definite characteristic of the plotted results cannot be found, it is to be noted that bacteria (Figure 25) have the widest variation of collection efficiencies and that the collection efficiencies of carbon particles (Figure 26) and fluorescent particles (Figure 27) are grouped somewhat closer together. In Figure 28, the collection efficiency of fluorescent particles is plotted versus the ionization voltage. An increase in efficiency with increasing voltage could perhaps be interpreted here. Of interest is the total efficiency distribution (Figure 29) of all samples and all precipitants evaluated for Figure 25 through 28. No distinct characteristic for the efficiency versus flow rate can be seen.

In connection with the experiments using a filter cartridge as the precipitator wall material, tests were made to study the precipitation effect of ferric oxide (Fe_2O_3), a contaminant of CIE fuel when stored in steel tanks. Approximately 300 mg of ferric oxide were added to 10 gal of CIE fuel. The fuel was then passed through the precipitator. After at least one full circulation of the liquid, the precipitator was removed and cut lengthwise into two halves. The precipitation and penetration effect of the ferric oxide particles upon the cartridge was easily observed by the reddish coloring of the otherwise white material.

These results with ferric oxide indicated that this new type of precipitator wall had promising aspects. The efficiency was estimated at 70 percent and it seemed to increase somewhat with increasing ionization voltage. Both ionization voltage and flow rate were shown not to be critical even when the flow rate was increased to maximum and the ionization voltage was built up to the breakthrough field strength of the CIE fuel.

For an efficiency of 70 percent with one passage it should be possible to reach an efficiency close to 100 percent by using several precipitators in series. Because of the relatively small pressure drop in each precipitator. this setup would still consume less energy than a comparable mechanical filter.

D. Sampling with Inert Material

1. Deterioration of CIE Fuel

Our experimental filter is connected with pump and flowmeter to a 10-gal reservoir of CIE fuel. It is obvious that with a flow rate of 1 to 10 gpm the same liquid is flowing again and again through the electrostatic filter. It had been observed earlier that a certain decrease in ionization occurs if the same liquid is used very often. The decrease in ionization, however. was only a minor effect and not thought to be of significance to filter characteristics.

While experimenting on filter efficiency, we observed that filter action was always excellent when using a new supply of CIE fuel; however, by the time we were ready to take samples for numerical evaluation we observed different results (See Figures 30, 31 and 32). The samples were taken on different days with different filters under similar conditions of flow rates and voltages. We used the same liquid. While initial tests showed a very nigh efficiency. even the first row of samples had an average efficiency of only 77 percent. Later the efficiency decreased to insignificant values even with a new filter. Two explanations can be given: 1) we have filtered out all particles above the size limit of the filter (the average size then decreases to a value where efficiency is low); 2) some properties of the liquid deteriorate during filtering and decrease efficiency.

We experimented, therefore, with electrostatic filters where the deposit on the walls could be released into the stream electrically and we also added ferric oxide during the period of deterioration. We are
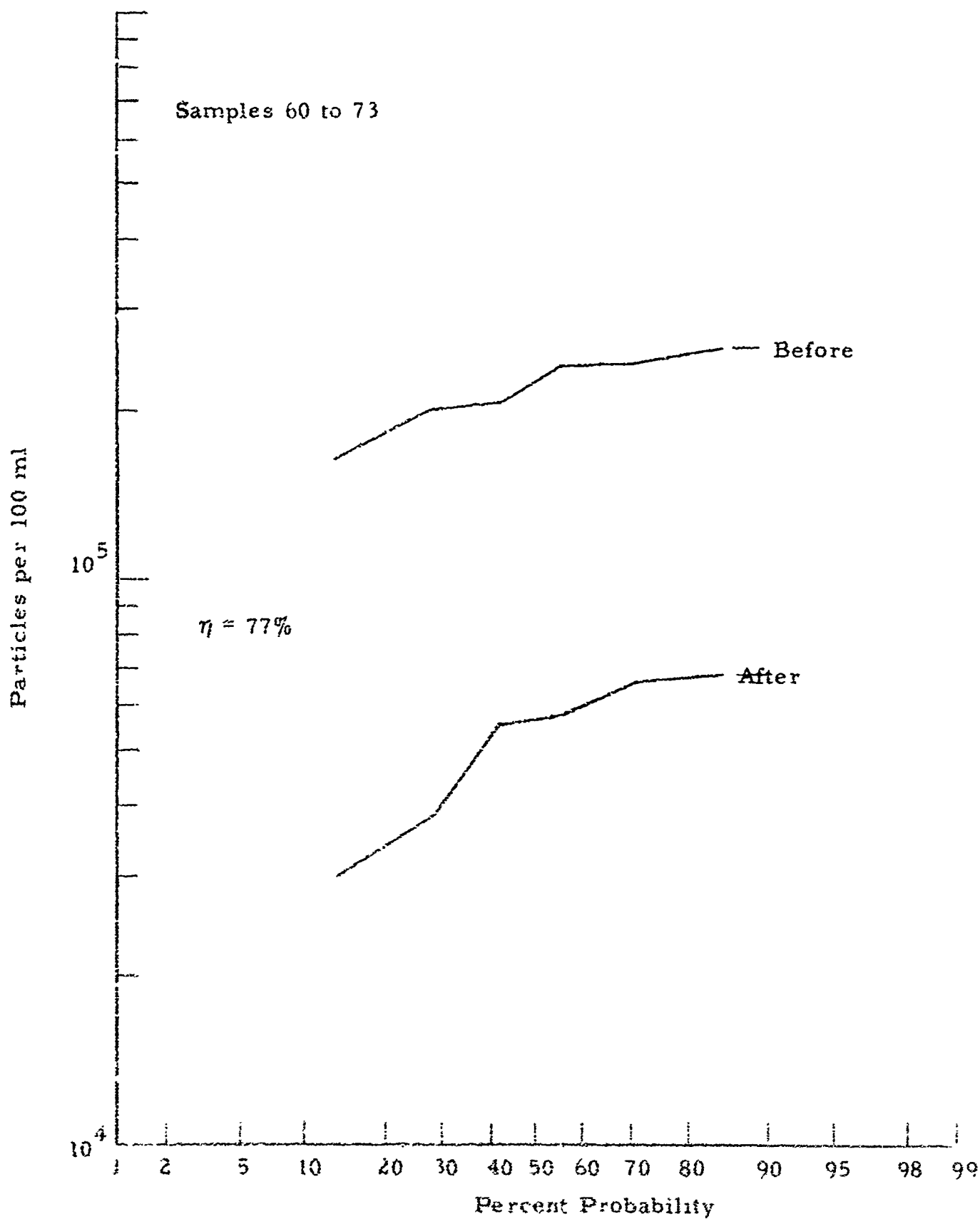
Figure 30. Particle Size Distribution Before and After Precipitation
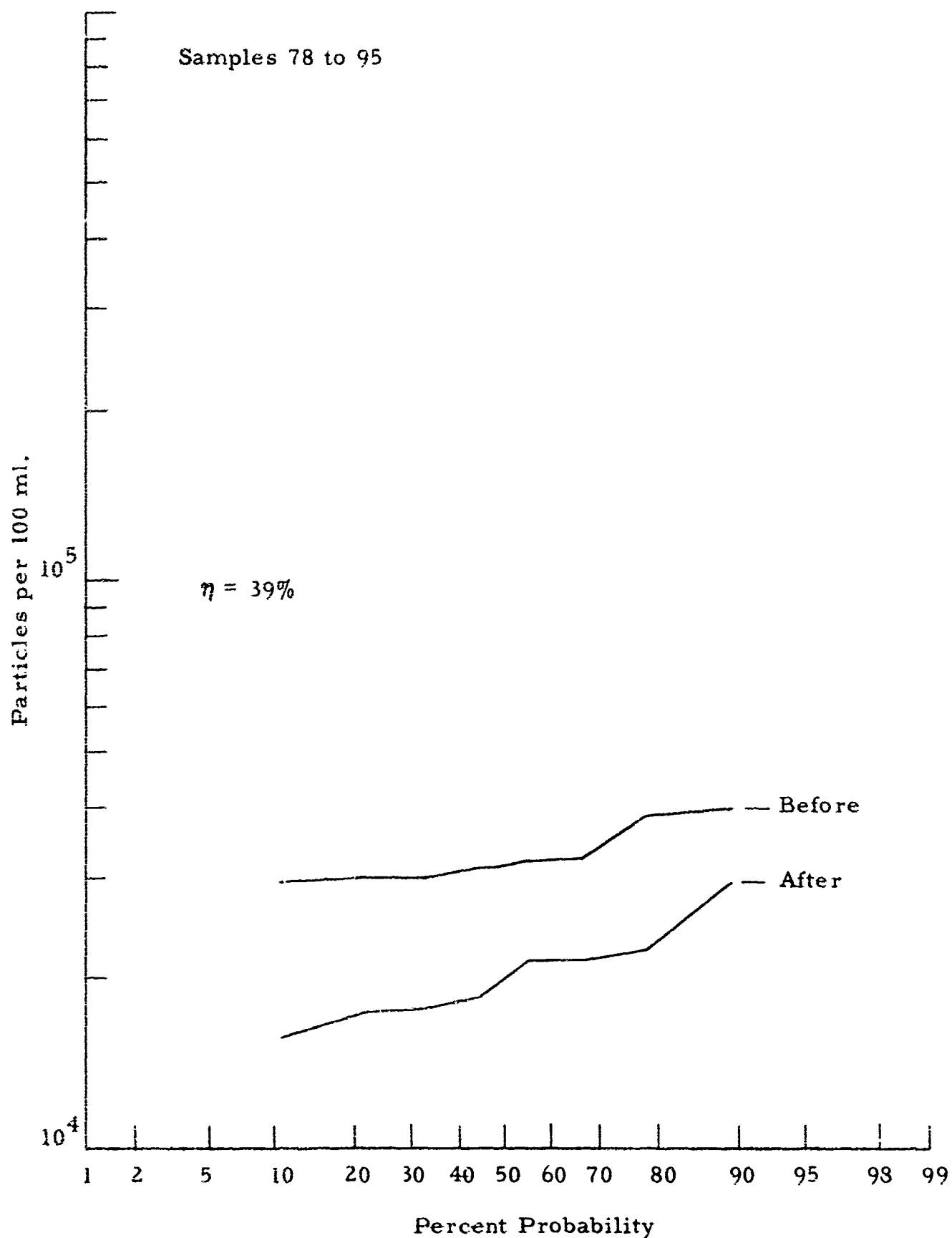
Figure 31. Particle Size Distribution Before and After Precipitation
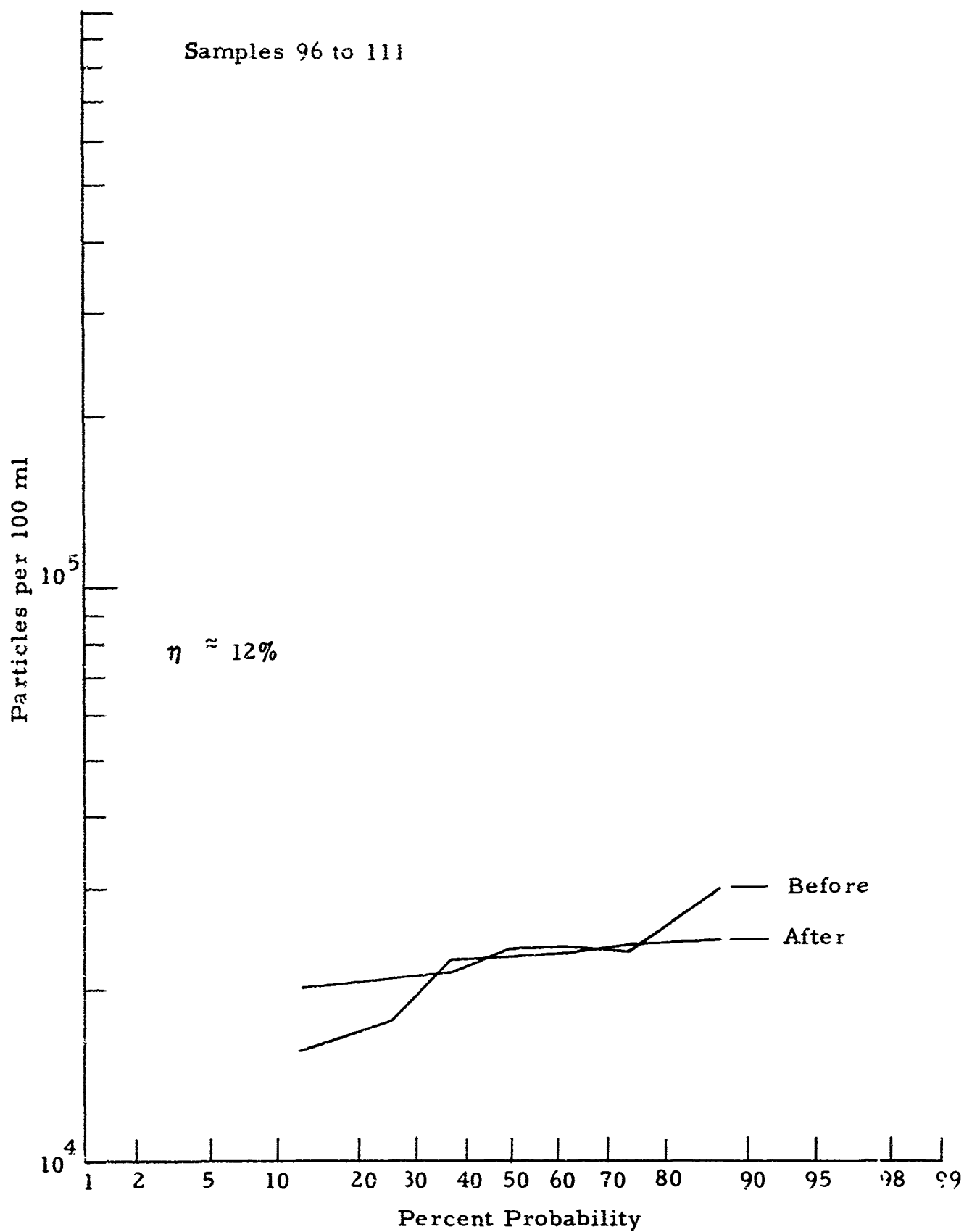
Figure 32. Particle Size Distribution Before and After Precipitation

now convinced that deterioration of liquid is the major cause of this effect, although a change of size distribution might be of some significance.

2. Filter Reliability

During the course of the investigation. we found that the distribution of particles scattered more widely after the liquid had passed the electrostatic filter (See Figure 33). Samples taken before passing through the filter had a standard deviation of the assumed lognormal distribution of about 0.07 while the distribution after the filter had a standard deviation of 0.37. Because the tests were made at varying flow rates and ionizing voltages. such a variability in results was to be expected. We can attribute some portion of the variation to the filter. Using Equation (57) we find a standard deviation of the filter characteristic to be 0.36. Flow rates varied 1:10 and ionizing voltages varied 1:5. No variation could be found at different temperatures of the liquid. No difference in filter behavior was observed when CIE fuel containing no additives was tested or after carbon particles, ferric oxide or small amounts of water were added to regular CIE fuel. It seems. therefore, that the developed electrostatic filter is reliable under conditions where the fuel is not often recirculated through the filter.

3. Filter Saturation

One of the important characteristics of any filter is the total amount of contaminants which can be deposited in a filter. This depends strongly on the filter volume or area of deposit. Earlier tests with Tygon, glass. or metal walls of the precipitator showed an astonishingly short sampling time until saturation. After a monolayer of particles had deposited on the wall, turbulence broke off portions of the deposit which went into circulation again. If lower concentrations of contamination were used, this effect was negligible.
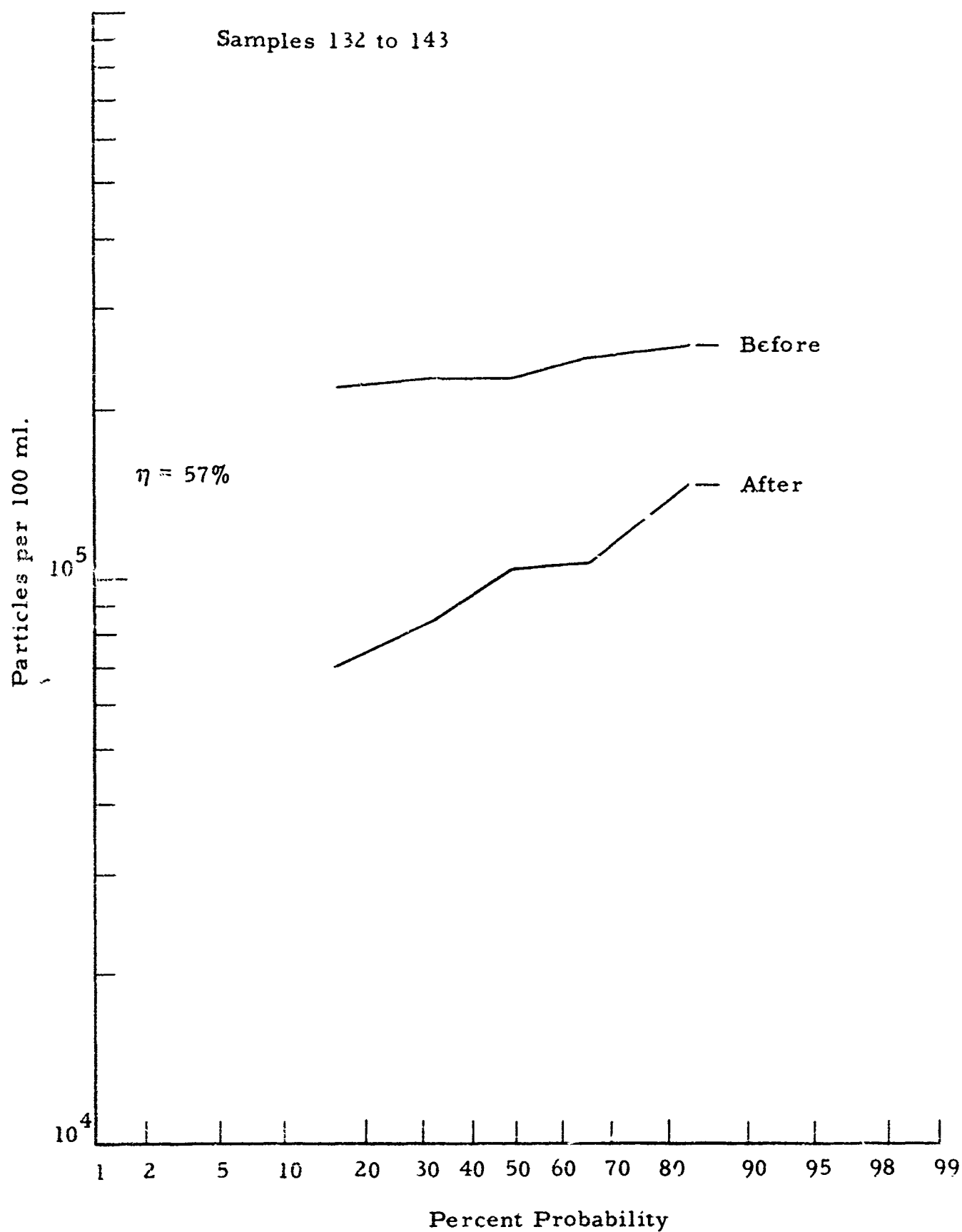
Figure 33. Particle Size Distribution Before and After Precipitation

Despite the difficulty of sampling the liquid for particles, data have been gathered on saturation using a precipitator with brass walls (See Figure 34). Particle concentration, flow rate and ionizer voltage were kept constant and it was made absolutely certain that the liquid passed through the filter the same number of times for each sample, to avoid any error due to liquid deterioration. Although only one sample at a time was taken and evaluated, there is a decrease in efficiency with time.

The first sample was taken after 4 seconds with an efficiency of 94 percent. After one minute, efficiency stayed below 50 percent. At saturation, a deposit density of 3×10^6 particles per cm^2 was determined from concentration of contamination, flow rate, deposit area and sampling time. This would equal a monolayer of particles assuming an average diameter of 5 microns. This is a realistic estimate. This test showed that for operational use of the electrostatic filter, about 10^9 particles can be filtered out before a cleaning process has to be applied. The average contamination of commercial CIE fuel we tested was 10^5 particles per gallon. With a flow rate of 50 gallons per minute, saturation would occur after 20 minutes.

Use of porous, non-conducting wall material to trap the deposited particles displayed no sign of saturation effect over any length of filtering time. Although efficiency was not very high initially, it improved with time as can be seen from Figure 35. This test was performed under the same conditions as the one shown in Figure 34. It was unfortunate that we could not follow this trend further but we could no longer maintain the condition of non-repeated use of CIE fuel.

However, we were able to perform a test where the same liquid was recirculated to determine the efficiency with several passes through the filter (See Figure 36). The same filter was used as for the test shown in Figure 35. The initial count was 6.25×10^7 particles per ml which decreased after 60 minutes to 8×10^4 particles per ml. The

Figure 34. Saturation Effect of a Solid Wall Material

The chart shows Particle Concentration (arbitrary scale) on the vertical axis and Filter Time (minutes) on the horizontal axis. A dashed line labeled "Concentration before Filter" is near the top. A curve of data points is labeled "Concentration after Filter."
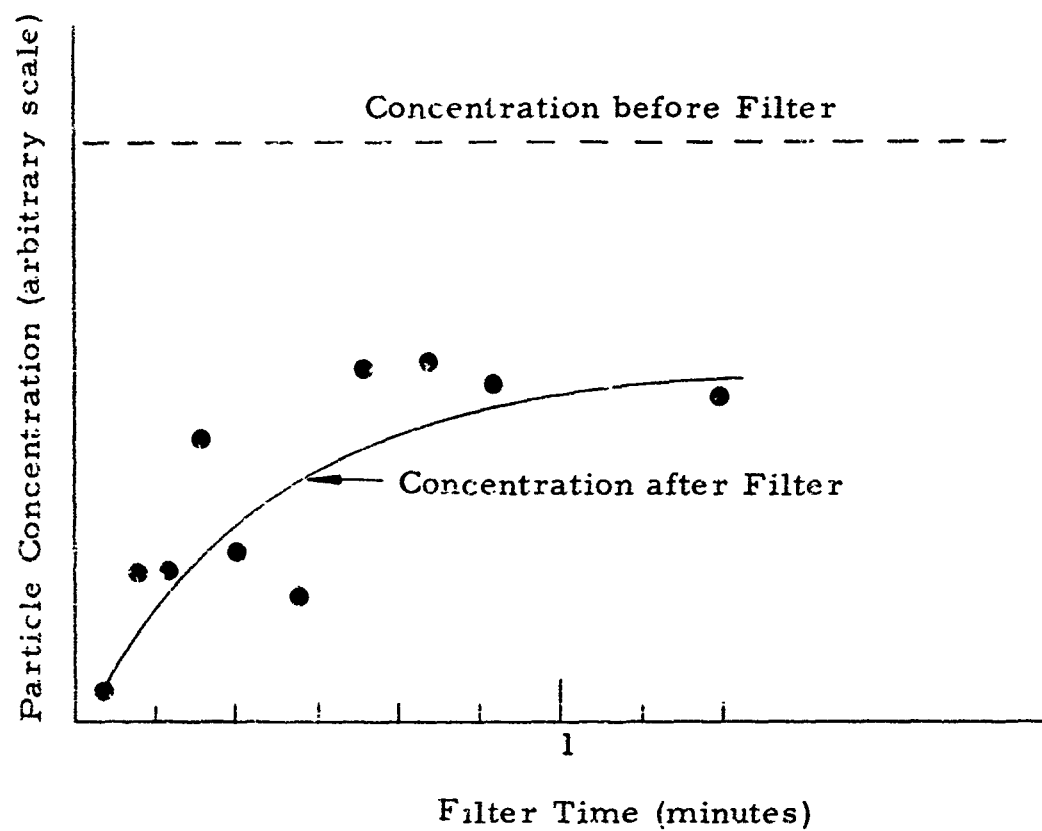
Flow Rate	- 30 ml/sec
Precipitator Length	- 18 cm
Precipitator Diameter	- 2.3 cm
Ionization Voltage	- 7.5 kv
Concentration of Contamination	- 7×10^5 particles per ml

Figure 35. Particle Retention Effect of a Porous Wall Material
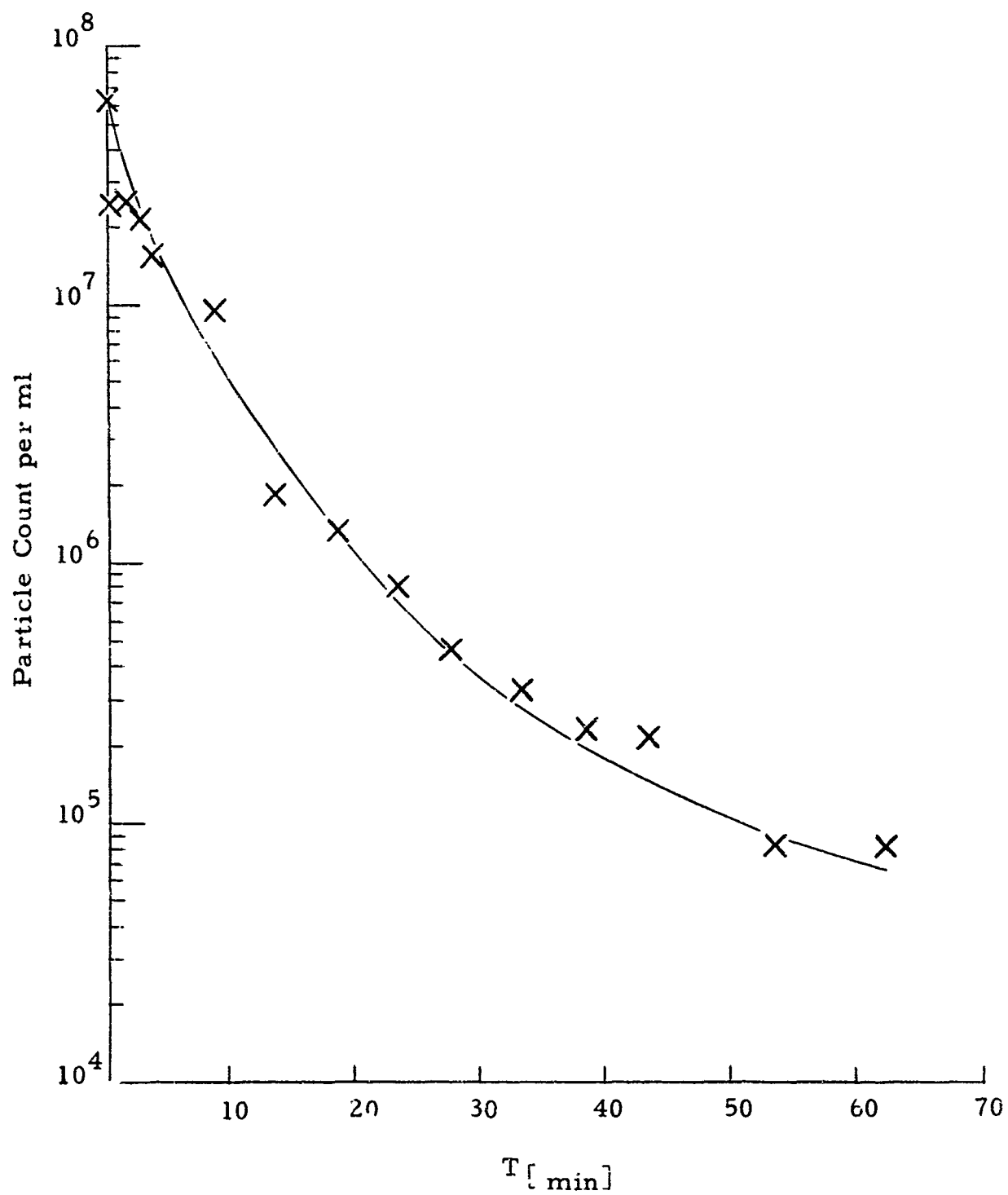
Figure 36. Decrease of Particle Count in a Recycling System

remaining concentration consisted only of particles of about 1 micron in diameter or about the cut-off size of the filter. The liquid made 23 passes through the filter. The efficiency of this filter cannot be derived easily from the data available, but was better than 65 percent in the beginning of the recycling process. Here, the influence of particle size on filter efficiency is very evident. A similar test is shown in Figure 37 in which all particles down to 0.8 micron were counted. It was observed that all particles above 3 microns were removed with the first or second pass through the filter.

4. Filter Efficiency

From the foregoing it can be seen that filter parameters in laboratory tests are influenced by a complexity of processes, each contributing to the standard deviation and the mean of the distribution of test results. To give an account on efficiency, with the exclusion of processes which are error terms, is difficult. For instance, in-homogeneity of the liquid produces a variance of readings taken at different locations on the filter and at different times and may make the measured efficiency appear higher or lower. Similar effects are to be expected by the process of sample analysis. Normally, for analysis, a small quantity of sample liquid is pumped through a Millipore filter. Such samples might already have some background count. Later, dust can collect on the filter material or filtered particles can be blown away from the surface.

Since a microscope is used to count the particles, inhomogeneities over the Millipore filter surface can also add errors. By counting through a microscope,a background count is possible through contamination of the scope. Usually a photograph is made and the slide analyzed later. Focusing of the picture will cause an error because not all particles will be equally in focus and the focus changes the apparent size of the particles. Finally, the count is performed by human eyes which are subject to errors and misinterpretations.
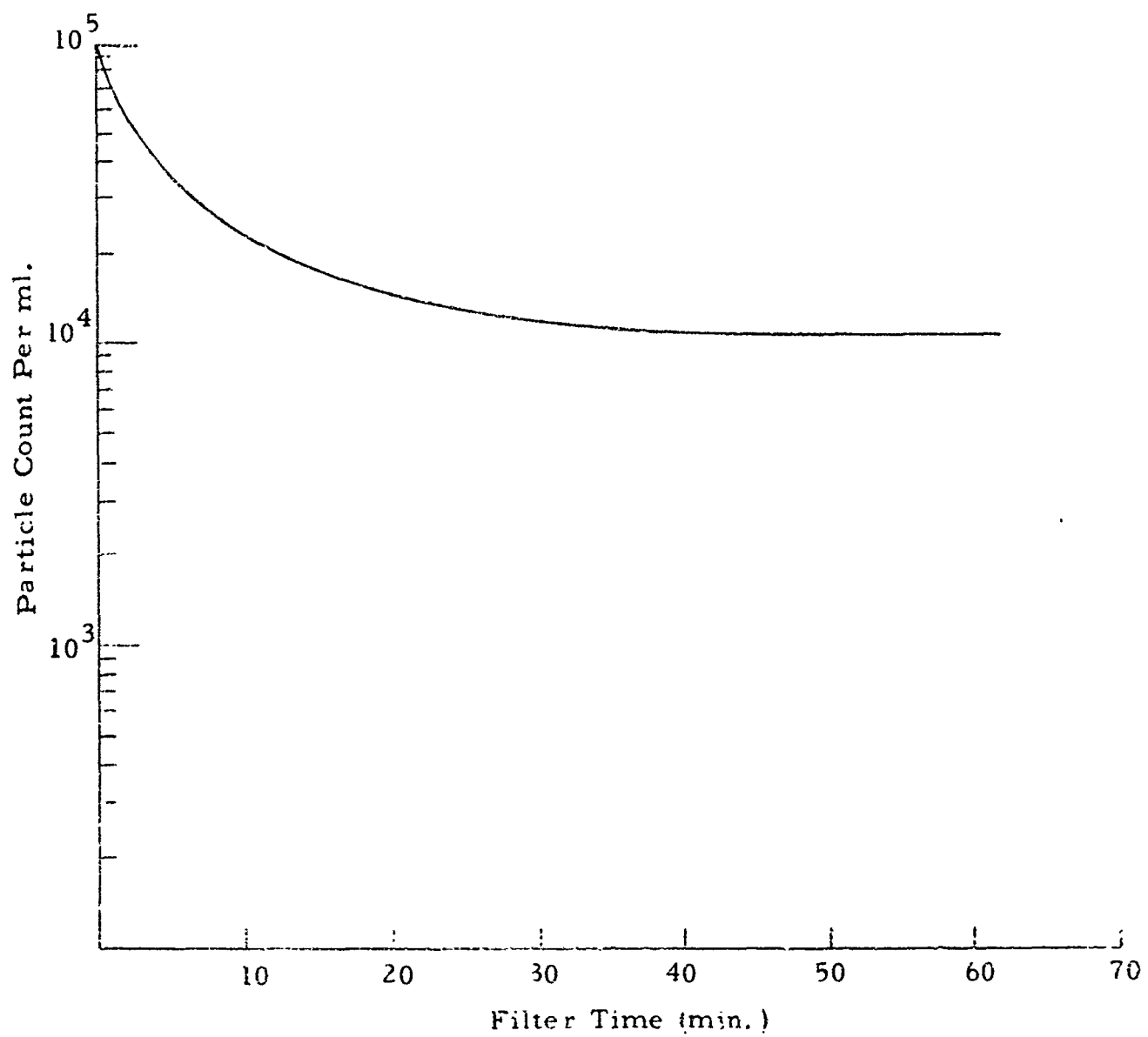
Figure 37. Count for Particles 0.8

83

Major difficulty is encountered where an estimate of the size has to be made by the observer and especially where two particles are close together. Figure 38 displays photographs of sample slides with a magnification of 1000 (1 cm = 10 microns). Figure 38(a) shows the background noise of the microscope; Figure 38(b) shows a sample taken before the filter while Figure 38(c) is an example of a probe after the liquid has passed the electrostatic filter. For analysis all particles from Figure 38(a) have to be subtracted from Figures 38(b) and 38(c). A decision then is made on the lowest size limit and as to which dots are particles. As can be seen, several dots do not have a sharp contrast and it is questionable whether they are really particles. To get reliable data on efficiency, this complete process of evaluation has to be repeated several times. From Figures 38(b) and 38(c) we deduced an efficiency of 95 percent. It is not difficult, however, to ascribe 99 percent efficiency or 50 percent number efficiency depending on the evaluator.

Up to this point. we have determined filter efficiency by use of particle numbers rather than mass or deposit a ea. Size distribution has not yet been considered. As deduced in quarterly reports the efficiency is dependent on particle size. From Equation (25) and Equation (32) we deduce that the size dependence of efficiency η (a) is given by,

$$\eta\ (a) = 1 - e^{-Aa} \tag{71}$$

with a being the particle diameter and A being a suitable constant. If we assume. for instance. a 63 percent efficiency for particles of 1 micron size, we obtain the relation of Figure 39.

In order to estimate the influence of particle size on total efficiency, we have to assume a size distribution of particles. One possible distribution can be deduced from the process of generation of particulates in fuel, namely, through grinding and break-off of larger particles.
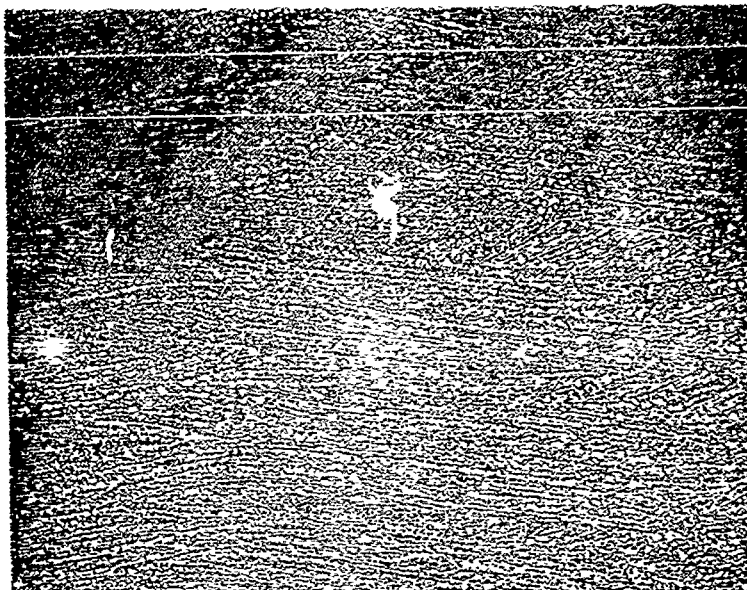
(a)
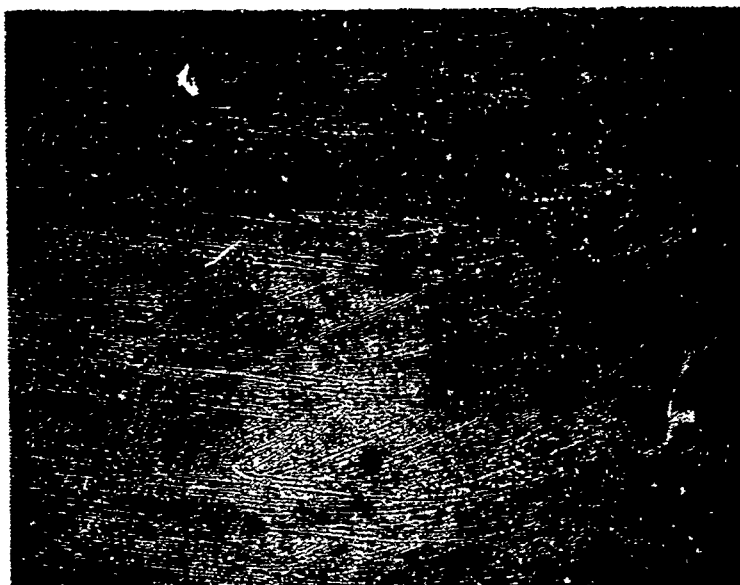
(b)
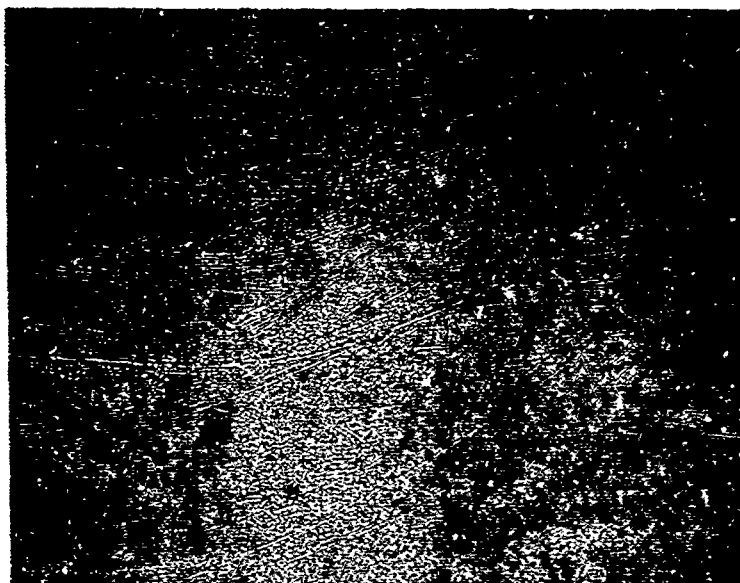
(c)

Figure 38. Photomicrographs of Fuel Samples
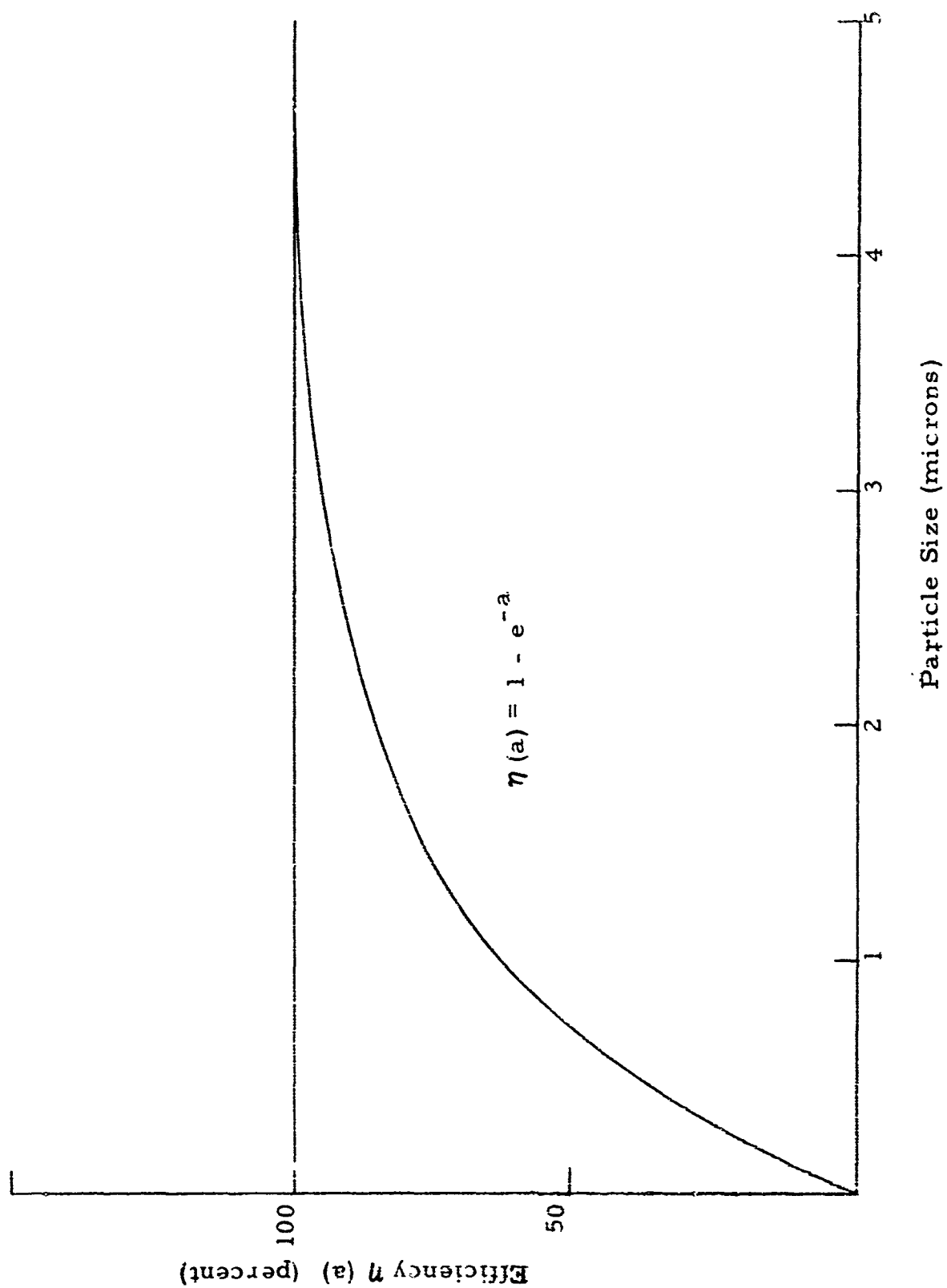
Figure 39. Dependency of Collection Efficiency on Particle Size

$\eta (a) = 1 - e^{-a}$

Particle Size (microns)

Efficiency η (a) (percent)

This would lead to a distribution where the number concentration decreases with the third power of the diameter. During the first stage of the program, we determined size distribution before and after the filter but for the moment let us discuss the influence of an analytically simple distribution of the efficiency. Let the total number N_1 of particles before the filter above size x be given by:

$$N_1 = N_o \int_x^\infty e^{-Ba} \, da. \tag{72}$$

After passing the filter, the total number of particles N_2 is:

$$N_2 = N_o \int_x^\infty (1 - \eta(a)) \, e^{-Ba} \, da, \tag{73}$$

which leads to

$$N_2 = N_o \int_x^\infty e^{-Aa} \cdot e^{-Ba} \, da \tag{74}$$

By defining a total efficiency η due to number concentration as determined by experiments, we have

$$\eta = 1 - \frac{N_2}{N_1}. \tag{75}$$

Combining (72) and (74), we get a total efficiency of

$$\eta = 1 - \frac{B}{(A + B)} \, e^{-Ax}. \tag{76}$$

It is evident from Equation (76) that for a decrease of particle concentration with increasing size, the total efficiency is given mainly by the filter efficiency at the smallest particle size x counted. Such a size distribution has been observed on all of our samples. The above conclusion is valid in general, even though the assumption of a size distribution was quite arbitrary.

To convert a given number efficiency into an efficiency of mass of material filtered out, we will assume the same number distribution as in Equation (72). The mass distribution of N_1 is given by

$$N_1 = N_0 \int_x^\infty a^3 e^{-Ba} \, da, \qquad (77)$$

with a distribution after the filter of

$$N_2 = N_0 \int_x^\infty a^3 e^{-(A+B)a} \, da. \qquad (78)$$

This will yield a mass efficiency of

$$\eta = 1 - e^{-Ax} \cdot f(A_j B_j x). \qquad (79)$$

$$f(A_j B_j x) = \frac{B}{A+B}^4 \cdot \frac{6 + (A+B)x + 3(A+B)^2 x^2 + (A+B)^3 x^3}{6 + Bx + 3B^2 x^2 + B^3 x^3} \qquad (80)$$

Here also the total efficiency, under certain conditions, is mainly determined by the efficiency at the smallest particle size considered. The mass efficiency η_m and the number efficiency η_n, under the assumption that A is equal to 2B, is shown in Figure 40. For A, the same value is assumed as in Figure 37.

It can be seen that the efficiency is much higher if masses are considered. We estimated earlier that the number efficiency obtained by experiments is better than 70 percent. This is equal to a mass efficiency of better than 99 percent.

Figure 40. Dependency of Collection Efficiency on Particle Mass

VIII. DEPENDENCE OF FILTER EFFICIENCY ON PARTICLE SIZE

As outlined in the previous section, an increase in efficiency can be expected for larger particles. Efficiency also can be defined in terms of mass rather than number. To express one in terms of the other, it is essential to know the size distribution of the contamination and the size dependence of the filter. We made several tests using a 1/2-gpm EHD filter and analyzed samples taken before and after the filter using Millipore filters of different pore sizes. The results are plotted in Figure 41. These tests indicate that filter efficiency increases with particle size to 3 microns (See Figure 42). Since no particles larger than 3 microns were present, it is not known what the efficiency would be with larger particles. However, from analytical considerations an increasing trend is expected. Similar tests conducted without our 10-gpm filter (results are plotted in Figures 43 and 44) show the same increase in efficiency with particle size.

Tests were made to determine the size distribution of natural background contaminants in CIE fuel. Samples were taken from fuel which had been stored in a 55-gallon steel tank for at least several months. The fuel was stirred vigorously before a sample was taken and was then filtered through a Millipore filter. Photomicrographs were made and all particles above a certain size limit counted (See Figure 45). Differentiation of the curve of Figure 45 gives the size distribution of the natural background material (Figure 46). As expected, there is a sharp decrease of count with increasing size. The number of particles decreases with the square of the diameter. This indicates that most of the mass of material is in the form of larger particles although the number of small particles is very much higher than the number of large particles.
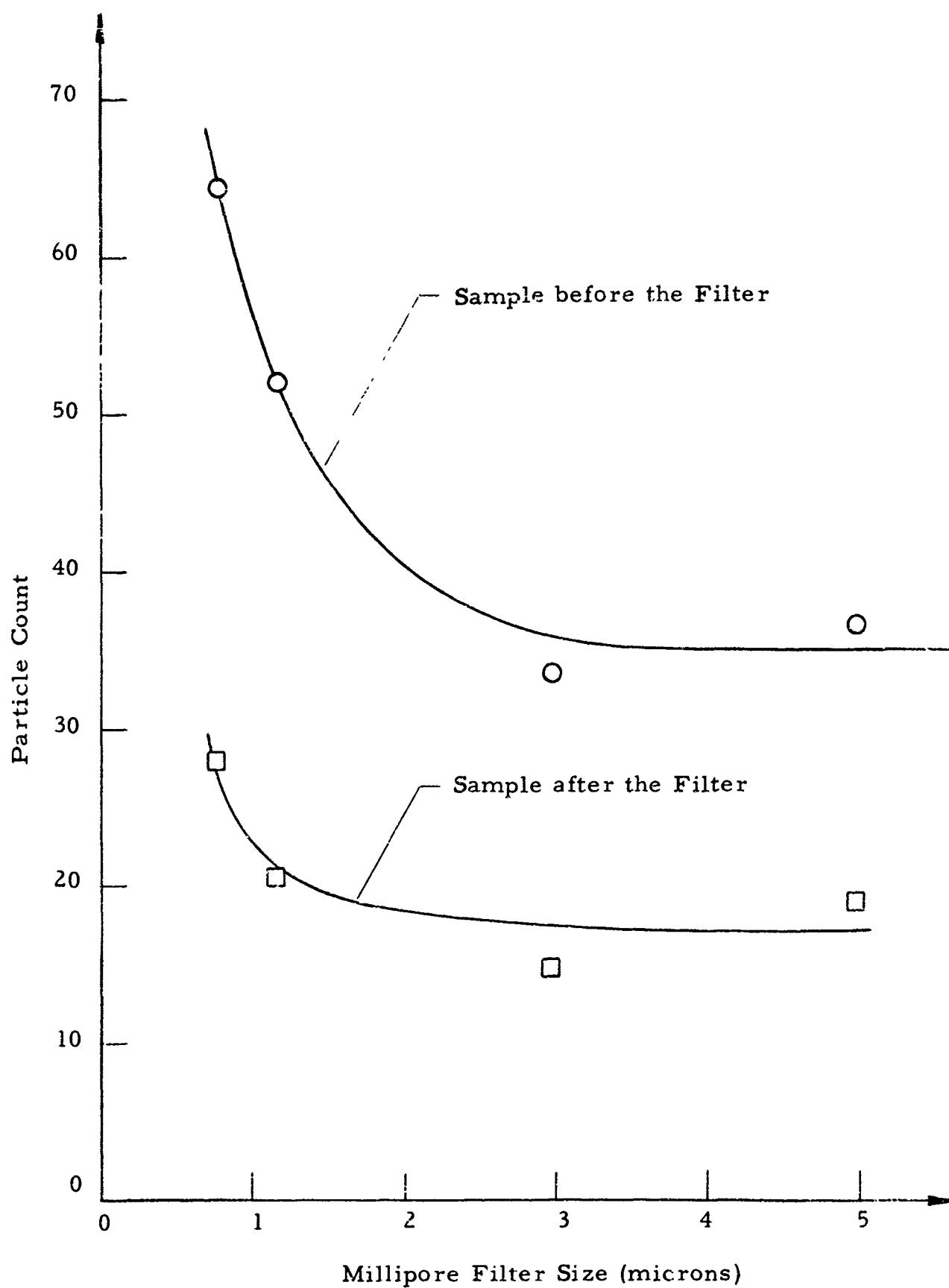
Figure 41. Particle Count vs. Millipore Filter Size (1/2-gpm EHD Filter)

- 91 -
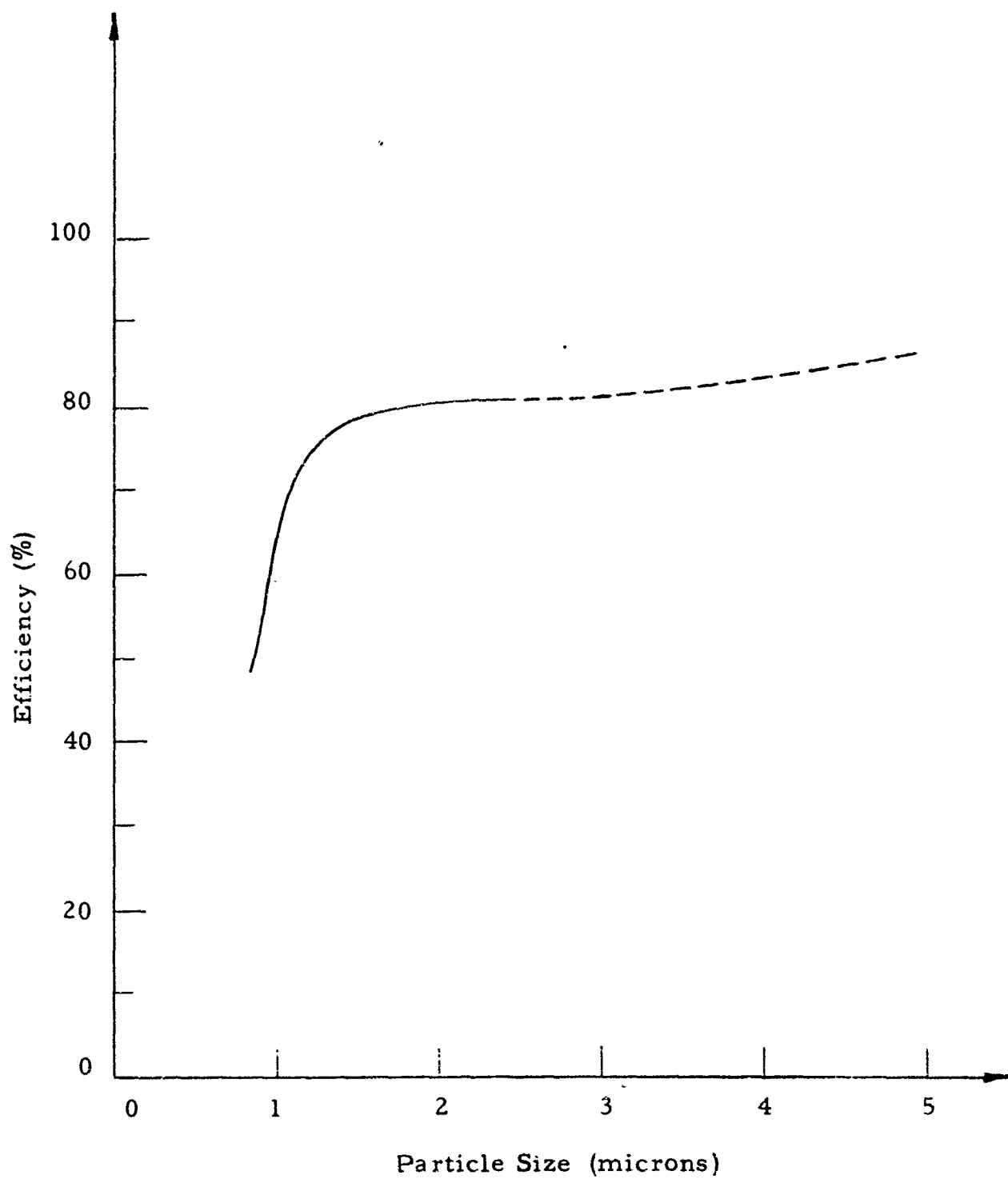
Figure 42. Efficiency vs. Particle Size (1/2-gpm EHD Filter)
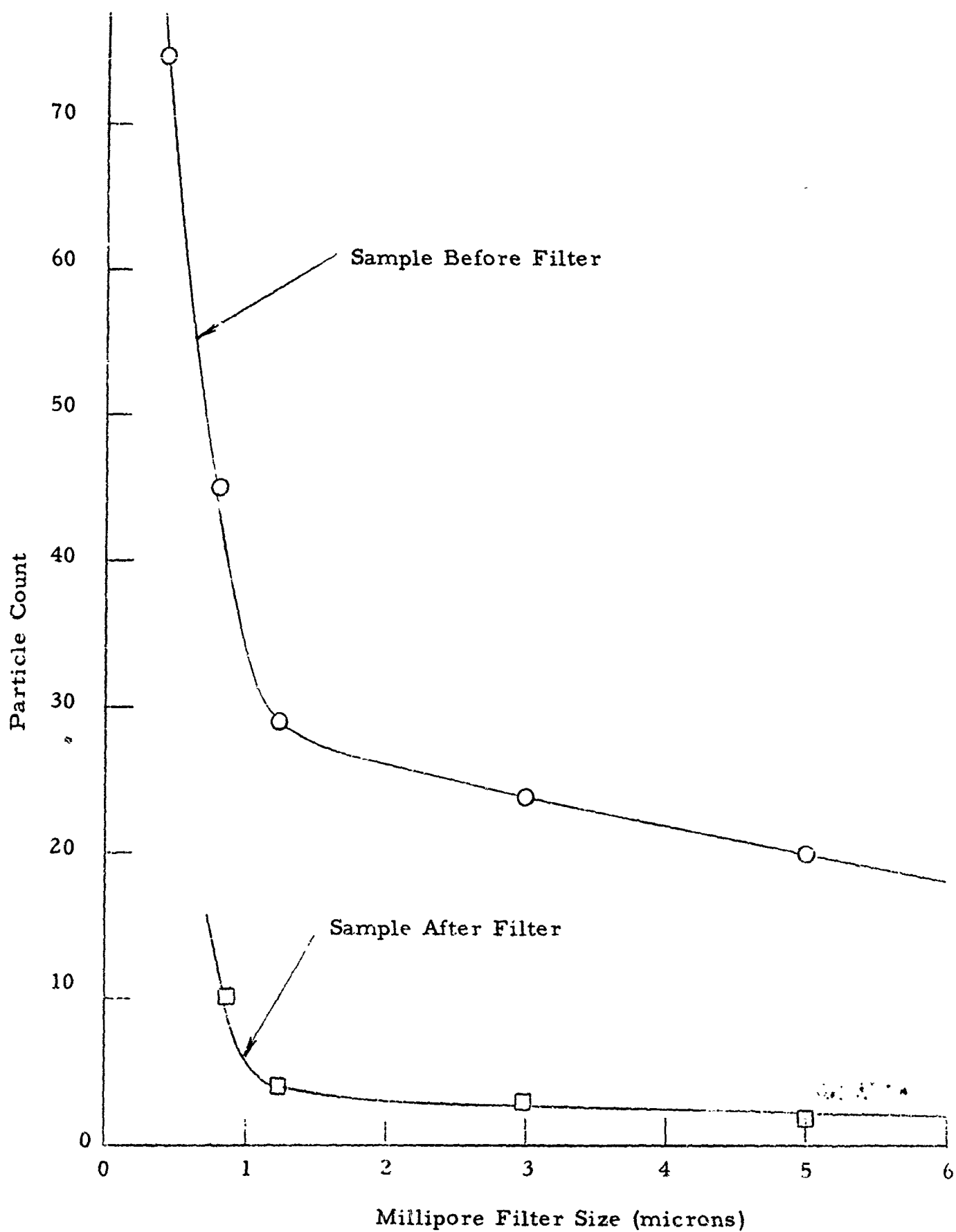
Figure 43. Particle Count vs. Millipore Filter Size (10-gpm EHD Filter)
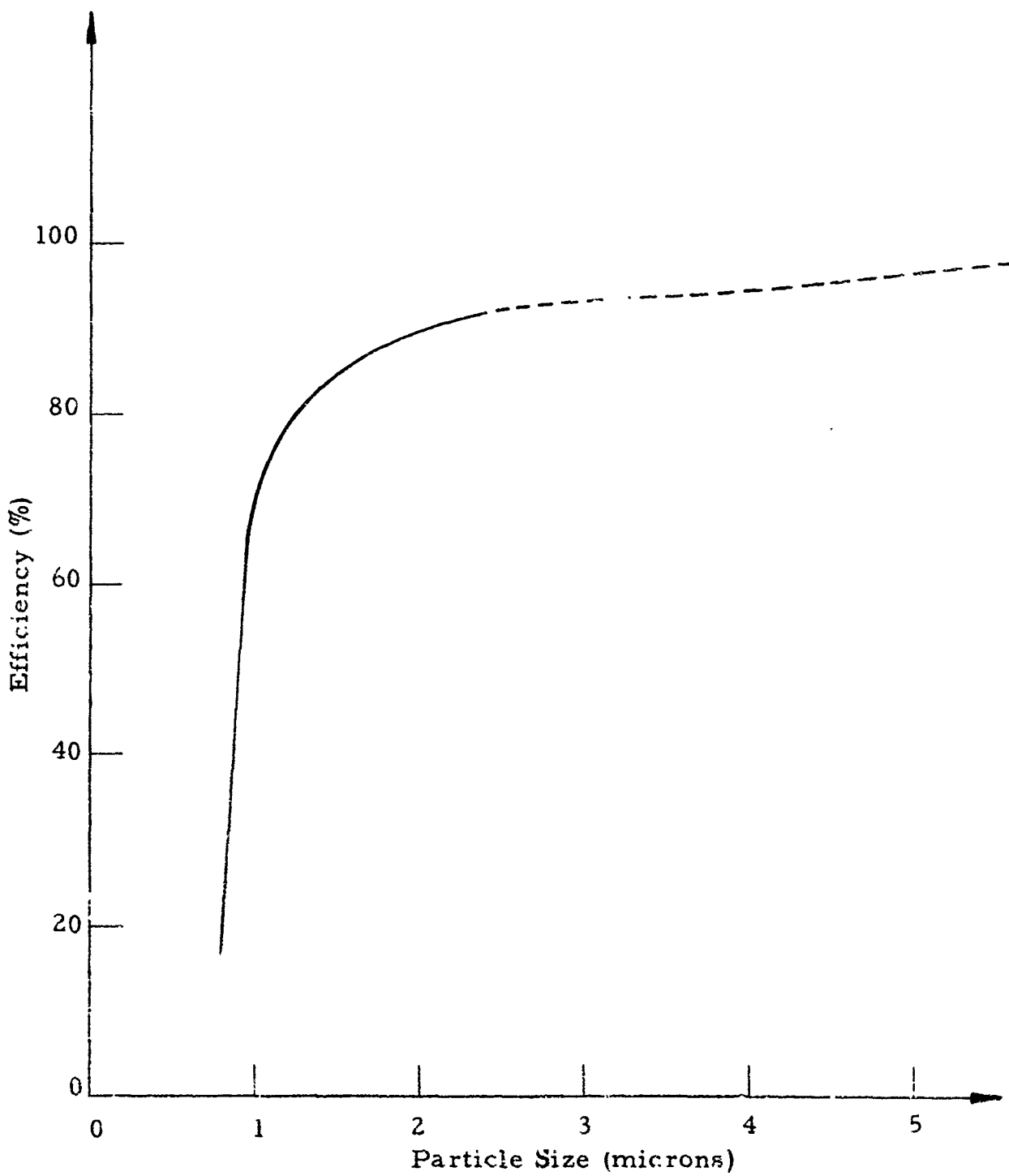
Figure 44   Efficiency vs. Particle Size (10-gpm EHD Filter)
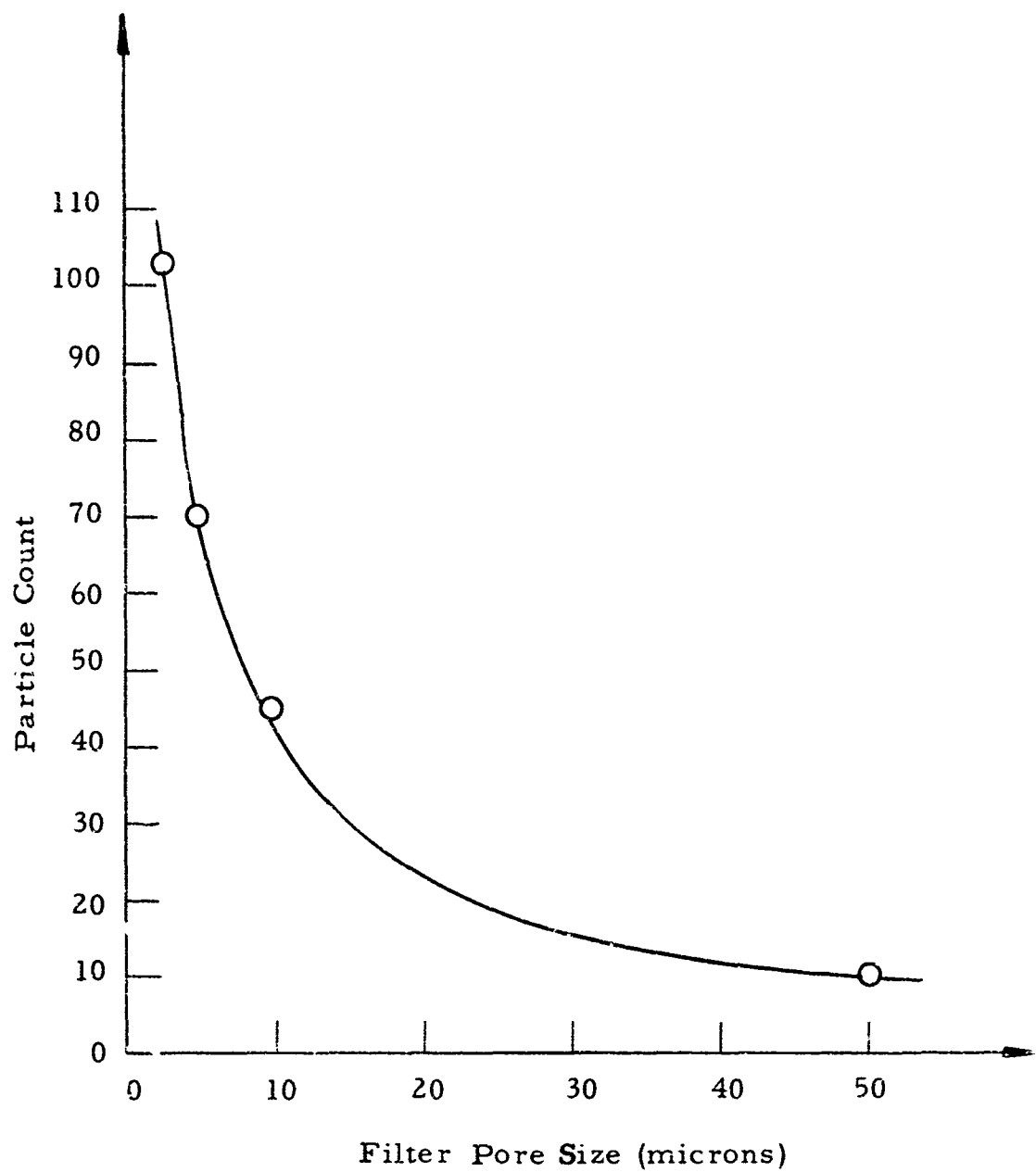
Figure 45.   Particle Count vs. Filter Pore Size
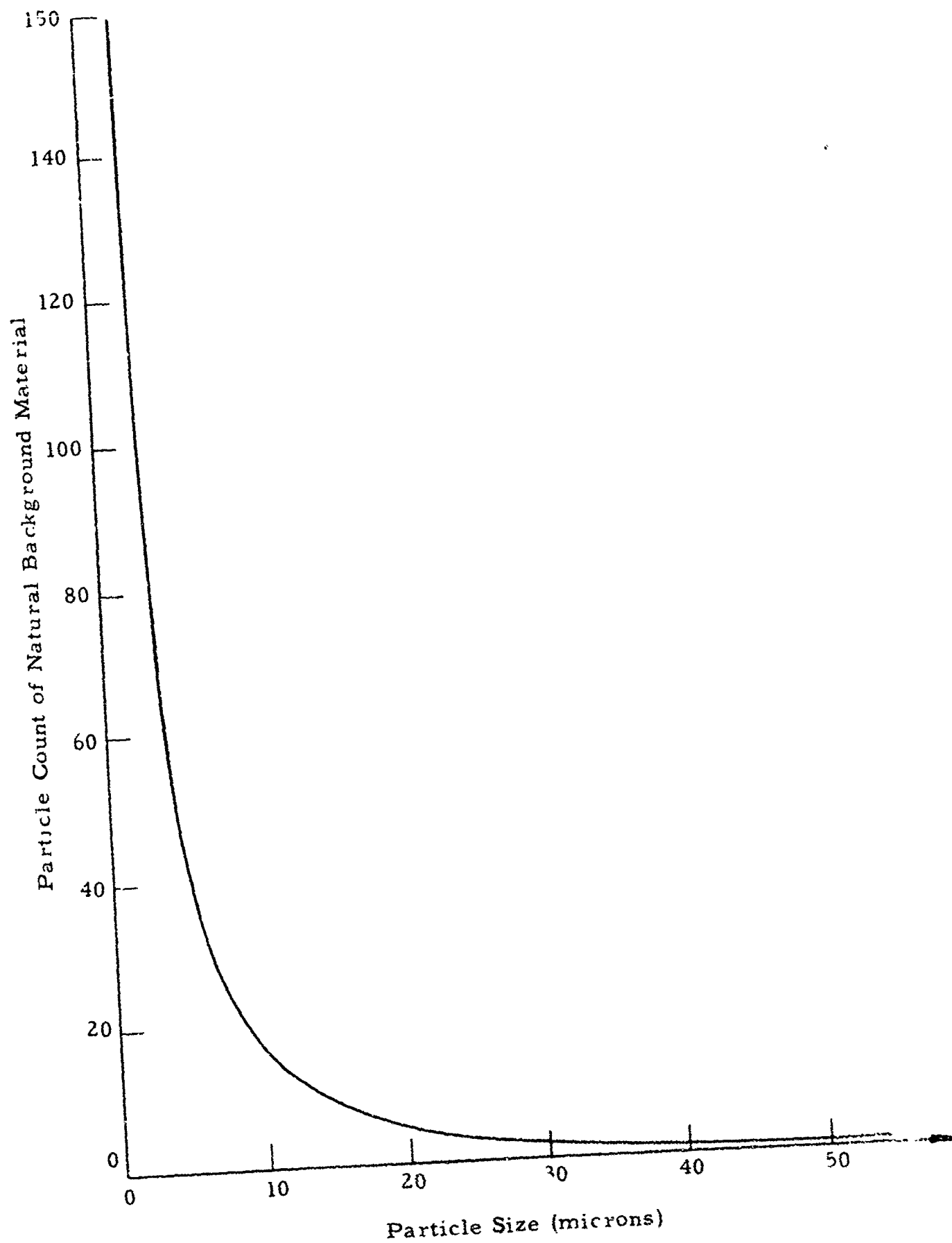
Figure 46.   Size Distribution of Natural Background
Contaminants in CIE Fuel

IX. DEVELOPMENT OF A PROTOTYPE FILTER

Efforts to improve the ionization and precipitation effect of the precipitator with a non-conducting, porous wall material as described above led to the design of two precipitators. No better wall material could be found, and at the present time it is considered to be an excellent solution to the difficult problem of trapping the particles out of the charged stream. All experiments were conducted using CIE fuel and artificial contamination by ferric oxide. Our preliminary studies of the behavior of the porous wall material were conducted primarily on a 1/2-gpm filter setup. This device was part glass to enable the experimenter to observe the precipitation effect which can be seen as a change from a turbid stream to a clean stream. Many tests were performed and numerous samples were evaluated by microscopic means. The experience and data gained in this work proved to be most useful in setting up a 10-gpm filter in a test stand.

A. Construction of the 10-gpm Filter

The ionizer used for the 10-gpm setup is designed with a total length of the corona edge of 78 mm, divided into 4 parallel emitters of equal length. The voltage applied across the ionizer is 6 kV dc positive and the current drawn reaches a maximum of 30 μ A.

The velocity of the stream at 10 gpm through the rectangular openings opposite the emitters is 10.8 m/sec. A velocity of 12 m/sec is considered a safe, cavitation-free maximum for this type of fluid and application. The flow rate of 10 gpm through the precipitator tube (1-1/2-inch I.D.) yields a stream velocity of up to 80 cm/sec.

Of interest is the pressure drop across the ionizer-precipitator assembly. The manometer indicated $\Delta p = 8$ psi at 10 gpm. About 95 percent of this pressure drop appears across the rectangular openings opposite the emitters. The dimensions of these lots are of major importance for the correct ionization and cannot be changed in order to accomplish a decrease in Δp. A pump delivering 40 watts of power will be necessary to pump the fuel at 10 gpm through the filter. The operation of this filter could not be observed since glass parts were not used; the setup was intended to be a useful prototype model. Efficiency was determined by taking samples before and after the filter and analyzing these samples by using micropore filters of different pore sizes and counting the total number of particulates. From Figure 43 the number efficiency can be calculated. An average of 85 percent can be deduced from the tests for particles larger than 1 micron. This is an improvement over the 1/2-gpm filter for which, from Figure 41, efficiency of 60 percent can be derived.

Since our test stand is only able to deliver 10 gpm, we are not able to test for higher flow rates. However, we can take our results in the range of 0.1 to 10 gpm and extrapolate to 100 gpm. In the ionizer section, maximum velocities are determined by cavitation. This means that the ionizer cross sectional area is increasing in proportion to flow rate. The same cross sectional area increase is necessary to maintain a constant ion density. Precipitator tube length and diameter are determined by flow rate and an established fixed time that the liquid stays in the precipitator; about 0.5 seconds. Ionizing potential will be unchanged in models of higher flow rate.

B.   Construction and Operation of the 50-gpm Filter

Using all experience gained during the program we have devised what we believe to be a relatively simple and reliable design (See Figure 47) of a 50-gpm filter.
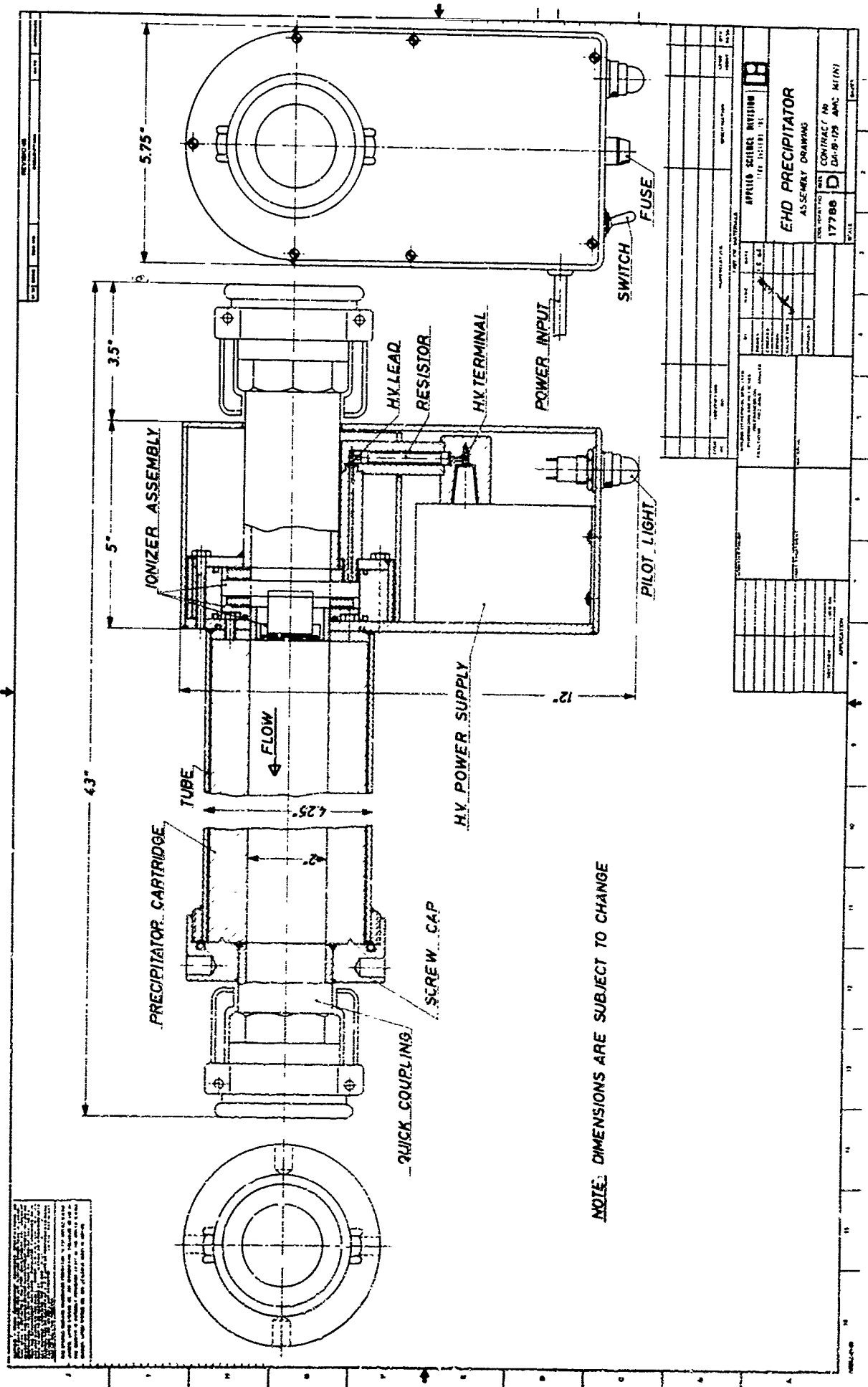
Figure 47. 50-gpm EHD Filter

It should be pointed out that this prototype filter is a relatively compact and completely enclosed unit involving no mechanically moving parts to wear out. The filter is constructed mainly of aluminum with only a few parts of the ionizer assembly being made of brass and stainless steel because of some delicate solder work involved. Some parts used in the high voltage hook-up and ionizer are made of Delrin, an excellent insulating plastic material. Where no disassembly is required, parts are welded or soldered, otherwise, screws are used in the assembly. Where seals are necessary, O-rings of an oil-resistant material are used.

The precipitator has 2-inch Evertite Standard Quick Couplings for connection to the pipeline. For filtration, the direction of flow must always be from the power-supply housing to the screw-cap end. The precipitator is designed for pressures not to exceed 100 psi. The pressure drop across the precipitator is less than 10 psi, therefore, no high-pressure pump is required. If regulation of the flow rate at 50 gpm of a high-pressure setup is anticipated, a valve should be installed upstream of the precipitator--that is, after the pump. It is desirable to provide a fuel line circuit which would make circulating of the fuel back into the tank possible. This would aid in the removal of trapped air from the precipitator before the ionizer is energized. The precipitator can be placed in any convenient position; however, the removal of air bubbles or trapped air is accelerated when the precipitator is installed vertically, with the power supply housing below.

The precipitator is designed for a nominal flow rate of 50 gpm. Since the action of precipitation depends on flow rate, therefore the upper and lower limit should be held between 60 and 30 gpm.

A strainer should be placed in the fuel line upstream of the precipitator to retain particles >300 μ. Such large particles tend to cause damage to the emitter by electrical shorting. In time, this can lower the performance of the precipitator.

The fuel flows through the ionizer where it is subjected to a high electrical field, thus receiving the charge necessary for proper precipitation. In the precipitator cartridge, which is right behind the ionizer, the contaminating particles in the fuel precipitate to the wall and penetrate into the porous material where they remain. The region of precipitation depends largely on the size of the individual particles and flow rate. The filtered fuel then leaves the precipitator.

The flow of 50 gpm requires an ionizer with total emitter lengths of 392 mm. Therefore, 14 individual emitters of 28 mm each are necessary. They are mounted opposite a plate having 14 rectangular openings of about 0.75 mm width and 28 mm length. The potential across the emitters and plate should be kept within the limits of about 5.5 kV to about 7.5 kV positive. The voltage will be supplied by a small 8 kV power pack. The high voltage lead from the power supply is heavily insulated and incorporates a 8-megohm resistor. This resistor serves two purposes: 1) it limits the current and protects the emitters in case of internal shorting and 2) lowers the voltage to provide the proper amount for ionization. The power input to the power supply is about 10 watts, 117 volts ac. The precipitator assembly is equipped with a 6-ft cable and a standard grounded 3-prong plug. The power supply is turned on and off by a toggle switch. The circuit also incorporates a 1/4-amp fuse.

In the statement of work the requirement was established for a filter with self-indicating features in case of an incorrect operation.

The electrical circuit of the precipitator (See Figure 48) incorporates two neon pilot lights (NE 51 H). The red light, connected across the 117-V ac input of the power supply, indicates whether or not the power supply is energized. The amber light gives a reliable indication of the electrical conditions at the ionizer in the following manner:

Connected in parallel to this second pilot light is a capacitor of .5 mFd. With a certain voltage applied to the ionizer, the capacitor will draw a small current over R_2 until it charges up to the firing voltage of
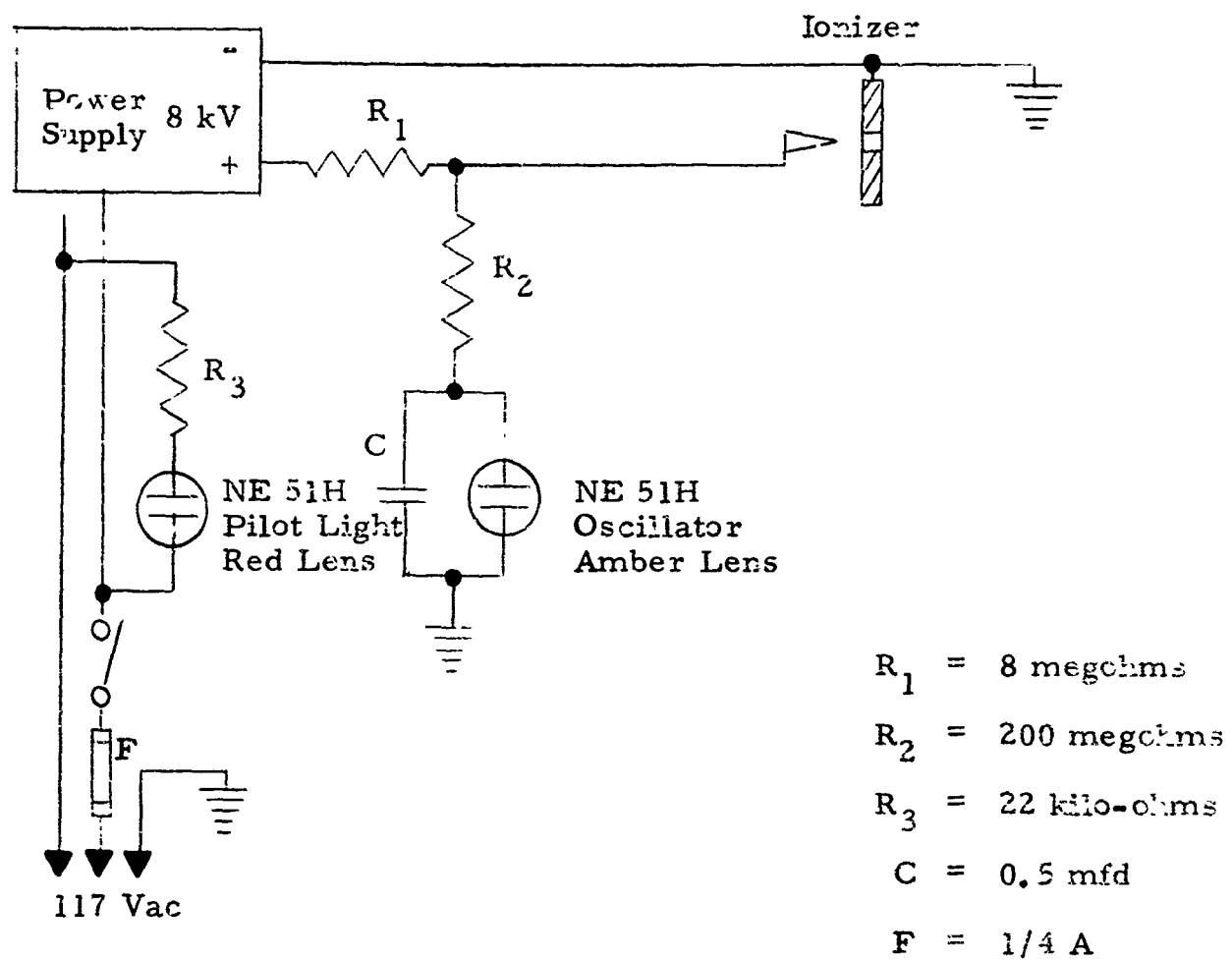
Figure 48. Circuit of the 50 gpm Precipitator

R_1 = 8 megohms

R_2 = 200 megohms

R_3 = 22 kilo-ohms

C = 0.5 mfd

F = 1/4 A

the neon bulb. The bulb then will discharge the capacitor and give a short flash. Now the capacitor will charge up again and the oscillation will be repeated. This circuit itself represents a low-frequency oscillator.

If for any reason the ionizer does not ionize the fuel, the ionizer will draw very little current and the voltage drop across R_1 becomes small. The rising voltage at the ionizer will increase the current across R_2 and results in an increase of the oscillator frequency. As an extreme, the bulb could stay on. If the ionizer is shorted out, say by water or a very large particle, the current across R_1 increases and causes a high drop. This in turn prohibits the capacitor from charging up and the oscillation stops.

While operating the EHD precipitator, the frequency limits of the flasher should be between about 75 and 105 flashes per minute. The frequency should be checked periodically.

When the frequency leaves the above limits, the flow should be stopped and the power to the unit cut off. A calibration curve has been supplied with the instruction manual.

After the power to the precipitator has been switched off, the flashing of the oscillator will continue for a short while. The oscillator bleeds the remaining charges from the capacitors within the high-voltage power supply. The precipitator cartridge is exchanged by removing the screw-cap. Holes for a face spanner wrench are provided. The pressure drop across the precipitator will not change with increasing contamination of the cartridge (as in conventional filters). Therefore, the pressure drop cannot be used as an indication of a clogged cartridge.

The cartridge used in our filter has the dimensions of 4-in. O. D., 2-in. I. D., and 32-in. length. This is quite a large volume and capable of retaining a large amount of particles. However, the lifetime for dependable service cannot be predicted because f the unknown concentration

of contaminants in the liquid. The cartridges required for the EHD precipitator are not commercially available; they were manufactured by the contractor for this project. Several extra cartridges have been delivered with the precipitator.

C. Safety

The safe and correct operation of the EHD precipitator depends to some extent on the operator. We have taken special care to ensure safe operation of the filter. Its unusual construction makes it mandatory that we instruct the operators and point out the safety measures to be taken. An instruction manual with reliable information and helpful suggestions has been delivered with the instrument.

No maintenance inside the housing is required. The high-voltage power supply and high-voltage carrying components are completely encased within the housing. Accidental touching is impossible. Pilot and indicator lightbulbs can be replaced only by removing the cover.

D. Maintenance

Other than periodic changing of the filter cartridge and checking the ionizer voltage, the precipitator (See Figure 49) requires no maintenance. The design involves no mechanically moving parts to wear out. Ionizer, power supply, and associated components are completely enclosed in a splashproof housing.

The precipitator described above has been designed on the basis of experimentation data and tests. Great care has been taken in machining and assembling parts. We have checked the precipitator and especially tested the ionizer to the degree possible before shipment. We were, however, not in the position to test the filter in a 50-gpm flowthrough because of our limited supply of fuel and equipment.
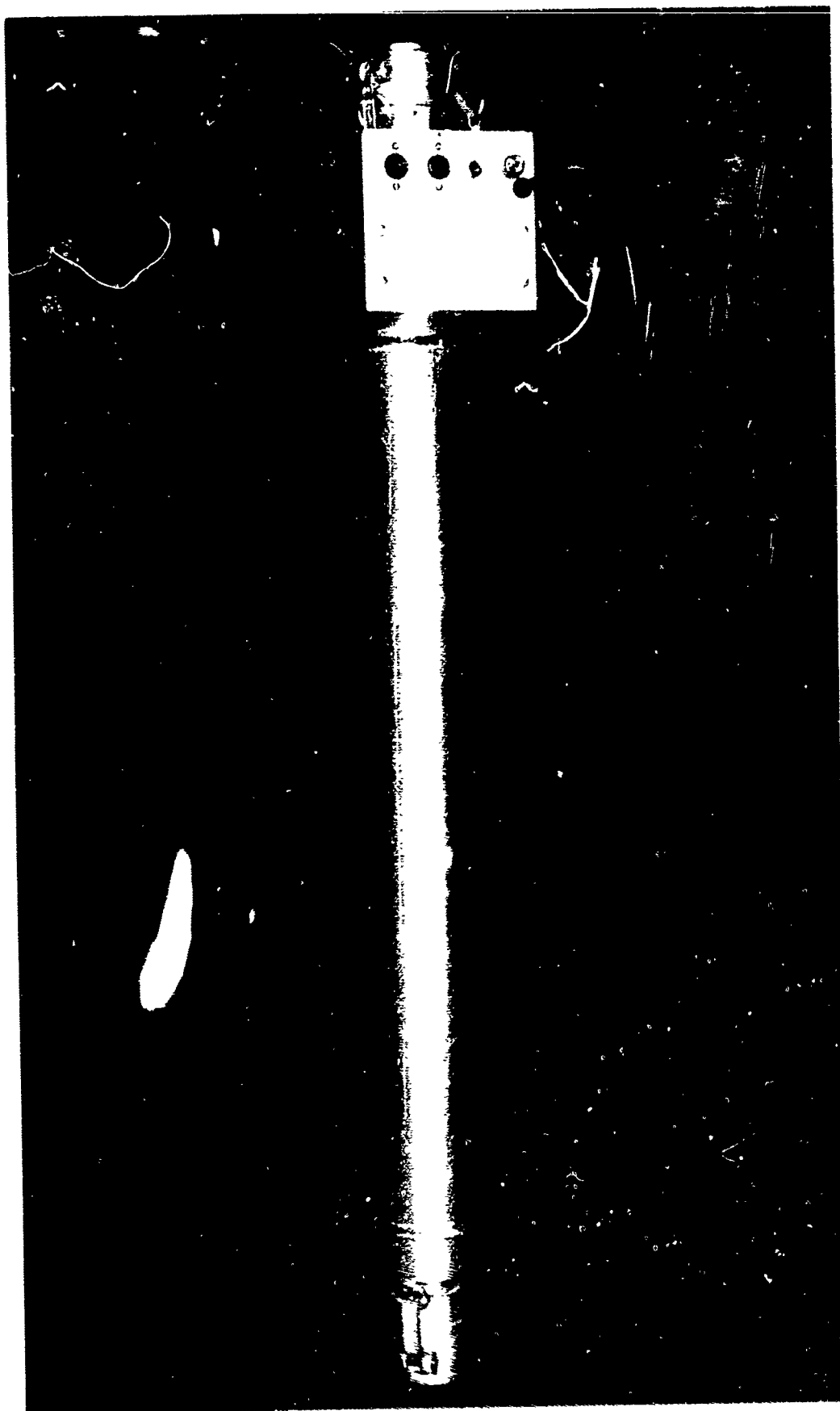
Figure 49. 50-gpm EHD Precipitator

X. TESTS OF THE EHD PRECIPITATOR USING MICROORGANISMS

The experimentation of this phase of the contract was designed to evaluate the microbiology of fuels associated with the EHD precipitator.

A. Experimental Design

Containers for storage of fuel were fabricated from a low carbon steel conforming to the American Petroleum Institute-Standard 12C. Twelve 9-in.^{2} tanks were constructed.

These storage tanks were divided in two groups. One group of six tanks was treated with a solution of 1×10^4 ppm peracetic acid followed by rinsing with sterile distilled water. All tanks were then rinsed with normal (as received) CIE fuel. Each tank of the two groups (treated and untreated with germicide) received 0.250 liter H_2O and 8 liters fuel. Two of the treated and untreated tanks received the following inoculation of organisms:

1) CIE fuel having the organisms and particulate removed by the EHD precipitator.

2) CIE fuel containing 200 bacteria and 200 fungi per liter.

3) CIE fuel containing 1×10^4 bacteria and 1×10^4 fungi per liter.

All tanks were stored at room temperature and sampled at 2-week intervals. The contents of one tank to each set were not altered after sampling (static test). In the dynamic test, the fuel sampled was replaced with the same microbial content per liter as indicated; i.e., if 500 ml fuel was withdrawn that originally contained 200 fungi and 200 bacteria per liter, 100 of each organism would be returned to the tank with the fresh replacement fuel. A schematic diagram of the test program is shown in Figure 50.

Tanks Soaked with Germicide

Tanks not Soaked with Germicide

Tanks under Static Conditions

Tanks under Dynamic Conditions

Tanks

(a) = Filtered Fuel
(b) = 200 Each Organism/Liter
(c) = 10^4 Each Organism/Liter
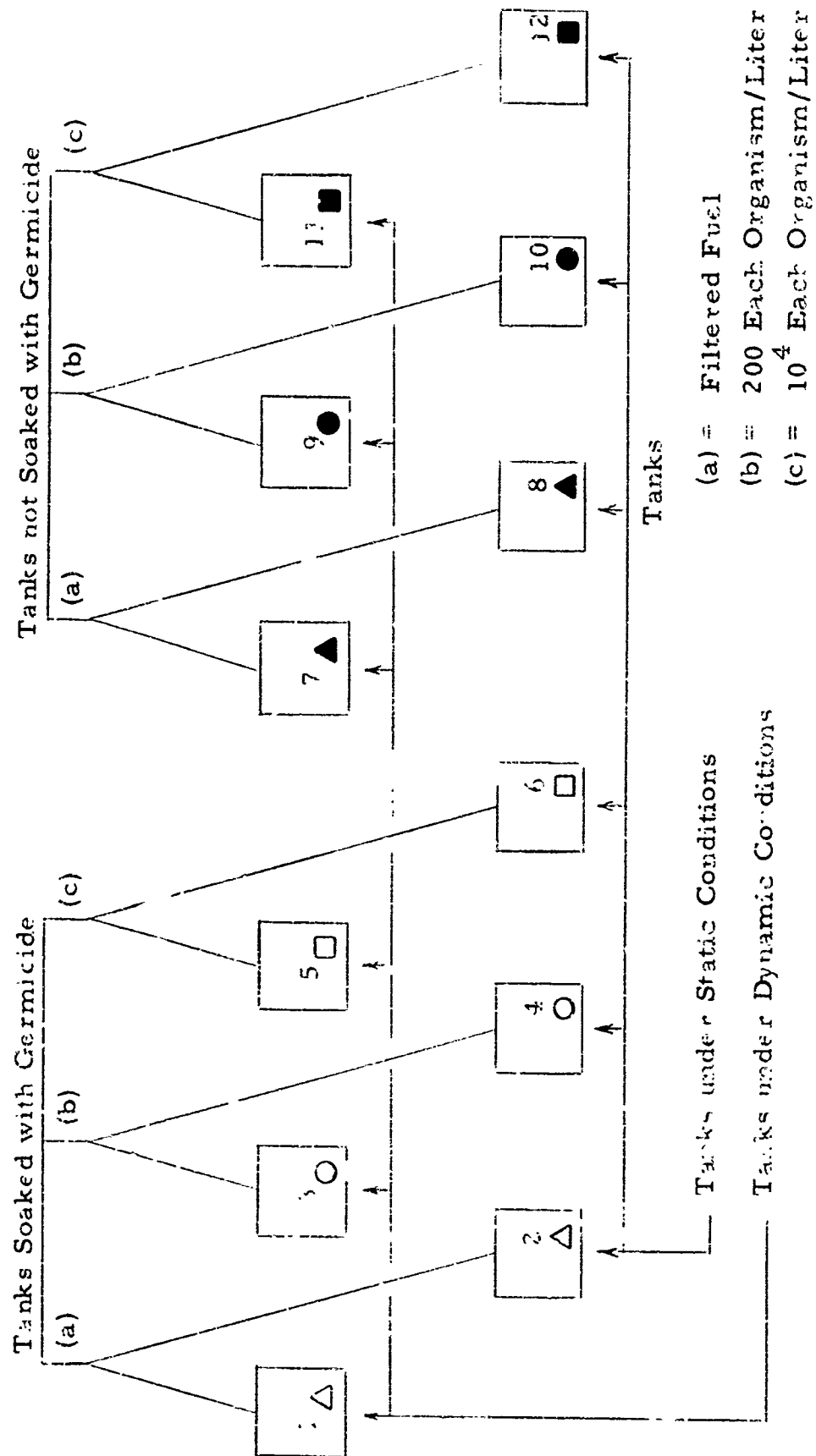
Figure 50. Test Program

B.   Sampling and Microbial Evaluations

The first sample was obtained at 0 time; immediately after adding the organisms to the tanks. Thereafter, samples were withdrawn at 2-week intervals for a period of 8 weeks.

1.   Preparation of Test Organisms for Inoculation

Pseudomonas aeruginosa was prepared by cultivation in Bushnell-Haas mineral salts medium with a CIE fuel overlay. After incubation at 30°C, aliquots were removed, diluted, and plated employing the pour plate technique to determine viable Ps. aeruginosa/ml.

Cladosporium resinae was also prepared in a Bushnell-Haas fuel medium with the incubation carried out at room temperature. The culture containing C. resinae spores was dispersed in a Waring blender, diluted, and surface plated on solid Sabourauds dextrose agar to determine number of viable units. After determination of viable units, calculation of appropriate dilution was made for inoculation into storage tanks.

2.   Sampling

Prior to withdrawal of a sample, the contents of the tank were stirred with a sterile probe. Approximately 700 ml of the fuel layer was siphoned into a flask. The water layer was withdrawn by insertion of a pipette to the tank bottom, exhausting the fuel-water phases and aspirating a sample. All receptacles, tubes, and pipettes employed were sterile. Replacement fuel and organisms were added as indicated by the experimental design.

3. Assay of Tank Contents

a. Fuel Phase

The microbial content of fuel was assessed by membrane filtration.[23] Duplicate samples of 1, 10, 100 and 200 ml CIE fuel were filtered. One sample of each volume was plated on tryptone glucose extract (TGE) and Sabourauds dextrose agar. Bacterial counts were obtained from the TGE and fungi were enumerated from the Sabourauds medium.

b. Water Phase

Two media were also used for water assay. Bacteria were enumerated employing standard dilution pour plate procedures with TGE agar. Numbers of fungi in the water phase were determined by spreading aliquots of dilutions over the surface of solid Sabourauds agar.

c. Turbidimetry

Due to the fact that turbidity of a nutrient fuel complex may be an indication of microbial growth or corrosion, these measurements were conducted on the fuel phase. Preliminary tests indicated no significant differences and was not further pursued. The water phase proved to be a better indication of amount of growth or corrosion. The test was conducted by diluting a 1-ml sample of the water phase with 5 ml distilled water and measuring the percent transmission at 505 millimicrons in a B&L colorimeter.

d. Hydrogen Ion Concentration

pH measurements were made on the water phase employing a Beckman Model 72 meter.

C. Results

1. Fuel Phase

The microbial flora recovered from fuel did not show a uniform
growth trend. Individual counts were subject to great variation from
one time interval to the next. However, certain definite relationships
between fuel treatment and microbial population were evident.

Table 4 shows the bacterial counts per 100 ml of fuel obtained at
the various sampling time intervals. The data are ranked at each time
interval by tank number from the highest to lowest microbial count
observed.

Table 4. Rank of Microbial Count in Fuel Sampled at
Various Time Intervals

Rank No.	2 Weeks		4 Weeks		6 Weeks		8 Weeks	
	Tank No.	Count/ 100 ml	Tank No.	Count/ 100 ml	Tank No.	Count/ 100 ml	Tank No.	Count/ 100 ml
1	8	1010	11	580	6	316	12	3780
2	4	500	10	400	12	199	3	2560
3	10	419	12	400	11	190	10	1990
4	2	350	4	400	9	164	11	1850
5	6	348	5	360	8	106	9	1580
6	1	336	9	210	7	103	6	1190
7	12	241	6	186	10	74	2	220
8	3	86	3	176	5	48	5	150
9	9	84	1	20	4	3	4	134
10	7	79	2	0	2	2	7	114
11	11	61	7	0	1	0	1	9
12	5	21	8	0	3	0	8	1

At the end of two weeks, there was no relationship whatsoever between the microorganism count and the fuel treatment. This phenomenon is probably caused by a prolonged lag phase in the establishment of a consistent type of flora in the fuel phase. By the fourth week the microorganism count showed a direct relationship to the fuel treatment; inoculated tanks showed the highest counts and filtered fuel uninoculated tanks the lowest counts. In general this persisted through the sixth and eighth weeks with the eighth week showing a marked increase in population of all tanks except 1, 7, and 8.

No significant differences were found in the bacterial counts of tanks under static conditions vs. dynamic conditions. Likewise, no significant difference was found at the end of 8 weeks between tanks treated with germicide and those not treated.

Cladosporium was not recovered in significant number during any of the sampling sequences. P. fluorescens was present in all inoculated samples. The absence of C. resinae may be due to the differences in growth rates of the two organisms. P. fluorescens has a more rapid rate of growth and may have overgrown the fungi. Differential media were employed to aid in obtaining separate quantitation but unfortunately the bacteria were capable of growing on both media.

Another explanation, and probably the most plausible, is the physical growth characteristics in a fluid medium. Psuedomonas will probably grow as a diffuse, turbid, rather uniform suspension. Cladosporium, however, grows as microcolonies or pellets in a fluid, and is held together by hyphal strands of the fungal thallus. The rate of dispersion of these colonies or pellets would possibly be absent or at best nonuniform, resulting in sporadic or entire lack of information. Because of lack of data on Cladosporium, microbiological results express total organisms recovered.

Turbidimetric assay of fuel was initiated at the second week of the experiment, but was discontinued after no significant variation in optical density was found. Membrane filters which contained particulate from fuel passed through the EHD precipitator had much lower concentrations than fuel not electronically filtered and inoculated with organisms. The membrane filter readily revealed these differences due to the large concentration factor but quantitation was not possible with simple turbidimetric techniques.

2. Water Phase

The original conception of the experimental design called only for sampling and analysis of the fuel at regular intervals. After the analysis at zero storage time, results were variable and it was decided to examine other parameters that may indirectly indicate the amount of biological activity in the fuel-water system.

Table 5 shows the microorganism count per ml of the water layer at the time intervals sampled. The counts are ranked from high to low and the tank number is indicated.

Unlike the fuel, analysis of the water phase reflected addition of the test P. fluorescens. Two weeks of storage resulted in a marked increase in all tanks inoculated, compared with maintenance of a low level ($\sim$100) in all uninoculated (filtered) tanks. The growth rate in the inoculated tank was great enough to negate the addition of fuel plus inoculum found in the dynamic test series. Comparison of tanks treated with the antimicrobial agent used showed no real differences except during the first few weeks of storage when the treated tanks contained slightly fewer inoculated organisms in the water phase. The microbial population changes under static and dynamic conditions are shown in Figures 51 and 52 respectively.

Table 5. Tank of Microbial Count in Water Layer
Sampled at Various Time Intervals

| Rank No.	2 Weeks Tank No.	Count/ml	4 Weeks Tank No.	Count/ml	6 Weeks Tank No.	Count/ml	8 Weeks Tank No.	Count/ml
1	12	5.44×10^6	12	1.7×10^6	11	4×10^6	12	$>10^7$
2	11	3.59×10^6	11	1.6×10^6	5	3.72×10^6	11	$>10^7$
3	9	1.97×10^6	3	9.6×10^5	9	2.48×10^6	9	$>10^7$
4	10	6.7×10^5	5	8.4×10^5	12	2.44×10^6	10	5.05×10^6
5	6	5.67×10^5	9	8.2×10^5	3	1.56×10^6	6	1.40×10^6
6	3	3.92×10^5	6	6.1×10^5	10	1.25×10^6	3	1.21×10^6
7	4	3.17×10^5	4	4.0×10^5	6	5.6×10^5	5	1.17×10^6
	5	2.53×10^5	10	3.5×10^5	4	4.5×10^5	1	1.15×10^6
9	2	210	2	<100	1	1.32×10^4	8	8.5×10^5
10	7	90	7	<100	7	7.9×10^3	4	7.9×10^5
11	1	<10	1	<100	8	600	7	5.4×10^4
12	8	<10	8	<100	2	<100	2	4.8×10^4
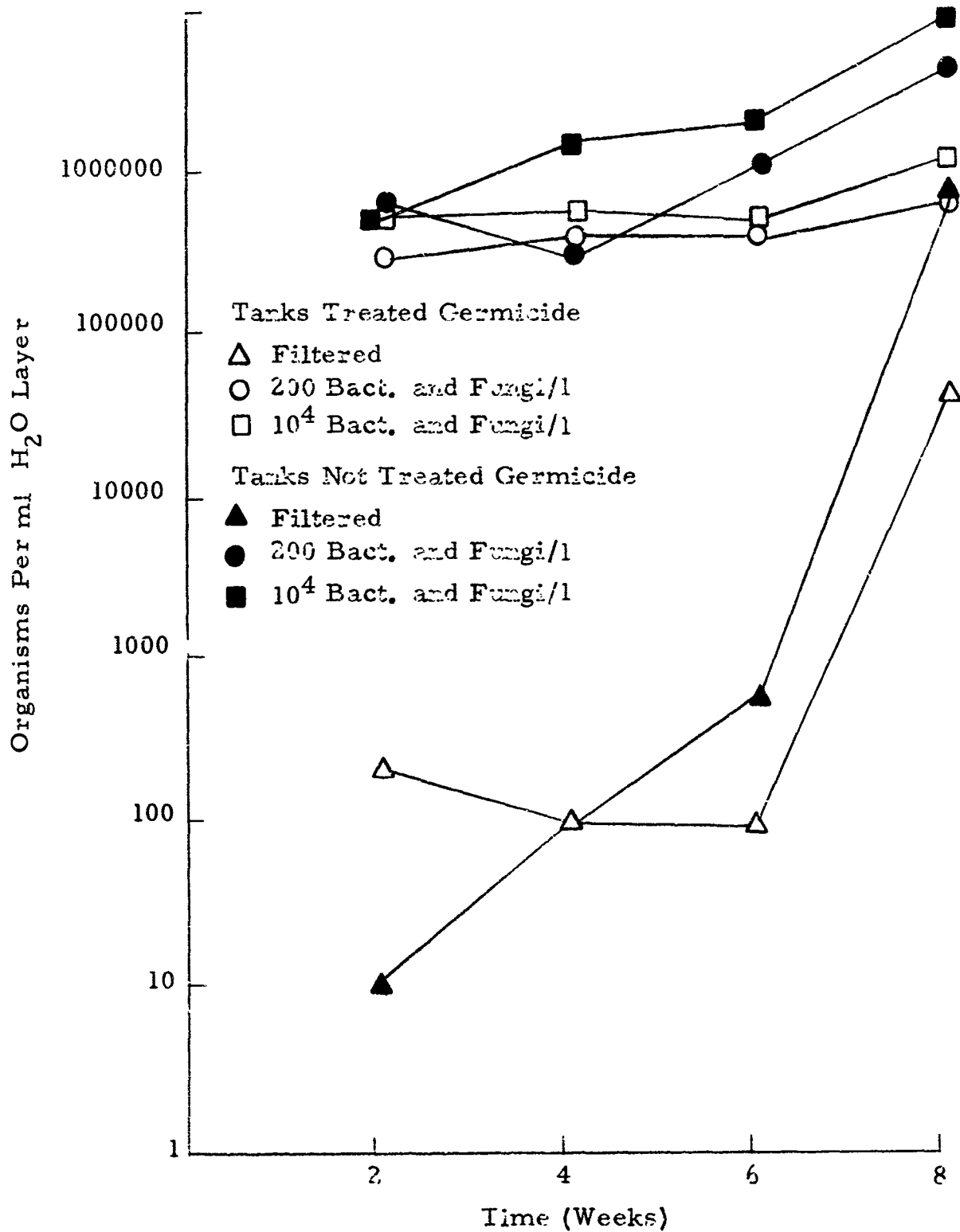
Figure 51. Microbial Population Changes in Water Layer Under Static Conditions
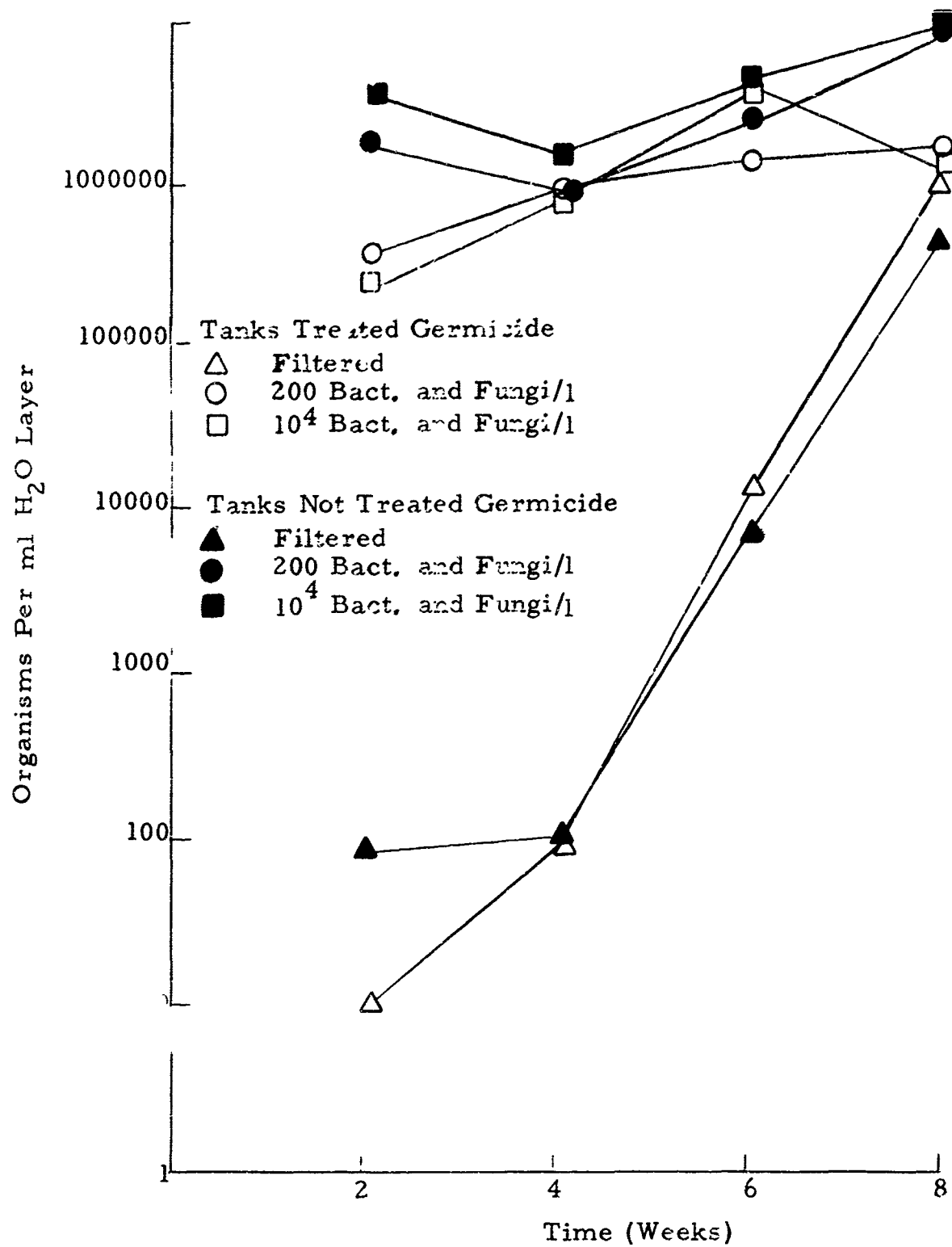
Figure 52. Microbial Population Changes In Water Layer Under Dynamic Conditions

Examination of the data curves indicates that all tanks will reach an equilibrium if allowed enough time. Under the test conditions, the time required would be on the order of 10 weeks. If the microbial content of the water phase is assumed to be at least a partial function of the microbial load in the fuel, then tank decontamination would have no effect over prolonged storage. It would seem that treatment with germicide would be applicable only if the fuel were sterile when placed in the tank. If sterile conditions are not met, the growth of microorganisms indigenous to the fuel quickly replaces those killed on the storage tank walls during germicidal treatment.

3. Turbidity of the Water Phase

Measurement of turbidity was selected as an indirect measure of microbial growth. The data obtained are shown in Table 6. The turbidity resulting from corrosion of the iron storage tank proved to be greater than that expected from the growth of fuel microorganisms. The water phase of all tanks except 8 and 11 had varying degrees of rust coloration. Analysis of data indicated that a lower percent transmittance was associated with storage tanks treated with the germicidal solution. A plot of the mean of values without treatment with a mean of all values with treatment (Figure 53) illustrates this effect. Separate analyses of data from each tank show that all do not conform; some tanks treated with the germicide have a turbidity about that of the untreated tanks. Variability in decontamination or preliminary degree of oxidation of the tank surface may be a partial cause.

The peracetic acid was selected for the following reasons: 1) rapid action, 2) broad spectrum, 3) no residual activity, 4) low concentrations being effective. Ethyl alcohol was not used due to its ineffectiveness as a germicide under these conditions.
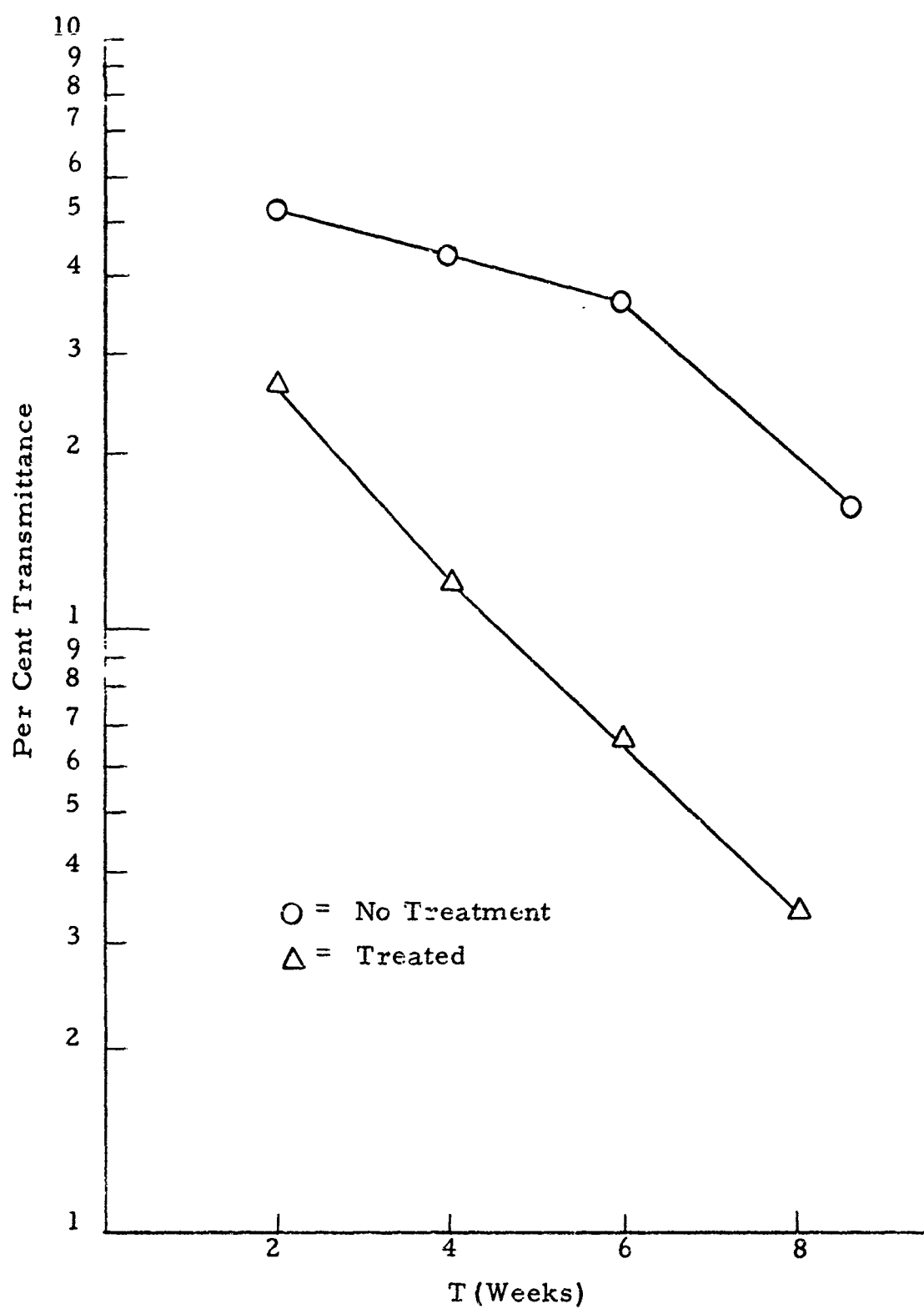
Figure 53. Effect of Peracetic Acid Germicide on Turbidity of Water Phase

Table 6. Transmittance of 1:5 Dilution of Water Layer
(Light Absorbed at 505 Millimicrons)

Tank No.	Time (Weeks)				
	0	2	4	6	8
1	—	30	12	24	0
2	—	25	8	2	1
3	—	21	8	2	1
4	—	26	13	6	0
5	—	31	20	6	12
6	—	26	13	0	0
7	—	25	8	5	0
8	—	85	76	81	77
9	—	45	25	15	5
10	—	30	23	5	2
11	—	78	79	70	51
12	—	72	50	40	45

4. pH of Water Phase

The determined pH values are shown in Table 7. No significant
change in pH was observed during the course of storage. After the
second week, all water phases were slightly acid, remaining at this
level for the duration. The pH ranged from 5.6 to 6.8.

Table 7. pH of the Water Layer During Storage

Tank No.	Time (Weeks)				
	0	2	4	6	8
1	—	6.15	6.2	6.2	6.4
2	—	6.2	5.9	5.7	6.0
3	—	6.6	6.5	6.5	6.4
4	—	6.43	6.0	6.8	6.0
5	—	6.65	6.1	6.4	6.7
6	—	6.55	6.4	6.5	6.0
7	—	5.95	6.1	6.1	5.6
8	—	6.30	6.1	5.6	6.1
9	—	5.85	6.4	6.5	6.4
10	—	6.39	6.4	6.1	6.8
11	—	6.30	6.4	6.0	6.3
12	—	6.20	6.5	6.3	6.5

D.   Conclusions

1)   Uninoculated filtered fuel consistently showed the lowest
     microbial count of all tanks studied throughout the 8-week
     storage.

2)   There was no significant difference in bacterial count between
     tanks previously soaked with germicide and tanks not soaked
     with germicide after 8 weeks of storage.

3)   There was no significant difference in bacterial count between
     tanks tested under static conditions and dynamic conditions.

4) Studies on the water layer showed that the microbial growth rate was greatest in the inoculated tanks. The uninoculated tanks maintained a low level of growth through the fourth week and then rapidly increased.

5) Turbidity of the water layer was greater in the tanks stored with germicidal treatment.

6) No significant change in pH was observed in the water phase during the course of storage.

XI. REFERENCES

1. Pohl, H. A. Some effects of nonuniform fields on dielectrics. J. Appl. Phys. 29: 1182-88 (1958).

2. Stuetzer, O. M. Ion transport high voltage generators. Rev. Sci. Instr. 32: 16-22 (1961).

3. ----. Ion drag pressure generation J. Appl. Phys. 30: 984-94 (1959).

4. ----. Magnetohydrodynamics and electrohydrodynamics. Phys. Fluids 5: 534-44 (1962).

5. ----. Electrohydrodynamic precipitator. Rev. Sci. Inst. 33: 1171-77 (1962).

6. White, H. J. and G. W. Penney. Electrical precipitation fundamentals. University Park, Pennsylvania State Univ., 1961.

7. Stuetzer, O. M. Apparent viscosity of a charged fluid. Phys. Fluids 4: 1226-31 (1961).

8. Kao, K. C. Some electromechanical effects on dielectrics. Brit. J. Appl. Phys. 12: 629-32 (1961).

9. Hoerner, S. F. Fluid dynamic drag. (1958). Published by author.

10. Aitchinson and Brown. The log normal distribution. Cambridge University Press (1957).

11. Jorgenson, G. V. and E. Will. Improved ion drag pump. Rev. Sci. Instr. 33: 55-56 (1962).

12. Middendorf, W. H. and G. H. Brown. Liquid dielectrics in an electric field. AIEE Trans. 77, Part 3: 795-99 (1958).

13. Stewart, G. W. X-ray diffraction in liquids. Phys. Rev. 30: 232-44 (1927).

14. Zaky, A. A., H. Tropper and H. House. Electrical conduction in organic liquids. Brit. J. Appl. Phys. 14: 651-56 (1963).

15. Kasemir, H. V. and L. H. Ruhnke. Antenna problems of measurement of the air-earth current. In Conference on Atmospheric Electricity, Proceedings, 2nd, 1958. Recent advances in atmospheric electricity, ed. by L. G. Smith. N. Y., Pergamon Press, 1958. pp. 137-47.

16. Adamczewski, J. Ann. Phys. 8: 309- (1937).

17. Bragg, J. K., A. H. Sharbaugh and R. W. Crowe. Cathode effects in the dielectric breakdown of liquids. J. Appl. Phys. 25: 332-91 (1954).

18. Stuetzer, O. M. Ion drag pressure generation. J. Appl. Phys. 30: 984-94 (1959).

19. Gemant, A. Phys. Rev. 58: 904- (1940).

20. Whitby, K. T. and A. R. McFarland. The decay of unipolar small ions and homogeneous aerosols in closed spaces and flow systems. In International Conference on Ionization of the Air, Philadelphia, 1961. Proceedings, vol. 1, Sect. 7. Philadelphia, 1961.

21. Standard handbook for electrical engineers. 9th ed. N. Y., McGraw-Hill, 1957. p. 409.

22. Crowe, R. W., J. W. Bragg and A. H. Sharbaugh. On the electric strength of aliphatic hydrocarbons. J. Appl. Phys. 25: 392-95 (1954); Electric strength and molecular structure of saturated hydrocarbon liquids. J. Appl. Phys. 25: 480-84 (1954).

23. Society for Industrial Microbiology. Special Publication no. 1. Proposed procedures for microbiological examination of fuels (1963).

24. U. S. Quartermaster Research and Engineering Center. Microbiological Deterioration Series. Report no. 6. A field survey of the microbiological contamination in JP-4 fuel and 115/145 AVGAS in a military fuel distribution system, by M. R. Rogers and A. M. Kaplan (1963).

25. Australia. Defence Standards Laboratories. Report 252. Fungal growths in aviation fuel systems, Part 2. Test methods, by G. F. Hazzard and E. C. Kuster (1962).

APPENDIX A

MATHEMATICAL NOMENCLATURE

MATHEMATICAL NOMENCLATURE

Symbol	Definition	Unit	Conversion Units
A	filter characteristic	m^{-1}	
a	particle radius	m	
B	size distribution characteristic	m^{-1}	
b_e	electric mobility	$m^2 \, volt^{-1} \, sec^{-1}$	$1 \, cm^2$ per esu sec $= 3.3361 \times 10^{-7} \, m^2 \, volt^{-1} \, sec^{-1}$
C	capacitance	amp sec $volt^{-1}$	
E	electric field	vm^{-1}	1 esu per cm $= 2.9966 \times 10^4$ volt m^{-1}
E_{max}	breakdown field	vm^{-1}	
E_r	radial field component	vm^{-1}	
E'_r	radial field component	vm^{-1}	
E_z	longitudinal field	vm^{-1}	
F	force	newton	1 dyne $= 10^{-5}$ newton
F_d	dielectrophoretic force	newton	
F_F	friction force	newton	
F_L	longitudinal Coulomb force	newton	
F_r	radial Coulomb force	newton	
f	liquid and time dependent term		
g	geometric factor		
h	flow rate dependent term		
K	dimensionless collection parameter		

Symbol	Definition	Unit	Conversion Units
I	current	amps	
m	mean		
m_e	median		
N_o	initial particle density	m^{-3}	
N_1	total particle density before filter	m^{-3}	
N_2	total particle density after filter	m^{-3}	
Q	electric charge	amp sec	1 esu = 3.3361×10^{-10} amp sec
q	electric charge density	amp sec m^{-3}	1 esu per cm^3 = 3.3361×10^{-4} amp sec m^{-3}
Q_{max}	maximum charge	amp sec	
q_o	initial charge density	amp sec m^{-3}	
R	resistance	volt amp^{-1}	
R_x	Reynold's number of length x		
r	radial distance	m	
r'	radius parameter	m	
r_o	radius of pipe	m	
r'_o	radius of center electrode	m	
T	time constant	sec	
t_c	characteristic time constant	sec	
U	voltage	volt	
U*	voltage to start corona ionization	volt	

A-3

Symbol	Definition	Unit	Conversion Units
v	velocity	$m\ sec^{-1}$	
y	distance from wall	m	
z	distance from ionizer	m	
z_c	characteristic distance	m	
δ	thickness of sublayer	m	
ϵ	dielectric constant	$amp\ sec\ volt^{-1}\ m^{-1}$	$1\ esu = 8.859 \times 10^{-12}\ amp\ sec\ volt^{-1}\ m^{-1}$
η	dynamic viscosity or efficiency	$newton\ sec\ m^{-3}$	$1\ poise = 1.02 \times 10^{-2}\ newton\ sec\ m^2$
η_m	mass efficiency		
κ	friction coefficient between particles and cylinder wall		
ν	kinematic viscosity	$m^2\ sec^{-1}$	$1\ stoke = 10^{-4}\ m^2\ sec^{-1}$
ρ	density of liquid	$kg\ m^{-3}$	
σ	electrical conductivity	$amp\ volt^{-1}\ m^{-1}$	$1\ esu = 1.11318 \times 10^{-10}\ amp\ volt^{-1}\ m^{-1}$
π	constant		3.14

c

DOCUMENT CONTROL DATA - R&D

Security classification of title, body of abstract and indexing annotation must be entered when the overall report is classified)

1. ORIGINATING ACTIVITY (Corporate author)	2a. REPORT SECURITY CLASSIFICATION
Applied Science Division, Litton Systems, Inc., Minneapolis, Minnesota 55413	Unclassified
	2b. GROUP

3. REPORT TITLE

ELECTROHYDRODYNAMIC REMOVAL OF MICROORGANISMS FROM HYDROCARBON FUELS

4. DESCRIPTIVE NOTES (Type of report and inclusive dates)
Final: 25 June 1963 - 20 November 1965

5. AUTHOR(S) (Last name, first name, initial)

Ruhnke, L., Will, E. and Pederson, P.

6. REPORT DATE	7a. TOTAL NO. OF PAGES	7b. NO. OF REFS
20 November 1965	122	25

8a. CONTRACT OR GRANT NO.	9a. ORIGINATOR'S REPORT NUMBER(S)
DA19-129-AMC-141(N)	ASD Report No. 2905
b. PROJECT NO. 1k012501A031(05)	
c.	9b. OTHER REPORT NO(S) (Any other numbers that may be assigned this report)
d.	

10. AVAILABILITY/LIMITATION NOTICES

Distribution of this document is unlimited.
Release to CFSTI is authorized.

11. SUPPLEMENTARY NOTES	12. SPONSORING MILITARY ACTIVITY
	U. S. Army Natick Laboratories, Natick, Mass. 01762

13. ABSTRACT

The feasibility of removing microorganisms and other particulates from hydrocarbon fuels by electrostatic precipitation was studied. Theoretic investigations describe the physics of electrohydrodynamic precipitation and essential parameters influencing collection efficiency. Measurements of fuel characteristics and filter parameters have been made which led to the development of an electrohydrodynamic filter. Particulates and a liquid are unipolarly charged in a corona edge ionizer and then are flushed into a precipitation tube in which particulates are moved by Coulomb forces into porous non-conducting walls. A 10-gpm model showed filter efficiencies of at least 85 percent by number of particles larger than 1 micron diameter. The basic advantages of the method investigated are the low pressure drop over the filter element and the small size of the unit.

14. KEY WORDS	LINK A		LINK B		LINK C	
	ROLE	WT	ROLE	WT	ROLE	WT
Ren.	8		4			
Micr ·ganisms	1,2		4			
Fuels	1		4			
Particles	1,2		4			
Precipitation	10					
Electrostatics	10					
Development			3			
Magnetohydrodynamics			2			
Filters(Fluid)	2					

INSTRUCTIONS

1. ORIGINATING ACTIVITY: Enter the n me and address of the contractor, subcontractor, grantee, Department of Defense activity or other organization (corporate author) issuing the report.

2a. REPORT SECURITY CLASSIFICATION: Enter the overall security classification of the report. Indicate whether "Restricted Data" is included. Marking is to be in accordance with appropriate security regulations.

2b. GROUP: Automatic downgrading is specified in DoD Directive 5200.10 and Armed Forces Industrial Manual. Enter the group number. Also, when applicable, show that optional markings have been used for Group 3 and Group 4 as authorized.

3. REPORT TITLE: Enter the complete report title in all capital letters. Titles in all cases should be unclassified. If a meaningful title cannot be selected without classification, show title classification in all capitals in parenthesis immediately following the title.

4. DESCRIPTIVE NOTES: If appropriate, enter the type of report, e.g., interim, progress, summary, annual, or final. Give the inclusive dates when a specific reporting period is covered.

5. AUTHOR(S): Enter the name(s) of author(s) as shown on or in the report. Enter last name, first name, middle initial. If military, show rank and branch of service. The name of the principal author is an absolute minimum requirement.

6. REPORT DATE: Enter the date of the report as day, month, year; or month, year. If more than one date appears on the report, use date of publication.

7a. TOTAL NUMBER OF PAGES: The total page count should follow normal pagination procedures, i.e., enter the number of pages containing information.

7b. NUMBER OF REFERENCES: Enter the total number of references cited in the report.

8a. CONTRACT OR GRANT NUMBER: If appropriate, enter the applicable number of the contract or grant under which the report was written.

8b, 8c, & 8d. PROJECT NUMBER: Enter the appropriate military department identification, such as project number, subproject number, system numbers, task number, etc.

9a. ORIGINATOR'S REPORT NUMBER(S): Enter the official report number by which the document will be identified and controlled by the originating activity. This number must be unique to this report.

9b. OTHER REPORT NUMBER(S): If the report has been assigned any other report numbers (either by the originator or by the sponsor), also enter this number(s).

10. AVAILABILITY/LIMITATION NOTICES: Enter any limitations on further dissemination of the report, other than those imposed by security classification, using standard statements such as:

(1) "Qualified requesters may obtain copies of this report from DDC."

(2) "Foreign announcement and dissemination of this report by DDC is not authorized."

(3) "U. S. Government agencies may obtain copies of this report directly from DDC. Other qualified DDC users shall request through
_____."

(4) "U. S. military agencies may obtain copies of this report directly from DDC. Other qualified users shall request through
_____."

(5) "All distribution of this report is controlled. Qualified DDC users shall request through
_____."

If the report has been furnished to the Office of Technical Services, Department of Commerce, for sale to the public, indicate this fact and enter the price, if known.

11. SUPPLEMENTARY NOTES: Use for additional explanatory notes.

12. SPONSORING MILITARY ACTIVITY: Enter the name of the departmental project office or laboratory sponsoring (paying for) the research and development. Include address.

13. ABSTRACT: Enter an abstract giving a brief and factual summary of the document indicative of the report, even though it may also appear elsewhere in the body of the technical report. If additional space is required, a continuation sheet shall be attached.

It is highly desirable that the abstract of classified reports be unclassified. Each paragraph of the abstract shall end with an indication of the military security classification of the information in the paragraph, represented as (TS), (S), (C), or (U).

There is no limitation on the length of the abstract. However, the suggested length is from 150 to 225 words.

14. KEY WORDS: Key words are technically meaningful terms or short phrases that characterize a report and may be used as index entries for cataloging the report. Key words must be selected so that no security classification is required. Identifiers, such as equipment model designation, trade name, military project code name, geographic location, may be used as key words but will be followed by an indication of technical context. The assignment of links, rules, and weights is optional.